COMPUTATIONAL STUDY OF C-H BOND CLEAVAGE AND C-C BOND FORMATION PROCESSES CATALYZED BY TRANSITION METAL COMPLEXES

Abel Jean Serge Locati

Dipòsit Legal: T. 278-2012

Abel Locati

Computational study of C-H bond cleavage and C-C bond formation processes catalyzed by transition metal complexes

DOCTORAL THESIS

Supervised by Prof. Feliu Maseras

Institute of Chemical Research of Catalonia (ICIQ)

UNIVERSITAT ROVIRA I VIRGILI

TARRAGONA
2011

Institute of Chemical Research of Catalonia (ICIQ)
Avgda. Països Catalans 16,
43007 Tarragona (Spain)

I STATE that the present study, entitled "Computational study of C-H bond cleavage and C-C bond formation processes catalyzed by transition metal complexes" presented by Abel Locati for the award of the degree of doctor, has been carried out under my supervision at the Institute of Chemical Research of Catalonia (ICIQ), and that it fulfils all the requirements to be eligible for the European Doctorate Award.

Tarragona, December 2011

Feliu Maseras

UNIVERSITAT ROVIRA I VIRGILI
COMPUTATIONAL STUDY OF C-H BOND CLEAVAGE AND C-C BOND FORMATION PROCESSES CATALYZED BY TRANSITION METAL COMPLEXES
Abel Jean Serge Locati
DL:T. 278-2012

Acknowledgments

I would like to thank Feliu Maseras for the opportunity to join his group to undertake this thesis. I really appreciated his kindness, his scientific integrity, and the freedom he allowed me regarding the way to perform my work. I believe this was scientifically very emancipating. Thank you.
I would like to thank Jonathan M. Goodman for his hospitality in his group in Cambridge during the summer of 2010. This was a very fruitful experience, where I had the opportunity to learn new computational tools and where I could explore a new research field. It was also the occasion to discover another country, and another culture.
I also had the opportunity to visit the laboratory of Odile Eisenstein and Eric Clot. This was a very interesting, but too short, experience. I really appreciated the guidance of Eric Clot.
I would like to thank Nuria Vendrell for the huge help she gave me regarding all the administrative problems when I arrived in Tarragona (and on many occasions afterwards).
I would like to thank Michel Etienne for all the very interesting and relaxed scientific discussions we had during his stay in Tarragona (and also afterwards). It was very rewarding to work on these niobium systems.
Of course, I would like to thank all the people I met in the lab through the years. In alphabetic order, I sincerely thank Neyvis Almora, Carina Backtorp, Hugo Barrera, Luca Bellarosa, Maria Besora, Fabienne Bessac, Piotr Blonski, Carles Bo, Laureline Bonniard, Ataualpa Braga, Oriol Caldero, Giuliano Carchini, Fernando Castro, Gemma Christian, Silvia Diez, Steven Donald, Ruth Dorel, Laura Estévez, Daniel Fernandez, Torstein Fjermestad, Monica García, Mickael Gicquel, Adrià Gil, Charles Goehry, Jaime Gómez, Christophe Gourlaouen, Martín Gumbau, Alexander Hamilton, Elena Herrero, Joan Iglesias, Jesús Jover, David Karhánek, Chunhui Liu, Núria López, Laura Mateus, Maxime Mercy, Pere Miró, Ainara Nova, Gerard Novell, Rob Paton, Rene Petz, Simon Pierrefixe, Jose Javier Plata, Cristina Pubill, Rocio Recio, Chamil Sameera, Gladys Tasso Ansaldi, Crisa Vargas, and Eric Zuidema.
I am particularly indebted to Fabienne, Ata, and Sameera for the many things they taught me.
There are also many people in ICIQ that I am really happy to have met. They are too many to name them all, but I am pleased to mention the following: Olivier, Amol, Blaise, Ala, Nicolas, Xisco, Ana, Mathieu, Eloisa, Giovanni.
In my three months stay in Cambridge, I had the chance to meet some interesting people: Jack (thanks for Marmite!), Russell, Bruno, David, Richard, Steven and Carlos.

I would also like to thank some of the many people I met in Tarragona over these last five years, outside the institute. I would like to name Juan, Spike, Tafti, Alfredo, Cyril, Roc, Luca, Yannick, Rebeca, Pascal, Andor, and many many more. Even if they will never read these lines, their names have their place here because they highly contributed to make these five years very exciting.

At the beginning of my thesis, I had the chance to pass one month in Santander to follow some doctoral classes. This was an stimulating experience, socially very rich, where I met many friends, such as Mireia, Ramon, Pablo, Ceila, Miquel, Ana, Pablo, Max, JuanJo and many more. I would like to thank Josep Mª Poblet for being my tutor on that occasion.

I need to thank three of my friends from my hometown: Aurélien Gasnier, David Schleck, and Matthieu Herr. Their philosophical thoughts helped me putting all these things in their appropriate perspective. It was nice to have been permanently connected, even with such large distances between us.

I would like to thank my parents Hélène and Serge. Without their love and constant support, this PhD thesis would have been much more difficult to complete.

I would also like to thank Manolo and Reme from "el Delta" for providing me with enough energy at lunchtime, day after day. I also have to mention Xian ("La Coimbra"), and Josep-Maria ("Bodegas Gras").

Finally, last but not least, I would like to express all my gratitude to Asia. Numerous are the reasons why I should thank her, and most of them don’t have their places here. I am particular grateful to her for all the good and bad moments we shared over these last few years.

UNIVERSITAT ROVIRA I VIRGILI
COMPUTATIONAL STUDY OF C-H BOND CLEAVAGE AND C-C BOND FORMATION PROCESSES CATALYZED BY TRANSITION METAL COMPLEXES
Abel Jean Serge Locati
DL:T. 278-2012

The work of this thesis has been possible thanks to financial support from the "Ministerio de Ciencia e Innovación" and the Institute of Chemical Research of Catalonia (ICIQ). The work has been carried out within the framework of the project "Diseño de Catalizadores para una Química Sostenible: Una Aproximación Integrada" (CONSOLIDER CS2006-0003) belonging to the program CONSOLIDER-INGENIO 2010 of the "Ministerio de Ciencia e Innovación".

Contents

UNIVERSITAT ROVIRA I VIRGILI
COMPUTATIONAL STUDY OF C-H BOND CLEAVAGE AND C-C BOND FORMATION PROCESSES CATALYZED BY TRANSITION METAL COMPLEXES
Abel Jean Serge Locati
DL:T. 278-2012

Chapter 1

Introduction

UNIVERSITAT ROVIRA I VIRGILI
COMPUTATIONAL STUDY OF C-H BOND CLEAVAGE AND C-C BOND FORMATION PROCESSES CATALYZED BY TRANSITION METAL COMPLEXES
Abel Jean Serge Locati
DL:T. 278-2012

Computational chemistry[1, 2] has gained a wide popularity over the last decades. Computational techniques are now routinely used in many fields of chemistry and they are valuable tools in several fields such as material science,[3] computational biochemistry[4] (like protein folding)[5], catalysis,[6, 7] and many more. And the list is growing. Among the many potential applications for computers, mechanistic studies of chemical reactions has been constantly developed since the use of accurate techniques is nowadays accessible with reasonable computer times. The scale of computable systems started with only a few atoms, and was progressively expanded to several decades. Currently, it is feasible to compute chemical systems of 150-200 atoms through DFT with accurate functionals in an acceptable range of time. The Nobel Prize awarded to Walter Kohn and John A. Pople in 1998 recognized both the development of computational methods and the major contribution of DFT techniques in the realm of computer modelling. The constant improvement of computer power has no doubt played a major role in such an expansion. Many chemical concepts which were impossible to envision computationally are now easily computable. Very large systems are accessible with the implementation of QM/MM techniques.[8, 9] Computing enzymes is one of the long-lasting challenges which recently became affordable for standard equipments.[10, 11] We can also mention the implementation of solvation effects through continuum electrostatic models which significantly improved the accuracy of the systems computed.[12]

If it is accepted that the technical problems inherent to computation which previously impeded its progression will be constantly reduced in the future, the relevance of computers in chemistry has not always been considered obvious. Why computing chemical processes? Chemical reactions have long been developed without an accurate understanding of the exact sequence of events taking place along a reaction. Various experimental optimization methods allow the development of optimum reaction conditions. More generally, chemistry has indeed been performed successfully for centuries without the help of computation. As a consequence, theoretical approaches have not always being recognized by the general community of chemists as a valuable tool. However, computation can definitely relieve the synthetic chemist in his goal to obtain better reactions. For instance, the choice of appropriate experimental conditions usually requires some long and fastidious tests of large amount of possible ligands, additives, solvents, which usually require long performing times and generate large amounts of waste. The use of computation can potentially relieve the synthetic chemist by pointing out the optimal parameters of a reaction. If impossible experimentally, the identification by computational means of the most important steps and the key intermediates of a reaction can help determine where the efforts towards better conditions should be directed. Examples of mechanistic elucidation through computation in homogenous catalysis are now numerous. Nonetheless, the direct improvement of catalytic processes through computationally elucidated

mechanisms are still scarce, but they start to emerge. Optimizing the conditions of a chemical reaction is not the only goal. We believe in the utility of studying reaction mechanisms, even for reactions that are already working well. Apart from technical considerations, the chemical understanding of the precise mechanism of a reaction is of prime importance by itself. Performing science is inherently directed to a better understanding of our world and the chemical concepts which govern it are still far from being understood. The utility of reaction mechanism might not be seen immediately, but its realization will be part of a general comprehension of chemistry, and, by extension, science.
It is believed that the continuous improvement of both computer power and computational methods will allow faster and more efficient mechanistic elucidations which will reduce the time between experimental outcomes and the results of the computational efforts. Ultimately, the gap between bench and *in silico* experiments will be reduced to the point that both experimentalists and theoreticians will work hand in hand, joining their tools in a coordinated effort towards more efficient chemical processes.

Among the myriad of bond formations and bond cleavages which take place in chemical reactions, two have been the topic of intense research in the last decades: the carbon-carbon bond formation and the carbon-hydrogen bond cleavage. They share the particularity to be considered as very inert bonds. Chemists usually took advantage of the functional groups in molecules because they are typically more reactive. Sulfur, oxygen, phosphorous, and nitrogen groups are typically considered as the groups of choice to structurally modify a molecule. Nonetheless, the realm of transition metal allowed the discovery of less obvious reactions, and soon emerged the idea that carbon-carbon bonds, and then carbon-hydrogen bonds were also fruitful patterns.[13] This triggered many studies which aim at developing valuable chemistry from inert bonds, sparing their prior functionalization step.

1.1 C-H bond cleavage

1.1.1 Challenges and mechanistic overview

Saturated hydrocarbons are the main components of petroleum and natural gas, and their availability makes them interesting targets for the conversion into more practical and useful compounds. Activation of the inert carbon-hydrogen bond of such saturated molecules has become an important challenge to overcome the major energetic challenges of the 21st century.[14] So far, a broad applicability of the C-H activation techniques in synthetic chemistry has been hampered by the high dissociation energy of the inert C-H bonds (101 kcal/mol^{-1} for ethane, 105 kcal/mol^{-1} for methane),[15] which make their functionalizations a hard task.[16] Alkanes, and more generally saturated hydrocarbons do react under very high

temperatures, and industrial processes allow their conversion into more valuable compounds. However, the very harsh conditions of the combustion processes inherently prevent the development of smooth, controllable and well-defined exploitations into fine chemicals. Enzymes can also be very efficient activating agents, but applications to large scale processes are not easy. The use of transition-metal based homogeneous catalysis has been explored, and significant breakthroughs over the last three decades have seen the development of catalysts operating under mild conditions, which lead the C-H activation processes to the doors of economical viability and practical development.[17-20] In the middle of the sixties of the past century, Chatt reported the ability of a zerovalent ruthenium complex to perform oxidative addition with naphtalene.[21] The so-called Shilov catalytic systems were another breakthrough in the field.[22] We also mention the case of the alkane oxidation and the important discovery of mercury and platinum catalysts which promote the transformation of methane to methanol through a carbon-hydrogen activation mechanism.[23, 24] Since then, the field received permanent attention, and the quest for a general catalyst that can operate in mild conditions is far from fully achieved.[10, 11] Much effort has been devoted into the mechanistic understanding of the C-H activation processes over the last decades, and many of such reactions are now rather well understood.[25]

Figure 1.1.1 collects the mechanisms generally accepted for C-H bond activation by transition metal complexes. The first mechanism, reported in equation (1), is the oxidative addition process that starts with a metal complex (L_nM) bearing a vacant site, usually generated *in situ* from a stable 18-electron complex. Coordination of the hydrocarbon fragment R-H to the metal vacancy is followed by formation of a metal-hydrogen and a metal-carbon bonds concomitantly with the cleavage of the carbon-hydrogen bond. The oxidation number increases by two units during the process. This mechanism is typically operative for electron-rich low-valent late transition metals, such as Ir, Ru, Pt, Os, Re…. The complexes involved should not be too sterically demanding at the metal center, and the electron count of the reactive intermediate should be 16 or less. Such a mechanism is impossible in early transition metal complexes where the metal is in the configuration d^0. Many transition metal complexes with the metal in the electronic configuration d^{10}, d^8, d^6 or d^4 are able to activate alkane or arene compounds through an oxidative addition mechanism, and this has been reviewed on several occasions.[26-28] Early reports include iridium complexes such as $(C_5H_5)Ir(PMe_3)$, or related complexes.[29-31] The first oxidative addition in a complex with a d^6 metal center was also reported by Bergman. $Cp^*Ir(PMe_3)(Me)(OTf)$ appeared to activate mildly the C-H bonds of several alkanes.[32] Studies of the mechanism of oxidative addition started several decades ago,[33] and computational mechanistic reports helped rationalize this process in many occasions.[34, 35] The second process represented in equation (2) is the sigma-bond metathesis, which is usually operative at electrophilic early transition metal centers (or rare-earth metal complexes), *i.e.* at metals that cannot be further oxidized (d^0 complexes). This process is characterized by the concerted cleavages of the R-H an M-R' bonds and formations of the M-R and R'-H bonds through a four-center transition state. One of the first reports features some

scandium derivatives $Cp^*_2Sc\text{-}R$ ($Cp^* = (\eta^5\text{-}C_5Me_5)$ and R = halide, alkyl, alkenyl…).[36, 37] Numerous examples can also be found in the literature.[28]

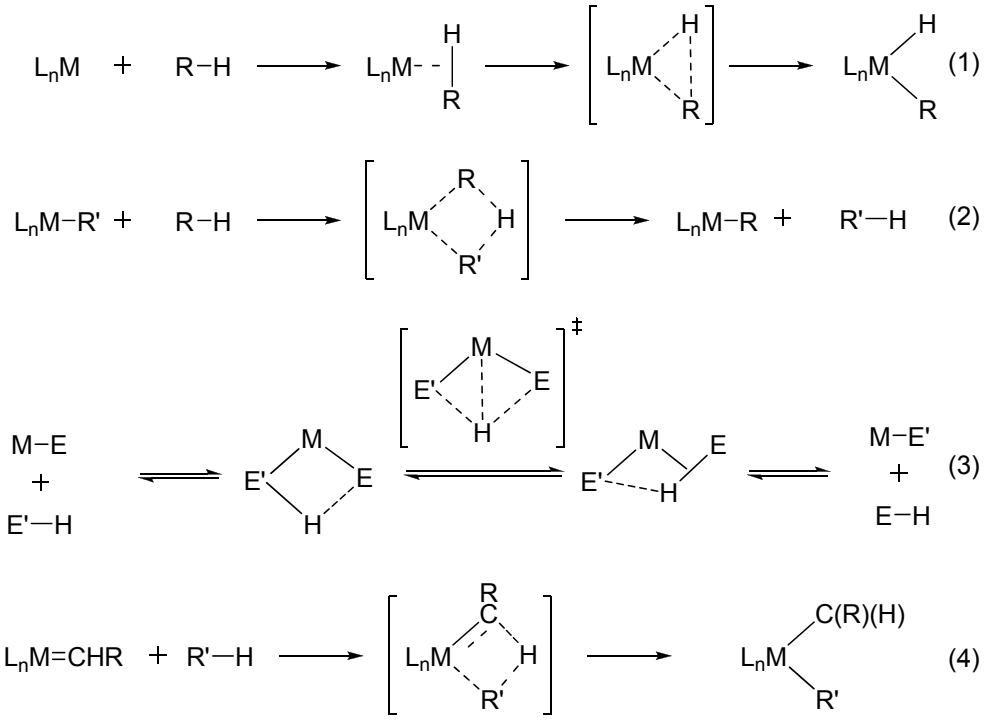

Figure 1.1.1 General mechanisms traditionally considered for a C-H activation process.

We note that the border between these two mechanisms is sometimes rather blurred and a combination of the two can be operative and was indeed reported in several occasions.[28, 38] The importance of σ complexes in C-H activation processes by late transition metals under constant oxidation state emerged recently.[39] The σ-CAM mechanism (see equation (3)) recognizes the adaptability of sigma-bond metathesis mechanisms to late transition metal fragments. The mechanism depicted in equation (4) is an 1,2-addition across a metal-ligand double bond. This process is also an important strategy for C-H activation reactions, and it has been used in the case of C-H activation of benzene across a Zr-N double bond.[40] Similarly, C-H bond activation of various hydrocarbons across a titanium-carbon triple bond was reported.[41, 42] A related process is the carbene insertion of a alkane onto a metal-carbene double bond,[43] where the metal is not directly involved in the activation process, but bind the active carbene fragment.[44] We also mention the Lewis-base assisted deprotonation, which has also been called the concerted metalation deprotonation (CMD), which involves the cooperation of a base to perform intra- or intermolecular C-H activation.[45-47]

1.1.2 Agostic interactions in organometallic systems

The term "agostic" is derived from the ancient Greek language, and means "to hold close to oneself". Agostic interactions are very important in organometallic chemistry due to their potential implications in various processes.[48, 49] They are indeed believed to have a role in the formation of intermediates in many organometallic reactions. Among others, the β-H elimination process assisted by a γ agostic interaction in zirconium complexes is usually highlighted.[50] They might also be involved in the mechanism of the Green-Rooney olefin polymerization, along the formation of the metal hydride bond.[51] Any covalent bonds in close proximity from a metal center can be potentially considered as agostic. The agostic interaction has been first contemplated as a three-center two-electron interaction between the metal and the C-H bond involved.[52, 53] This was described by Brookhart and Green as the "donation of C-H bonding electron into a vacant atomic orbital on the transition metal atom".[52] We note that the close contact of a C-H bond and a metal center does not suffice to define such proximity as agostic interaction.[54] The difficulty is to delimitate a clear definition of what should be considered as agostic, and what should not. Since the term was coined, the exact definition has been the subject of debate in the chemical community, and a clear way of defining these interactions has not emerged yet.[49, 55] However, it is usually considered that the distortion of a covalent bond in close contact with a metal center is the main attribute of such interactions, and we will thus consider such distortion as its definition.
Experimental characterization techniques of agostic interactions include gas electron diffraction, and NMR spectroscopy.[55] X-Ray diffraction is also used but the difficulty to locate the hydrogen atoms close to the metal makes this technique rather unreliable. A well-defined way to characterize an agostic bond has not emerged, being experimental or theoretical.

1.2 C-C bond formation

1.2.1 Cross-coupling reactions

The overwhelming importance of carbon-carbon bond formation reactions was recently acknowledged by the attribution of the 2010 Nobel Prize in chemistry to Richard F. Heck, Ei-ichi Negishi and Akira Suzuki for their work in the development of cross-coupling reactions. Many efforts have been devoted around the world to develop this very rich chemistry[56] and cross-coupling reactions are commonly used in academia and in the industry.[57] The possibilities of such reactions are also exploited in the total synthesis of natural products.[58, 59] In the following, we will quickly review some of the fundamental carbon-carbon bond forming reactions.

The first coupling reaction was pioneered in 1855 by Charles-Adolphe Wurth, and consists of the reaction of two alkyl halides with sodium to form a new carbon-carbon bond (equation (1) of Figure 1.2.1). In 1901, Fritz Ullmann discovered the reaction depicted in equation (2), later called the Ullmann coupling. The reaction needs harsh conditions.[60, 61]

The Mizoroki-Heck coupling (eq.(3)) was originally reported by Mizoroki in 1971,[62] (although some contributions appeared earlier), and developed by Heck.[63, 64] Activated olefins were found to react with organic halides stereoselectively (the *trans* product is typically favoured).

Acetylenic coupling was primarily reported by Glaser in 1869.[65, 66] Some experimental issues (generation of explosive intermediates) prevented a broad applicability of this method. Improvements in the experimental protocol,[67] followed by the introduction of new ligands by A.S. Hay expanded the scope of the reaction.[68] We also mention the important contribution of Sonogashira (coupling schematically represented in equation (4)), whose main features is the presence of two catalysts : a Pd(0) species, and a copper salt.[69] The acetylenic coupling has many implications in various fields of chemistry.[70]

The Suzuki-Miyaura reaction (eq.(5) and (6)) consists of a palladium-catalyzed coupling between an organoboronic acid and an organic halide.[71] The mechanism has been thoroughly studied computationally,[72, 73] and the importance of the base has been rationalized.[74] The scope of this ubiquitous coupling has been hugely expanded.[75]

The palladium-catalyzed coupling of tin reagents was discovered in 1975 (eq. (7)).[76] This coupling has also been vastly developed,[77] and successfully applied to a vast amount of compounds. The mechanism is well-defined and is rather well understood.[78]

The Negishi coupling (eq.(8)) involves an organozinc, an halide and a palladium (or nickel) based catalyst.[79] Its scope is also very large, with various organohalides competent for the coupling.[80]

Coupling reactions are not limited to carbon-carbon bond forming reactions.[81] As an example, we mention that Buchwald and Hartwig developed a highly versatile palladium-catalyzed coupling affording aryl amines (eq.(9)),[82-84] originally discovered by Migita in 1983.[85]

More recently Fukuyama discovered a reaction depicted in equation (9), later coined the Fukuyama coupling, which consists of a palladium-catalyzed coupling between a organozinc and a thioester.[86]

Finally, the first coupling involving silicon reagents was reported by Hiyama in 1988, and is represented in equation (10).[87] However, most of the development of this reaction (fluoride-free processes, expansion of the scope) has been done by the group of Denmark.[88] The mechanism study of the fluoride-free coupling is one of the aims of this PhD thesis.

Since the primary reports of Wurtz and Ullmann, a wealth of cross-coupling reactions were thus reported over the last century.[89] The use of various metal catalysts and organic reagents allowed the development of an extremely rich chemistry. Their usefulness for the synthetic chemist, and the tremendous

importance of the applications derived from these, make the mechanistic studies of such processes of crucial importance. The use of DFT calculations has been shown reliable and useful on many occasions, in a variety of coupling reactions.[90]

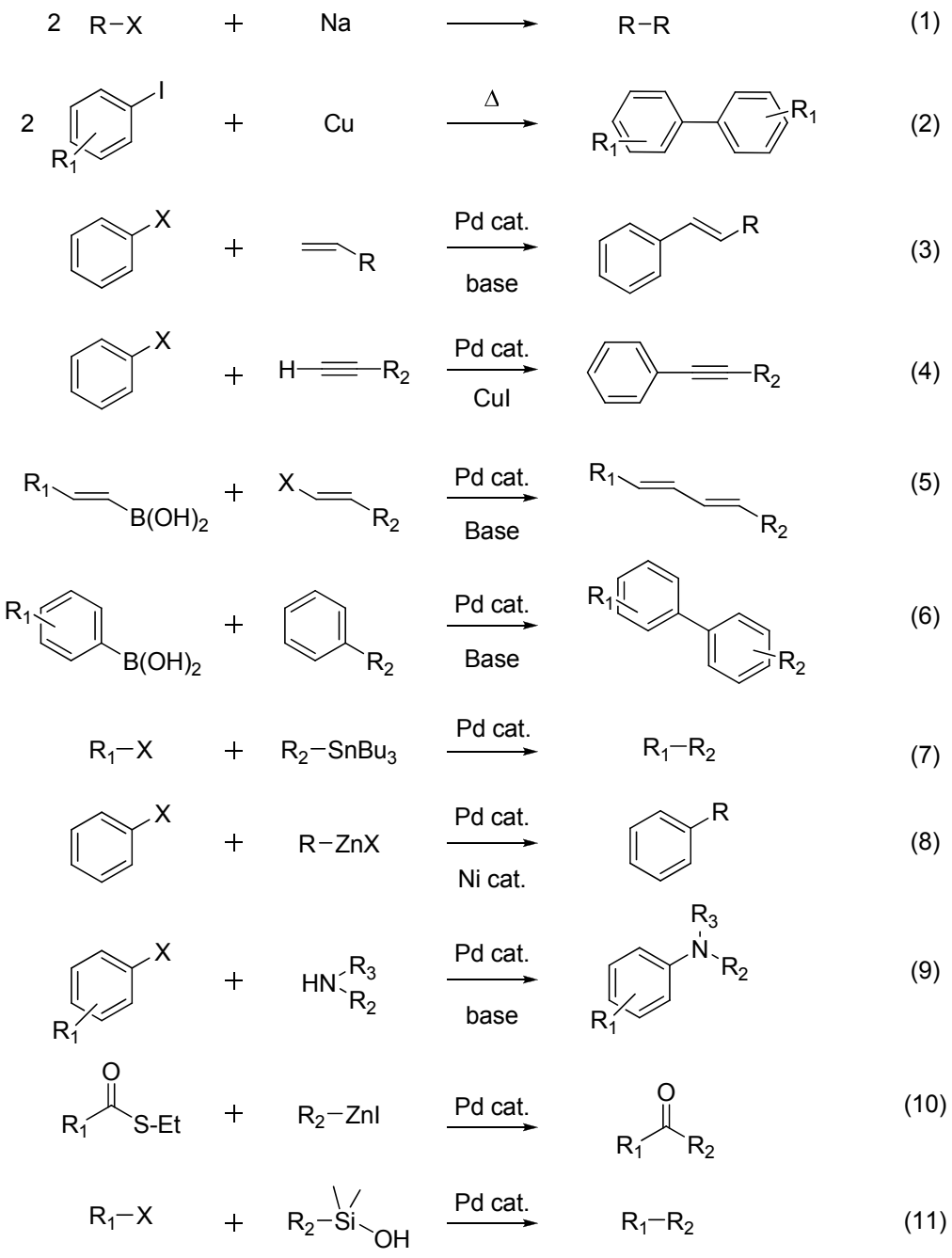

Figure1.2.1 Schematic representation of the main cross-coupling reactions.

Regarding the theoretical treatment of the cross-coupling reactions, the Suzuki-Miyaura coupling is among the most studied, and many computational reports were published over the last decade. An understanding of the full catalytic cycle has been reached. [73, 91, 92] The elucidation of the Heck coupling has also been the topic of several theoretical reports.[93, 94] The transmetalation step of the Stille cross-coupling was thoroughly analyzed by Yates *et al*, and the phosphine ligand effect was rationalized.[95]

Regarding the cross-coupling of organosilicon compounds (Hiyama coupling), Sakaki and co-workers studied the role of fluoride on the activated transmetalation process between a vinylsilane and a palladium (II) complex.[96] To our knowledge, no other computational treatment of the Hiyama cross-coupling (and especially the fluoride free process) has appeared.

1.2.2 General mechanism of a cross-coupling reaction

The generally accepted mechanism of a cross-coupling is surprisingly homogeneous, in spite of the huge variety of metal catalysts, ligands, and organic reagents used. The three main steps are the oxidative addition, the transmetalation, and the reductive elimination and are represented in Figure 1.2.2. Oxidative addition and transmetalation are usually the most energetically demanding processes of the coupling, the reductive elimination being considered as the easiest step (even if this can be arguable in some cases).

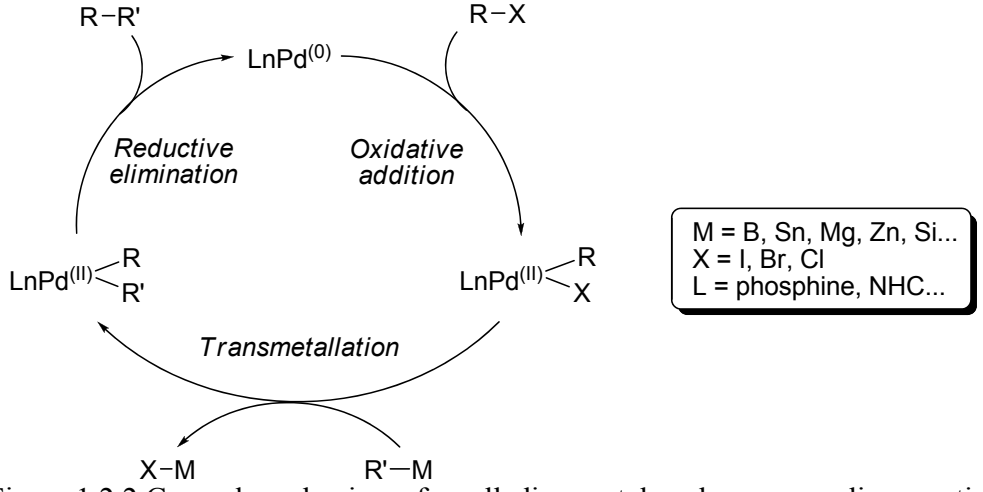

Figure 1.2.2 General mechanism of a palladium-catalyzed cross-coupling reaction.

However, even if the general three-steps pattern is followed by the vast majority of cross-coupling reactions, the precise mechanistic picture is more complex and highly dependant of the molecular components and the experimental conditions. The oxidative addition step has been extensively studied computationally.[97, 98] It is usually considered as one of the most energy demanding step of the catalytic cycle, but no general rules can be drawn. Three pathways are usually considered for this process, namely a dissociative pathway (with one of the ligands bound to the metal

which dissociates before addition of the organic halide), an associative pathway concomitant with displacement of one of the ligands (the organic halide binds the metal concomitantly with the loss of one ligand), and, in the case of bisphosphine complexes, a bisphosphine pathway where no ligands are leaving the coordination sphere of the metal during the oxidative addition (this last case is usually discarded for steric reasons, especially when very bulky ligands are used).

Reductive elimination has also been fairly studied in the past.[99] The rates of this process can vastly vary, depending on the electronic and steric properties of the complexes.[100] Nonetheless, computational efforts allowed the establishment of general trends and the influence of some ligands could be rationalized.[101, 102]

In contrast, the transmetalation step is highly dependant of the particular cross-coupling process, and the complexes involved. General rules are even more complicate to determine for this process, but it is usually considered that it is significantly demanding in energy.

The understanding of the precise events occurring in a cross-coupling will ultimately allow the design of new improved reagents and help the development of coupling using milder conditions. Part of this thesis is a modest attempt towards this elusive goal.

1.2.3 Olefinic ligands in cross-coupling reactions

Olefinic ligands are ubiquitous in chemistry, and their fundamental role has been highlighted recently.[103, 104] The effects of alkene ligands on the oxidative addition of a cross-coupling catalytic cycle are rather well-understood. The reaction rate for the olefin ligated palladium catalyst is believed to be slower than the non-ligated species for that particular step. Particularly, dibenzylideneacetone (dba) is widely considered as an olefinic ligand, and its behaviour has been studied in details by Amatore and Jutand.[105, 106] $Pd(dba)_2$ and $Pd_2(dba)_3$ are some of the most widely used palladium pre-catalysts and the non-innocent role of dba in the oxidative addition step has been established.[107] The presence of dba possibly stabilizes the palladium catalyst, preventing is decomposition. However, dba also participates in an equilibrium between the reactive species towards the oxidative addition (L_nPd, where L_n is typically a monodentate or a bidentate phosphine) and the much less reactive species (the dba ligated catalyst $L_nPd(dba)$). The dba ligated species is the main species in solution but the less reactive towards oxidative addition (as depicted in Figure 1.2.3, $k_2 < k_1$). The concentration of the active species is then controlled by the extent of the less reactive species. The type of ligand L (typically a phosphine) has also an influence on the reaction rate but the concentration of dba in solution is key in the process by affecting the availability of the reactive species. We note that dba controls the rates of the oxidative addition, but is probably absent from the transition state of this process.[108]

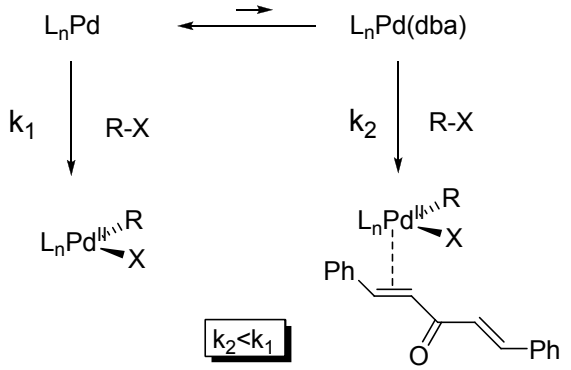

Figure 1.2.3 Reactive species in the oxidative addition step.

In contrast, olefinic ligands such as dba are known to have beneficial effects on the reductive elimination step. Regarding the transmetalation process, the effect of dba on the reaction rates or the mechanism is unknown. Figure 1.2.4 sums up the dba effects (and more generally that of the olefinic ligands) on a cross-coupling reaction.

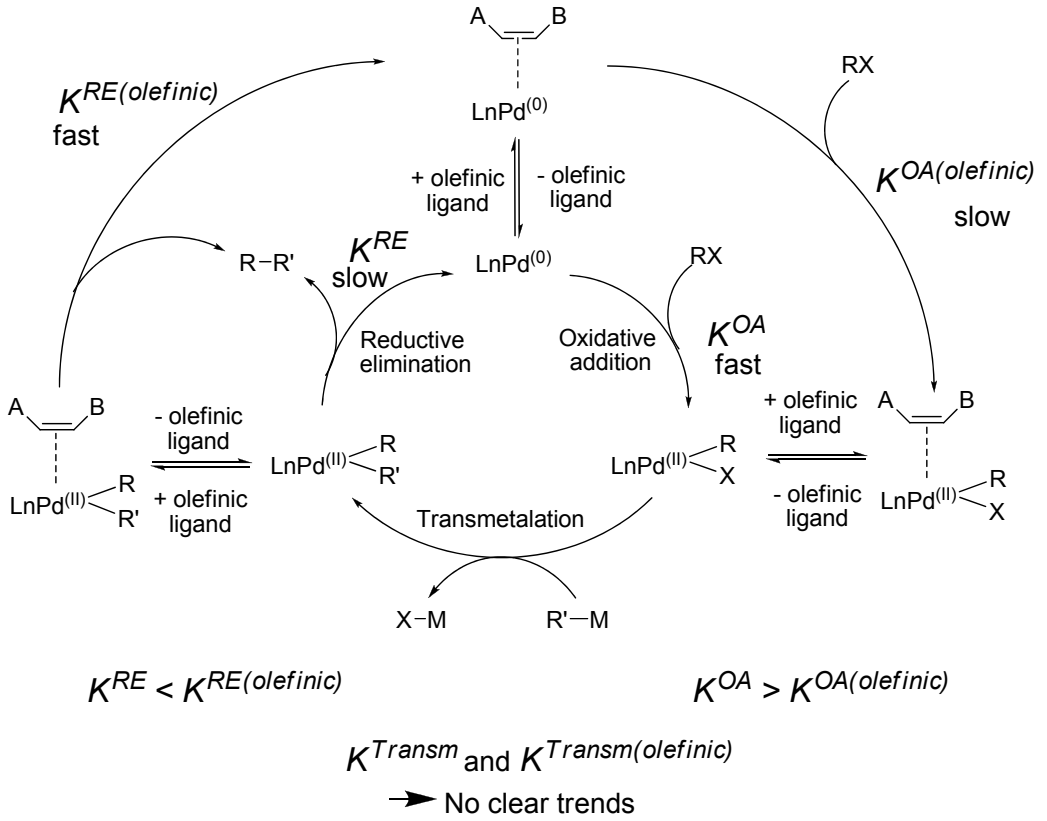

Figure 1.2.4 Olefinic effects along the general cross-coupling catalytic cycle.

The role of dba on the transmetalation step of the fluoride-free silanolate coupling will be studied in this thesis.

The quest for milder conditions is a guiding line in the chemistry of cross-coupling. The possibility to use aryl chlorides instead of aryl bromides and iodides has been an important step towards the use of cheaper reagents with easier availability.[109-111] The stronger R-X bond when going up the halogen part of the periodic table makes the oxidative addition step more difficult with chloride compounds than with bromide or iodide reagents. The challenging coupling of alkyl organic compounds was another major improvement.[112, 113] The use of simple alkane reagents (R-H) instead of halide compounds (R-X), taking advantage of C-H bond activation processes is now one of the forthcoming challenges.[114] C-H activation and carbon-carbon bond forming reaction are two very powerful tools for the synthesis of new molecules. The development of methods which would take advantage of both concepts will undoubtedly unravel exciting possibilities to build new molecular scaffolds.

1.3 Density Functional theory : An overview

Foundations of the Density Functional theory (DFT) emerged at the beginning of the 20th century, when the idea that the ground state energy of a given system and its properties could be defined as a functional of the ground state electron density. Enrico Fermi and Llewellyn Tomas independently developed a method, the so-called Fermi-Tomas method, which gave a central role to the electron density in a system of electrons.[115, 116] After the work of Slater,[117] P. Hohenberg and W. Kohn formally generalized this concept with two theorems that provided the basis of DFT.[118] The first theorem establishes that, in a given system consisting of electrons moving under the influence of an external potential, the total energy of the given system is a unique functional of the electron density. The second theorem demonstrates that the density that minimizes the total energy of the system is the ground-state energy of that system. A route to find the ground-state energy was provided by the formalism published by W. Kohn and LJ. Sham in 1965.[119] The Kohn-Sham equations can be expressed as follows:

$$E[\rho] = T_S[\rho] + \int dr\, \upsilon_{ext}(r)\,\rho(r) + V_H[\rho] + E_{XC}[\rho]$$

Where T_S is the Kohn-Sham kinetic energy, υ_{ext} the external potential, V_H the Coulomb energy, and $E_{XC}[\rho]$ is the exchange-correlation energy.[120] The exchange-correlation term is the most challenging term of the equation, and the quest for more accurate DFT functionals are variations and improvements on how to address this term. The $E_{XC}[\rho]$ is usually split in two separated terms, namely the exchange term E^X, and the correlation term E^C. The former term is associated with the interactions taking place between electrons of the same spin, when E^C is critical for electrons of opposite spins. This functional, and then the two terms of the exchange-correlation energy can be local or include the effect of the gradient. The first approximation was the Local density Approximation (LDA) which considers that the electron density is the same at each point of the space where the functional

is evaluated, and the electron density of a homogeneous electron gas can be used, even for inhomogeneous systems. This LDA approximation was first proposed by Dirac in 1920.[121] The Local Spin-Density Approximation (LSDA) included the electron spin dependence in the description,[117] and was designed for systems with unpaired electrons. LDA functionals typically overestimate the E^C term, while underestimate the E^X term, which results in a rather good description of the exchange-correlation term. This cancellation of errors compensates the raw approximation inherent to the LDA method.

The following major improvement was the consideration of the gradient of the density. The Generalized Gradient Approximation (GGA) method takes into account the fact that the electron density varies through the space, and as such, the approximation is more complex than that of the LDA method. Functionals following the GGA formalism typically estimate the energy of the systems with a reasonable accuracy, improving the results obtained with LDA functionals. Their performance is however limited in a number of cases. For example when accurate descriptions of van der Waals interactions is needed.[122] We also note that no significant improvement is found for calculations in the solid state.[123] In a series of publications, A.D. Becke developed this approximation,[124-128] together with Perdew.[129-131] The formalism developed by Becke is based on empirical parameters, while that of Perdew is derived through the physical concepts of quantum chemistry. Among the numerous functionals following the GGA approximation, are BP86,[124, 129] and BLYP.[124, 132]

A very popular class of functionals is the hybrid-GGA, which combine the exchange-correlation term of the GGA approximation with a part of the Hartree-Fock exchange. These functionals are now widely used because of the significant improvement obtained for the description of a wide range of molecular properties. The most popular hybrid functional is B3LYP,[124, 128, 132] but PBE1PBE[130, 133] is also part of this family. The pure functional of Perdew, Burke and Ernzerhof (PBE) was made into its hybrid form as the PBE1PBE or PBE0.

Meta-GGA (or kinetic energy) functionals, such as TPSS,[134] include some additional semi-local components to the gradient (the Laplacian). Truhlar and co-workers have developed the suite of meta-hybrid density functionals including M06, M06HF, M062X, M05, and M052X.[135] Meta-hybrid-GGA functionals are now increasingly used in chemical modelling, since some of them appear to describe accurately molecular systems containing weak interactions (such as van der Waals interactions).

In addition to mixing the HF-exchange into a given density functional, the extended hybrid functionals developed by Grimme and co-workers are composed of a fraction of the MP2 correlation energy calculated with hybrid DFT orbitals.[136]

Benchmarking the chemical system under study is a common practice in order to assess the accuracy of the chosen functional on a given problem.[137] Among the

huge number of functionals available to the computational chemist, B3LYP has been one of the most used since 1993.

It has been suggested that the progression in the DFT formalism development could be seen as a five-rung ladder.[138] In this pictorial representation, the first two rungs would be occupied by the functionals following the LDA and GGA approximations respectively, and the third one by the meta-GGA. The fourth rung would by occupied by the hybrid and the hybrid-meta-GGA approximations. The last one corresponds to the fully non local functionals, which are still under development.

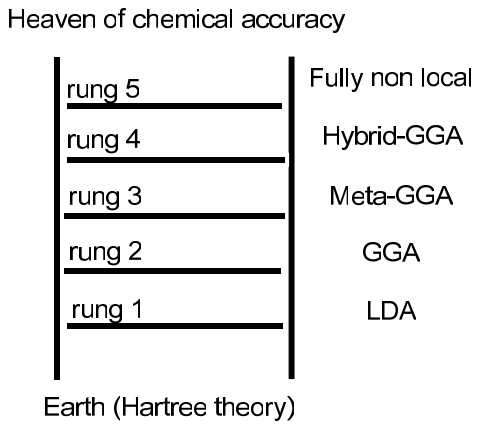

Figure 1.2.5 Ladder of accuracy comparing the generations of DFT functionals.

This scheme translates the idea that more complex functionals (developed through more complex approximations climbing the ladder) describe more precisely the electron density, and by extension provide more accurate descriptions of the molecular properties of the system computed. Nonetheless, we note that the complexity of the functional is not always translated in a better performance in the description of a given system. Indeed, one can climb or descend the ladder depending on their needs. In this line, the accuracy of the widely-used B3LYP functional has been seriously challenged, especially with systems including dispersion interaction.[139] The highly parametrized M06 suite of functionals,[140] and B97D,[141] and the inclusion of a dispersion factor on non-dispersive functionals are the main corrections proposed to date.[142] However, in a vast majority of cases, B3LYP has been found competent in providing satisfying results, especially for transition state search.[143]

In this PhD thesis, various functionals will be used, namely, PBE1PBE, B3LYP, M06 and B97D.

1.4 Objectives

The first major objective of this doctoral thesis is a better understanding of the chemical behavior of $TpNbCH_3(c\text{-}C_3H_5)(MeCCMe)$ and related complexes, in special their efficiency towards C-H activations recently reported by the group of Prof. Etienne. The coordination of the cyclopropyl group to the metal center is poorly understood. There seems to be a carbon-carbon agostic bonding between one of the C-C bonds of the cyclopropyl ligand and the metal center, but this is difficult to characterize from pure experimental data. The key reaction of this complex with benzene is still poorly understood, and a theoretical calculation of the energy profile can be helpful. The reaction of this complex with different dimethylbenzenes yields a diversity of products involving alkyl or aryl C-H activation which is difficult to understand. The migration reactions competing with intermolecular C-H activation are also poorly understood, and they will be investigated, in particular in terms of involvement of the alkyne ligand.

The second major objective of the thesis is the characterization of the mechanism of cross-coupling processes with fluoride-free silicon reagents reported by the group of Prof. Denmark. We will first aim to understand the transmetalation processes in the two mechanisms, unactivated and activated, that have been experimentally reported. The role of the phosphine ligand will be assessed, and the viability of the Pd-O-Si type complex as an intermediate in the transmetalation will be studied. The beneficial effect of dibenzylideneacetone (dba) on the coupling must be clarified, and the possibility of a dba-assisted intermolecular transmetalation will be investigated. Other interesting experimental observations that remain unexplained are the selectivity issues induced by the use of crotyl silanolates, and the role of chloroform when coupling heteroaromatic silanolates with aryl halides will also be studied.

Chapter 2

C-H activation by niobium tris(pyrazolyl) alkyne complexes

UNIVERSITAT ROVIRA I VIRGILI
COMPUTATIONAL STUDY OF C-H BOND CLEAVAGE AND C-C BOND FORMATION PROCESSES CATALYZED BY TRANSITION METAL COMPLEXES
Abel Jean Serge Locati
DL:T. 278-2012

The polypyrazolylborate anions (Tp) appeared as a new family of ligands in 1966.[144, 145] The general structure is $[R_nB(pz)_{4-n}]^-$, where R is a hydrogen, an alkyl or an aryl substituent, and pz is a pyrazol-1-yl group, with n = 0, 1 or 2 (see the schematic representation in Figure 2.0.1).

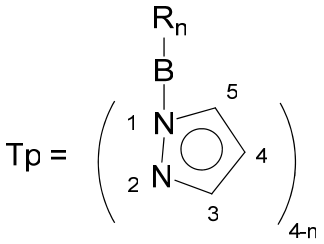

Figure 2.0.1 General representation of the polypyrazolylborate ligand.

One of the most commonly used is the tridentate ligand $[HB(pz)_3]^-$ (when n=1), which is negatively charged and provides six electrons. Three coordination sites are available, each pyrazolyl group being able to bind the metal. The ability of one of the pyrazolyl groups to dissociate from the metal center, affording a bidentate form of the ligand, keeping the last pyrazolyl group available to "sting" the metal over the course of the reaction, let people call them scorpionates, in analogy with the tail of a scorpion.[146] A very rich chemistry has been developed.[147] The group 5 of the periodic table shows some examples.[148]
Figure 2.0.2 represents the main complex which will be studied along this chapter and schematically summarizes its reactivity.

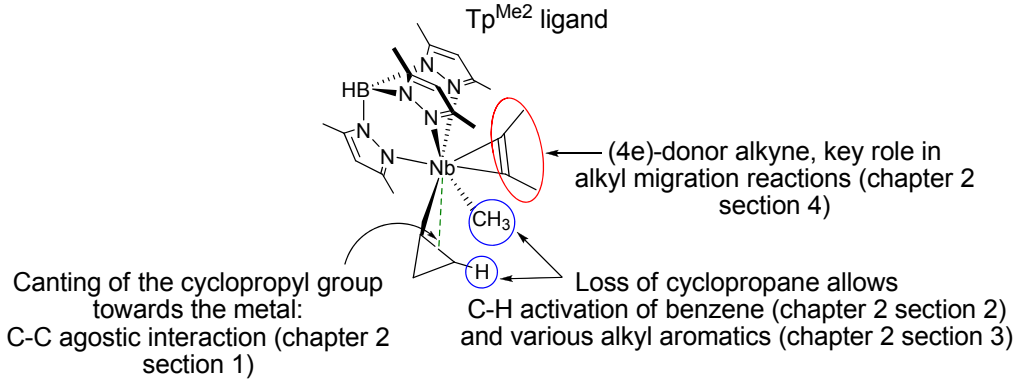

Figure 2.0.2 Representation of the niobium complex studied over chapter 2, and summary of its reactivity regarding its structural features.

This chapter will be built following the structural features of this complex. The first section will be devoted to the study of the agostic interaction observed between one

of the carbon-carbon bond and the metal center. Section 2 and 3 of the same chapter will deal with the C-H activation ability of this niobium complex. Finally, migration processes will be discussed in the last section.

2.1 A new criterion for the characterization of agostic C-C interactions

Agostic interactions were extensively studied over the last decades. Since the term was coined by Brookhart in 1983,[52] a multitude of complexes with agostic interactions were isolated, and several reviews attempting to rationalize the importance, the causes, and the consequences of these intriguing species were published.[48, 53, 55, 149] Among the possible type of interactions between a covalent X-H bond and a transition metal, the C-H agostic structures are indeed very well documented. In contrast, C-C agostic interactions are a more unusual phenomenon, and have been described in only a few complexes.[150-156] They are even scarcer when, together with the C-C agostic, some more common interactions between a C-H bond and a metal are possible in the same complex.[157, 158] In systems similar to the ones we studied over the course of this thesis, C-H agostic complexes were reported and analyzed exhaustively in the past.[159-162] We will instead focus on the measurements of C-C agostic interactions in cyclopropyl rings of niobium complexes, and the possibility to characterize them by NMR computed means.

In this section, we focus on a set of niobium complexes bearing a cyclopropyl ligand with structural parameters indicative of a C-C agostic interaction between one of the carbon-carbon bonds of the cyclopropyl and the metal. We will introduce the use of J_{CC} coupling constants as a tool to magnify weak structural parameters, and to reliably characterize C-C agostic interactions. The effect of the adjacent ligand on the C-C interaction will be analyzed by screening a spectrum of complexes, whose experimental isolation is challenging.

2.1.1 Computational methods

The stationary points were all computed using the Gaussian03 suite of program[163] at the PBE1PBE level,[130] which showed reliable results for agostic systems.[161] The Nb atom was described using an effective core potential (LANL2DZ) for the inner electrons in conjunction with its associated double-ζ basis set for the outer ones.[164, 165] An f-polarisation shell was added (exponent 0.9520).[166] The 6-31G(d) basis set was used at C, N, B, H, O, Cl, Si and F atoms.[167, 168] NMR shifts and coupling constants were computed using the Gauge-Independent Atomic Orbital (GIAO) method as implemented in Gaussian03.[169]

2.1.2 Agostic and nonagostic species studied

In our study of the characterization of the agostic C-C interaction, we focus on a small set of complexes which were experimentally isolated in the group of Prof. Michel Etienne. The general structure of the niobium complexes studied in this section is schematically represented in Figure 2.1.1, together with the atom labelling used.

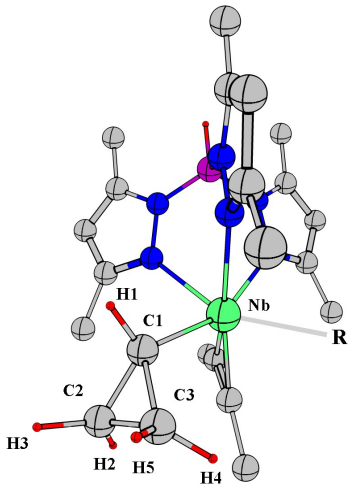

Figure 2.1.1 General structure of the complexes studied. Hydrogen atoms on the Tp backbone and on the alkyne ligand are omitted for clarity.

Figure 2.1.2 depicts three isolated complexes of niobium where agostic interactions are suspected: $Tp^{Me2}CH_3(c\text{-}C_3H_5)$(MeCCMe) (**1**), $Tp^{Me2}NbC_6H_5(c\text{-}C_3H_5)$(MeCCMe) (**Ph_ag**), and $Tp^{Me2}NbCl(c\text{-}C_3H_5)$(MeCCMe) (**Cl_ag**). Complex **1** should be logically labelled **Me_ag**, but since this complex will be referred continuously throughout this chapter, it was deemed convenient to name it in the simplest possible way. These three complexes were all synthetized and computed by DFT means. In those, the R group of Figure 1.1.1 corresponds to a methyl, a phenyl, and a chloride group respectively. The latter was the first to be synthetized[158] and a C-C agostic interaction was observed by means of X-ray spectra and computational analysis.[170] Later on, other complexes such as **1** and **Ph_ag** were described, and systematic studies corroborated the presence of a C-C agostic bonding between the C1-C3 bond and the niobium, when C-H agostic isomers with α-C-H and β-C-H bonds could have been seen as reasonable alternative.

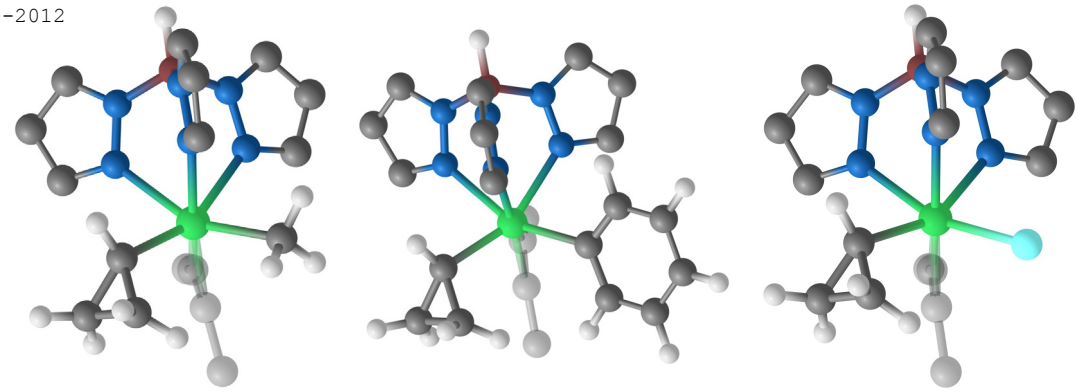

1 ***Ph_ag*** ***Cl_ag***

Figure 2.1.2 Computed structures of three isolated niobium complexes. Hydrogen atoms and methyl groups on the Tp backbone and on the alkyne ligand are omitted for clarity.

For comparison with the C-C agostic structures depicted in Figure 2.1.2, a non agostic iron complex was synthetized.[171] In contrast to the niobium species, compound CpFe(CO)(PPh_3)(*c*-C_3H_5) (**Fe_ag**) can be considered as unambiguously nonagostic. The electron count in this case is 18, and interaction between the carbon-carbon bond of the cyclopropyl group and iron is excluded. The structure, together with the numbering scheme, is shown in Figure 2.1.3.

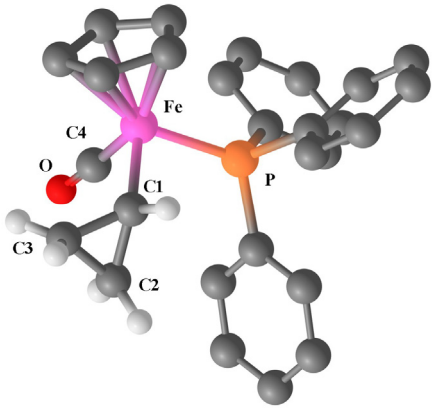

Fe_ag

Figure 2.1.3 CpFe(CO)(PPh_3)(*c*-C_3H_5) complex. Hydrogen atoms on the Cp ligand and on the phosphine are omitted for clarity.

2.1.3 Use of NMR coupling constants J_{CC} to characterize agostic interactions in niobium complexes

2.1.3.1 Structural parameters

In Table 2.1.1 we show the most relevant structural data for the four compounds presented above, namely **1**, **Ph_ag**, **Cl_ag**, **Fe_ag**. The available experimental data are collected together with the computed parameters. The key carbon-carbon distances of the cyclopropyl group are shown. Note that no reliable experimental values could be obtained for complex **1**, due to a disordered structure. The angles formed between these carbon-carbon bonds are also reported together with the Nb-C1-C2, Nb-C1-C3, and Nb-C1-H1 angles because these are the geometrical parameters traditionally used to characterize an agostic interaction with a metal center.

Table 2.1.1 Computed and experimental (in italics) structural parameters for **1**, **Ph_ag**, **Cl_ag**, **Fe_ag**.

	1	**Ph_ag**	**Cl_ag**	**Fe_ag**
d(C1-C2)	1.51 / *n.o.*[a]	1.51 / *1.51*	1.50 / *1.49*	1.51 / *1.49*
d(C2-C3)	1.49 / *n.o.*[a]	1.49 / *1.48*	1.49 / *1.48*	1.50 / *1.49*
d(C1-C3)	1.53 / *n.o.*[a]	1.53 / *1.52*	1.53 / *1.54*	1.50 / *1.48*
C1-C2-C3	61.4	61.5	61.6	59.9 / *59.4*
C1-C3-C2	59.9	59.8	59.7	60.2 / *60.3*
C2-C1-C3	58.6	58.7	58.7	59.8 / *60.2*
Nb-C1-C2	129.2	131.1	131.4	123.1 / *125.1*
Nb-C1-C3	118.6	112.2	115.3	129.8 / *130.7*
Nb-C1-H1	113.0	113.7	112.4	111.2 / *110.6*

[a] n.o. : Not measurable because of disorder.

A number of geometrical features are relevant in this set of compounds. In all four complexes, the computed C1-C2 distances are very similar, between 1.50 and 1.51 Å. The same is observed for the C2-C3 distances, with values around 1.49 Å. The C1-C3 distance is slightly elongated at 1.53 Å for **1**, **Ph_ag**, and **Cl_ag**. No such distortion is observed in the non agostic complex **Fe_ag**. We note that the computed distances mirror the available experimental values, with differences of only 0.01 Å. This gives confidence in the distances computed for complex **1**, where no distances could be obtained. The angles formed between the three carbons of the ring are very similar. They seem then unaffected by the presence or the absence of

an agostic interaction. In contrast, the Nb-C1-C3 angles appear significantly smaller than Nb-C1-C2 in the agostic complexes. In **1**, **Ph_ag**, and **Cl_ag**, the Nb-C1-C3 angles are more acute by around 15 degrees than Nb-C1-C2.

Put together, all these parameters (elongation of C1-C3 and acute Nb-C1-C3 angle) confirm the canting of the cyclopropyl group toward the metal centre for the three niobium complexes. The geometrical parameters then clearly account for an agostic interaction. In marked contrast, in the electronically saturated iron complex, no carbon-carbon distortion, neither canting of the cyclopropyl group can be observed. Even if the elongation of the C1-C3 bond distance is relatively significant, the distortions observed are rather small. From an experimental point of view, such tiny differences can be difficult to observe, and obtain some of the structural features is challenging with these niobium complexes (like for complex **1** where the X-Ray structure appears disordered). Even if the computational methods used allow us to be more confident for such small distortions, we looked for a more reliable probe of these agostic interactions.

2.1.3.2 Experimental J_{CC} values

Nuclear Magnetic Resonance (NMR) is a spectroscopic technique widely used in many scientific fields. Many different experiments are available to determine the structure of chemical compounds. Among them, some 1D-NMR techniques are used to get information on the connectivity between different types of nuclei (carbons, protons…), and elucidate the structure of challenging compounds. The use of the 1D INADEQUATE (Incredible Natural Abundance Double Quantum Transfer Experiment) sequence[172] enables the characterization of the coupling constants associated between neighbouring carbon centers. The main issue is that such measurements face some technical problems. Coupling constants between protons is a routine task because of the abundance of these in nature. It is different with the carbons. ^{12}C are inactive through NMR techniques, and the natural abundance of the measured ^{13}C is low (about 1%). The probability of having two neighbouring carbons in the same molecule is then very low. Nevertheless, suppression of the main carbon signal is possible through the INADEQUATE technique, which allows measurement of the ^{13}C-^{13}C coupling constant with a reasonable accuracy in most cases. The sensitivity of this method is not always optimal. Even if significant improvements have been made in the development of this technique, some issues preclude reliable measures in critical cases.

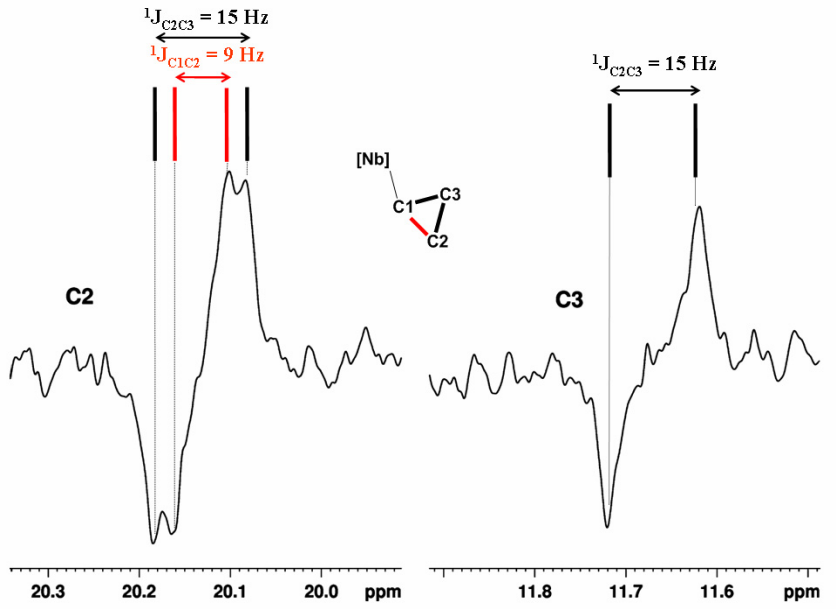

Figure 2.1.4 ^{13}C INADEQUATE spectrum of compound **1**.

Figure 2.1.4 shows the representative spectrum of complex **1**. C2 appears as a doublet of doublets, and C3 consists of a simple doublet. The coupling constant J_{CC} of carbon C3 can be assigned as 15 Hz. We can then assign the value of 15 Hz of one of the doublets of carbon C2 to that of the coupling constants between C2 and C3 and the second coupling constant of 9 Hz can then be assigned for J_{C2C1}. The fact that a single doublet is observed for C3 means that the coupling between C3 and C1 should be smaller than 3 Hz. No coupling constants could be experimentally determined for C1 for technical reasons, the signal appears too broad.

In the case of cyclopropane, all three J_{CC} values are around 12 Hz.

Concerning complexes **Ph_ag** and **Cl_ag**, the spectra obtained are similar. Coupling constants could be assigned for J_{C2C3} and J_{C2C1}, but only an estimation could be made for the bond where an agostic bonding is present. Specifically, with complex **Cl_ag**, J_{C1C3} was impossible to measure because the signal was masked by the methyl groups on the Tp backbone.

For complex **Fe_ag**, the J_{CC} values are all between 10 and 12 Hz. The values can be then considered as broadly homogeneous in the complex where no agostic interactions are suspected.

Table 2.1.2 collects all the experimental data for the coupling constants.

Table 2.1.2 Experimental coupling constants J_{CC} for **1**, **Ph_ag**, **Cl_ag**, **Fe_ag**.

	1	**Ph_ag**	**Cl_ag**	**Fe_ag**
J_{C1C2}	11	n.o.	9	10/11
J_{C2C3}	15	15	15	10/12
J_{C1C3}	<3	<3	<3	11/12

There is thus a significant lowering of the carbon-carbon coupling constant when an agostic interaction is present. Differences in J_{CC} are numerically much more significant than in the C-C distances. This looks thus as an appealing technique for agostic characterization. Experimental acquisition of the coupling constants is however a very challenging task. In our case, assignment of the coupling constants of the cyclopropyl group is incomplete. Characterization of the J_{CC} of the agostic bond by this method does not seem significantly more feasible than through the use of the structural parameters shown above. Therefore, we turned to computation to get the missing values.

2.1.3.3 Computed NMR parameters on experimentally isolated complexes

Computing NMR parameters by DFT means is generally a much easier task than performing experimental measures.[173] The reliability of computational NMR for organometallic compounds has been established in many occasions.[174] We first computed the chemical shifts for the niobium complexes. For the sake of comparison, the values of cyclopropane are also shown. The Gaussian 03 suite of program gives absolute values of magnetic shielding, and calculated values can be referenced to that of tetramethylsilane (TMS) which is the commonly-accepted standard for NMR spectroscopy. Nevertheless, we will not compare the chemical shifts to the experimental values, so only the absolutes values are reported here. The chemical shifts of the atoms of the cyclopropyl ring and that of the metal center are collected in Table 2.1.3.

Table 2.1.3 Computed values for the main chemical shifts (in Hz) for cyclopropane and complexes **1**, **Ph_ag** and **Cl_ag**.

	1	**Ph_ag**	**Cl_ag**	**Cyclopropane**
Nb	-372.0	-351.1	-346.6	—
C1	143.7	132.3	131.6	194.1
C2	179.4	179.5	177.4	194.1
C3	173.1	170.5	171.0	194.1
H1	30.5	29.7	29.8	31.7
H2	31.5	31.3	31.3	31.7
H3	30.5	30.0	30.1	31.7
H4	31.1	30.8	31.3	31.7
H5	30.8	30.2	30.8	31.7

The vicinal metal center has a clear (and expected) influence on the chemical shift of C1. C3 is slightly more upfield than C2. All the hydrogen chemical shifts are very similar, and no significant changes compared to the hydrogen atoms and carbons of cyclopropane are observed. We then computed the presumably more informative coupling constants J_{CC} (Table 2.1.4)

Table 2.1.4 Computed values for the main coupling constants (in Hz) of cyclopropane and complexes **1**, **Ph_ag** and **Cl_ag**.

	Ph_ag	**1**	**Cl_ag**	**Fe_ag**	**Cyclopropane**
J_{NbC1}	-1.4	-1.3	-1.5		
J_{NbC3}	-0.001	-0.07	-0.05		
J_{NbC2}	-0.2	-0.2	-0.2		
J_{C1H1}	144.2	141.3	145.9		150.3
J_{C3H2}	150.8	151.0	151.2		150.3
J_{C3H3}	155.2	153.8	157.6		150.3
J_{C2H4}	150.0	149.8	150.4		150.3
J_{C2H5}	153.6	152.9	152.2		150.3
J_{C1C2}	9.5	8.1	9.8	10.7	15.1
J_{C2C3}	16.5	17.2	16.8	15.5	15.1
J_{C1C3}	-1.0	1.0	0.5	13.8	15.1

As expected, the J_{CC} provide more information than the chemical shifts. Calculated values are in perfect agreement with the available experimental values collected in Table 2.1.2. The J_{CC} values associated to the C2-C3 distances are similar along the three computed complexes (values between 16.5 and 17.2), and are very close to the experimental observations (experimental values around 15). For the C1-C2 bond, the reported experimental values are also in the range of the computed ones. In the case of complex **Ph_ag**, where no assignment of J_{CC} for this bond was possible, a value of 9.5 Hz has been computed. In the case of the most distorted distance (C1-C3), J_{CC} experimental values were found to be below 3 Hz. The calculations allowed us to obtain more precise values. Thanks to these comparisons, we can consider that our method is reliable enough to characterize agostic interactions when no experimental data are available. We also note than the J_{C1C3} values are comparable along the three complexes, suggesting that the agostic interaction is rather similar for the three neighbouring ligands considered.

2.1.3.4 Computed NMR parameters of complexes not synthetized

Confident in the fact that the computing of the coupling constants is a more sensitive tool than measuring distances to characterize agostic interactions, we decided to study a series of niobium complexes. To analyze the influence of the ligand, we computed several complexes of the type $Tp^{Me2}Nb\mathbf{R}(c\text{-}C_3H_5)(MeCCMe)$, with R = F, SiH_3, H, Ø, CN, NO_2, NH_2, NMe_2, OMe. We thus widened the electronic and steric spectrum of the possible ligands bound to the metal centre. None of these complexes were synthetized, and their computations appear thus especially interesting. In Table 2.1.5, we report the key distances and the coupling constants of the cyclopropyl ring in these complexes.

Table 2.1.5 Coupling constants (in Hz) and key geometrical parameters (in Å) of the cyclopropyl ring of various computed niobium complexes.

R	F	SiH_3	H	Ø	CN	NO_2	NH_2	NMe_2	OMe
d(C1-C2)	1.51	1.50	1.49	1.48	1.50	1.51	1.51	1.51	1.51
d(C2-C3)	1.49	1.49	1.49	1.51	1.50	1.49	1.49	1.49	1.49
d(C1-C3)	1.53	1.54	1.54	1.54	1.54	1.52	1.52	1.52	1.53
J_{C1C2}	10.3	10.1	9.8	11.8	9.4	7.4	7.6	8.8	9.1
J_{C2C3}	16.8	17.1	15.0	11.5	15.4	16.8	16.9	17.3	17.2
J_{C1C3}	0.8	-1.5	-5.8	-8.7	-4.7	4.2	4.4	3.7	2.0

In all cases, we observe a dramatic lowering of the coupling constants J_{C1C3} compared to that of the other two. J_{C1C2} is also significantly below J_{C2C3}, but the magnitude of the lowering is smaller in all the complexes computed. It is

interesting to note than the geometrical parameters follow mainly the order of the coupling constants values. The compounds with negative values all have C1-C3 distances as elongated as 1.54 Å. In the case of coupling constants between 3.7 Hz and 4.4 Hz (when **R** = NO_2, NH_2, NMe_2), the distance is slightly less elongated at 1.52 Å. This supports again the vision of the coupling constants as a tool to magnify the elongated distances of an agostic geometry.

We observe than in the cases of a strong vicinal π donor ligand (**R** = NH_2, NMe_2), the values of the coupling constants J_{C1C3} are slightly higher than the values obtained with complexes **1, Ph_ag and Cl_ag**. The electronic saturation of the metal due to this strong π donor ligand might induce a weaker agostic interaction with the cyclopropyl group. On the opposite, strong σ donors such as SiH_3 or a simple hydride show stronger agostic characters translated by lower coupling constants values. The same is observed when no ligand is placed (**R** = ø). This might also be explained by steric reasons, especially if we consider the case where there is no adjacent ligand. In such case, the value is even lower, and the canting of the cyclopropyl group might be favoured by the larger amount of available space. The case of **R** = NO_2 is particular. A η^2 interaction is taken in that case. This can be explained by steric and electronic reasons. As previously mentioned, the electronic mechanisms of the agostic interactions observed in these complexes are beyond the scope of this thesis. The point we would like to emphasize here is that the agostic character can be tuned by the electronic properties of an adjacent ligand.

At this point, we should mention than such lowering in the coupling constants of a cyclopropyl backbone is not unprecedented. Lowering of J_{CC} was already reported in the literature in organic molecules, namely silyl-substituted cyclopropene molecules.[175, 176] But in these cases, the lowering appeared symmetrically in two of the bonds of the ring. Several works also reported the use of coupling constants in organometallic systems to account for an agostic interaction. In Figure 2.1.5, we show an example of a C-C agostic bonding where the coupling constants were used to studied the agostic character of the interaction.[151] Nonetheless, the current work is the first example where such a lowering in the coupling constants is described in the case of an organometallic system bearing a cyclopropyl ligand.

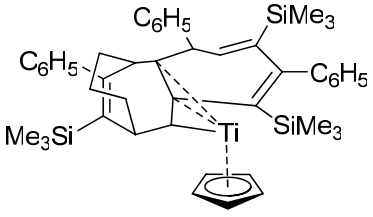

Ti_ag

Figure 2.1.5 Example of an organometallic system where coupling constants have been used to characterize a CC agostic interaction.

2.1.4 Concluding remarks

Computing the coupling constants of the cyclopropyl backbone is a reliable and affordable method for the identification of agostic C-C interactions. J_{CC} follows the trend of the affected geometrical parameters, magnifying the distortions observed. These can also be useful in the cases which experimental values are impossible to obtain for technical reasons. The relation between the electronic and steric features of the adjacent ligand and the strength of the agostic interaction is more difficult to assess. A combination of steric and electronic parameters can be responsible for this in every complex considered and a reasonable explanation can be found for each ligand.

2.2 Activation of benzene by a niobium complex

One of the most interesting features of compound $Tp^{Me2}NbCH_3(c\text{-}C_3H_5)$(MeCCMe) (**1**) is its ability to activate the C-H bond of benzene. The reaction depicted in Figure 2.2.1 has been experimentally reported by the group of Prof. Michel Etienne.[177] When complex $Tp^{Me2}NbCH_3(c\text{-}C_3H_5)$(MeCCMe) (**1**) is put in a solution of benzene, it activates sequentially two aromatic C-H bonds. Complex **1** first loses methane which allows activation of a molecule of benzene and formation of complex $Tp^{Me2}NbPh(c\text{-}C_3H_5)$(MeCCMe) (**2**). Then, complex **2** eliminates cyclopropane and generates the diphenyl complex $Tp^{Me2}NbPh_2(c\text{-}C_3H_5)$(MeCCMe) through activation of a second molecule of benzene. The first step occurs at room temperature, the second one at 323 K. To shed light on the putative intermediates, the general mechanism, and the reasons of the unusual reactivity of this niobium complex, we undertook a computational characterization of the key intermediates by DFT means.

We will first enumerate the common mechanisms admitted for C-H activation reactions. After determination of the key intermediates, the full computed profile will be shown. Structures of transition states and intermediates will be discussed. Finally, the key role of the cyclopropyl ligand will be highlighted.

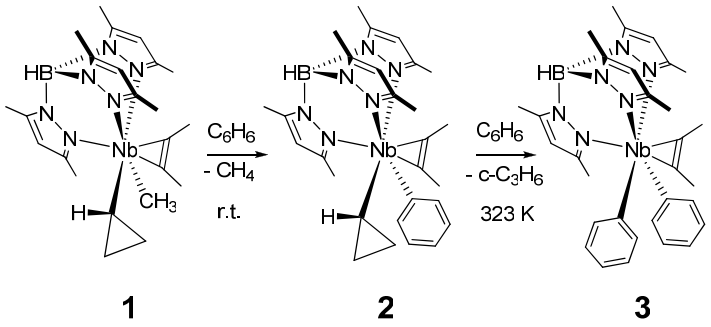

Figure 2.2.1 Activation of benzene by $Tp^{Me2}NbCH_3(c\text{-}C_3H_5)$(MeCCMe).

2.2.1 Computational methods

In this section, the M06 functional[135, 140] has been used as implemented in the Gaussian09 suite of program.[178] Nb was described with the SDD effective core potential for the inner electrons and its associated basis set for the outer ones.[179] All the other atoms were treated with the standard 6-31G(d) basis set.[167, 168] All energy values in this part are free energy values (in kcal/mol) including solvation (solvent treatment by the SMD method).[180] The reason why this functional was used in this part (instead of PBE1PBE[130] used in the agostic study) is the better agreement obtained with M06 regarding the kinetic constants. Experimental and computational values were indeed found very close. The whole profile was also computed by means of the PBE1PBE functional, and no substantial differences were found in the mechanism or in the structures. All transition states computed have only one imaginary frequency, and were connected to the corresponding minima by relaxing the transition state geometry towards the reactant and the product.

2.2.2 Possible intermediates and computed energy profile

The possibility of an oxidative addition mechanism could be discarded due to a zeroth order in benzene in the reaction depicted in Figure 2.2.1. Generation of alkylidene and alkene intermediates of equations (4) and (5) can be made through α-H abstraction and β-H abstraction respectively. Below are shown these two types of hydrogen transfer.

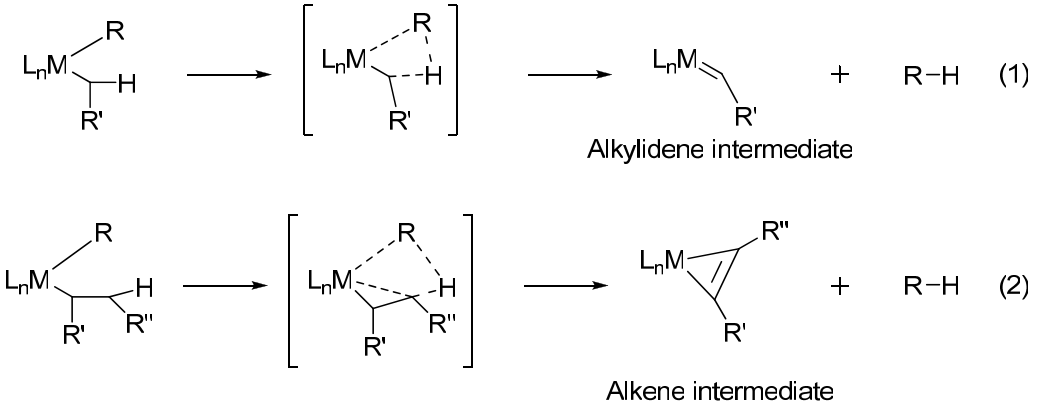

Figure 2.2.3 α-H and β-H abstraction mechanisms in $L_nM(alkyl)_2$ complexes.

The equation (1) depicted in the upper portion of Figure 2.2.3 corresponds to the formation of an alkylidene intermediate generated through an α-H abstraction. The hydrogen in α from the metal center is transferred to the alkyl group R, which generates the alkylidene concomitant with the release of a molecule of alkane. Such transformations are well known in dialkyl complexes of group 5.[181, 182] The group of Legzdins reported many C-H bond activation reactions by tungsten,[183-185] and molybdenum complexes where an alkylidene holds the key role in the activation.

Titanium[186] and chromium[187] alkylidene complexes were also reported. Reactive triple bond counterparts of such unsaturated intermediates, namely alkylidyne complexes (with a M≡C bond) were also synthetized for titanium.[41, 42] In equation (2), depicted in the lower portion of Figure 2.2.3, the β hydrogen is similarly transferred to the vicinal alkyl group which generates an alkene intermediate, together with loss of an alkane molecule. Examples of η^2-diene,[188, 189] η^2-alkyne,[190-192], η^2-allene[193, 194], or η^2-styrene[195] which activate C-H bonds are fairly common in the literature. However, facile loss of the simpler η^2-alkene ligand through β-H abstraction usually causes decomposition of the complex, making this type of intermediate typically unstable. Subsequent intermolecular C-H activation reactions are consequently more scarce with η^2-alkene intermediates.[196]

Consequently, in many C-H activation reactions with transition-metal complexes, an α-H abstraction type mechanism is intuitively the first mechanism considered, and alkylidene intermediates are the species more likely to be generated.

Guided by these general mechanistic considerations, we computed the two possible intermediates for the first C-H bond activation, between complex **1** and **2**. **A** is the intermediate generated by a β-hydrogen abstraction and **A'** is formed through an α-hydrogen abstraction. In both cases, there is concomitant loss of a molecule of methane. Figure 2.2.4 shows the two possible intermediates.

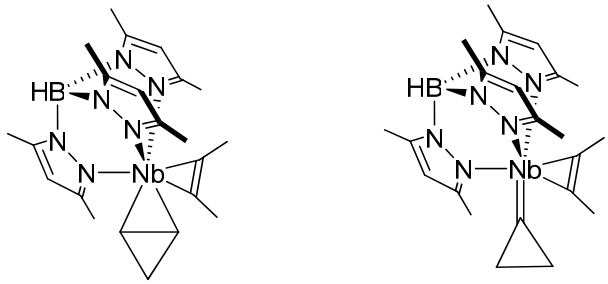

Figure 2.2.4 η^2-cyclopropene **A** and cyclopropylidene **A'** complexes proposed for the first activation of benzene by complex **1**.

Unexpectedly, the alkene intermediate appears more stable than the alkylidene complex. The energy difference between **A** and **A'** is 3.3 kcal/mol. Furthermore, **A** has been trapped in the reaction media by a Lewis base (pyridine), and X-Ray characterization could be obtained. This, together with the relative stabilities of these two species, allows us to be confident that the key intermediate between **1** and **2** is a η^2-cyclopropene complex. The structure of **A** will be commented later. The fact that the common alkylidene intermediate is unlikely in this reaction is of importance. As we previously said, many C-H bond activation reactions were found to occur through these species. In contrast, considering the known instability of alkene complexes arising from β-H abstraction, the C-H activation processes through this type of intermediates is highly unusual. With this in mind, we undertook the computation of the full reaction profile, depicted in Figure 2.2.5.

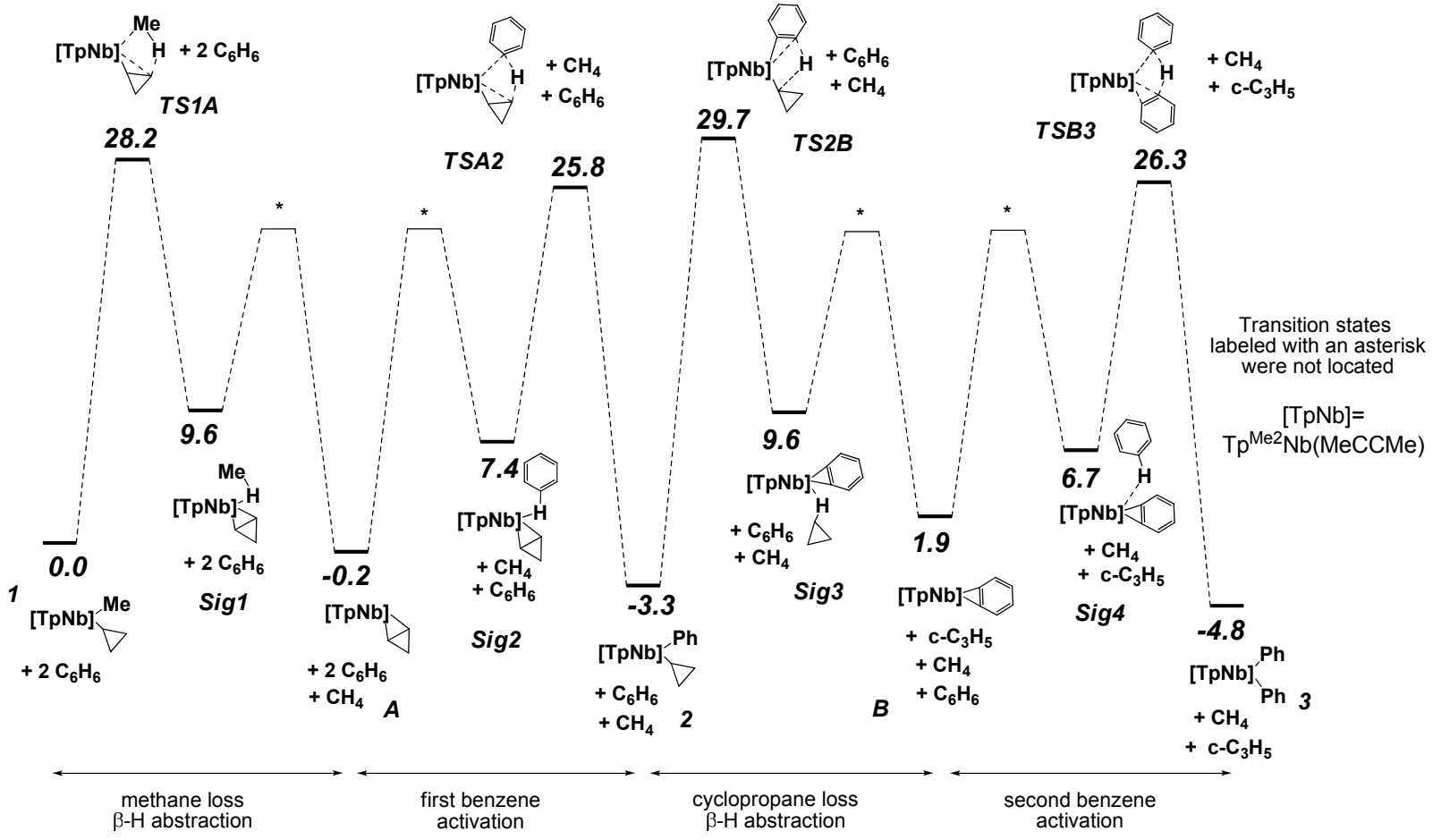

Figure 2.2.5 Full energy profile for the activation of benzene by complex **1**. Free energies in kcal/mol (including solvation).

In the profile depicted in Figure 2.2.5, the general reaction is split in four sections. After loss of methane (from **1** to **A**), C-H activation of a first molecule of benzene (from **A** to **2**) takes place. Subsequently, the cyclopropyl group is leaving the metal coordination sphere as a molecule of cyclopropane (**2** → **B**). Generation of **B** allows activation of a second molecule of benzene (**B** → **3**). **1**, **2** and **3** are the complexes isolated experimentally, and **A** and **B** are the key intermediates for each of the two activation steps.

In each of the transition states computed, a hydrogen transfer takes place which leads to a sigma complex where a molecule of alkane (methane, cyclopropane) or benzene is weakly interacting with the complex. Transition states between these weak van-der-Waals complexes and the corresponding intermediates were not computed, because the barriers are expected to be low. In any case, the barriers of the hydrogen transfers should be higher. Moreover, calculation of transition states for such dissociative processes are usually technically challenging. We focus on the four transition states and the key intermediates and leave aside the sigma complexes. The main structures of this profile are detailed below.

2.2.3 Key intermediate structures

Figure 2.2.6 depicts the key intermediates for the two activations. **A** is an unsaturated cyclopropene complex, and **B** an unsaturated benzyne complex.

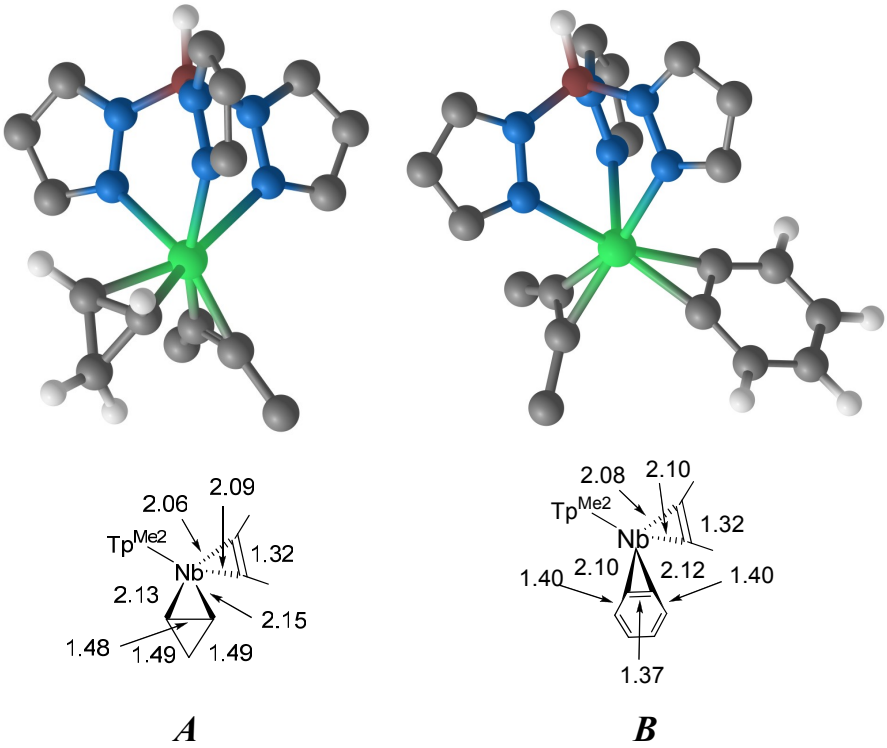

Figure 2.2.6 Unsaturated key intermediates **A** and **B** along the profile.

The cyclopropene and the benzyne complexes both interact with the metal in a η^2 fashion. In **A**, the carbon-carbon distance of the cyclopropyl group (1.48 Å) is notably elongated compared to the corresponding distance in free cyclopropene (computed at 1.29 Å at the same level of theory). This long distance reveals substantial back-bonding from the metal and is indicative of a metallacyclic resonance. This is why we use this type of bonding in the drawings along the manuscript. The Nb-C(alkyl) distances lie at 2.13 Å and 2.15 Å. The alkyne ligand parameters are also of interest. The 1.32 Å carbon-carbon distance is very close from that of a double bond, and the Nb-C(alkyne) bond lengths are 2.06 Å and 2.09 Å. All these bond lengths (short Nb-C(alkyne) and long C(alkyne)-C(alkyne)) are comparable to that of the trapped product $Tp^{Me2}Nb(c\text{-}C_3H_4)(NC_5H_5)(MeCCMe)$ characterized by X-Ray,[197] and support a four-electron donating alkyne ligand.[198, 199]

It is also important to note that two conformers of very similar energy have been found for **A**. The most stable one has the CH_2 of the three-member ring pointing towards the wedge formed by two of the arms of the Tp ligand. The other one is directed out of this wedge and is slightly less stable.

Intermediate **B** is found along the pathway between **2** and **3**. It has been trapped by addition of PMe_3 in the reaction mixture and the trapped products were fully characterized by X-ray diffractions which confirmed the η^2 coordination of the benzyne ligand. Contrary to cyclopropene complexes such as **A**, benzyne, and more generally aryne intermediates are fairly common in organometallic chemistry. Zirconium[200] and molybdenum[201] complexes are among the examples found in the literature for early transition metals. In group 5, niobium,[202, 203] vanadium,[204] and tantalum[203] complexes were reported. At the other side of the periodic table, ruthenium complexes which activate C-H (but also C-C, N-H, and O-H) bonds have been synthetized.[205] Such compounds are usually found as intermediate species in C-H activation processes, and a plethora of reactions have been reported.[206] In our case, the benzyne intermediate **B** has the carbon-carbon distance slightly reduced compared to the other bonds of the aromatic ring (1.37 Å vs. 1.40 Å for the other C-C distances, which are also the typical bond lengths of free benzene). Carbon-niobium distances are rather similar at 2.10 Å and 2.12 Å. Regarding the alkyne ligand, the bond lengths are comparable to that found in intermediate **A**, with a C(alkyne)-C(alkyne) distance of 1.32 Å, and C(alkyne)-Nb bond lengths of 2.08 Å and 2.10 Å. No substantial differences between complexes **A** and **B** for this ligand is thus observed.

2.2.4 Transition state structures

Figure 2.2.7 depicts the two first transition states corresponding to the activation of the first molecule of benzene: **TS1A** and **TSA2**.

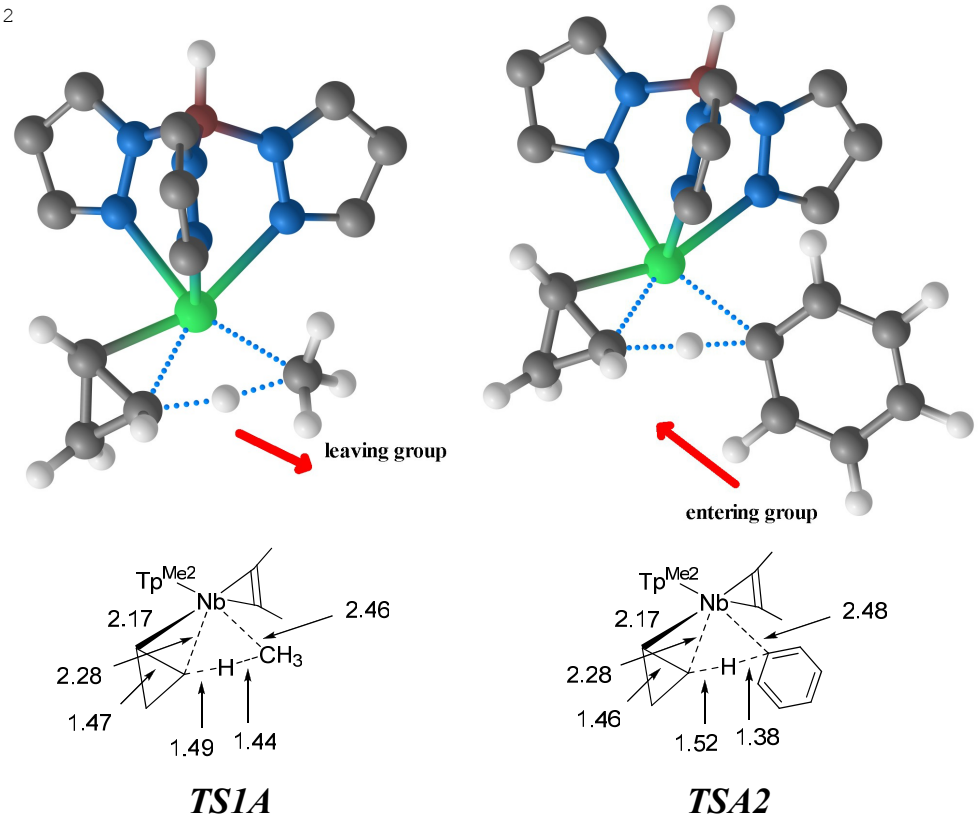

Figure 2.2.7 Computed transition states **TS1A** and **TSA2**.

TS1A corresponds to the hydrogen transfer from the cyclopropyl group to the leaving methyl ligand. The Nb-C(methyl) and the C(β)-H bonds are cleaved and the C(methyl)-H and C(β)-Nb bonds are formed. In **TSA2**, the Nb-C(Ar) and the C(β)-H bonds are formed while the C(Ar)-H and C(β)-Nb bonds are cleaved. This transition state illustrates the benzene entering the metal coordination sphere. In **TS1A**, the β carbon of the cyclopropyl group is rather close to the metal centre, with a C(β)-Nb distance of 2.28 Å. The C(α)-Nb distance is at 2.17 Å. The carbon-metal distances of the cyclopropyl ligand in **TSA2** are virtually the same with a C(α)-Nb distance of 2.17 Å and a C(β)-Nb distance of 2.28 Å. The C(α)-C(β) distance is 1.46 Å for both transition states. The C-Nb distances of the leaving / entering group are also very similar: 2.46 Å in the case of C(methyl)-Nb (**TS1A**) and 2.48 Å for C(Ar)-Nb (**TSA2**). In both transition states, the hydrogen atom is midway between the carbons of the two groups. In the case of **TS1A**, the hydrogen transferred is 1.49 Å away from the cyclopropyl ligand and 1.44 Å from the methyl. For **TSA2**, the H atom is 1.52 Å from the cyclopropyl and 1.38 Å from the methyl. These two transition states have then very similar structural features. Energetically they are also very comparable, **TS1A** being higher than **TSA2** by 2.4 kcal/mol only.

In Figure 2.2.8, we reproduce the two transition states corresponding to the second step of the reaction.

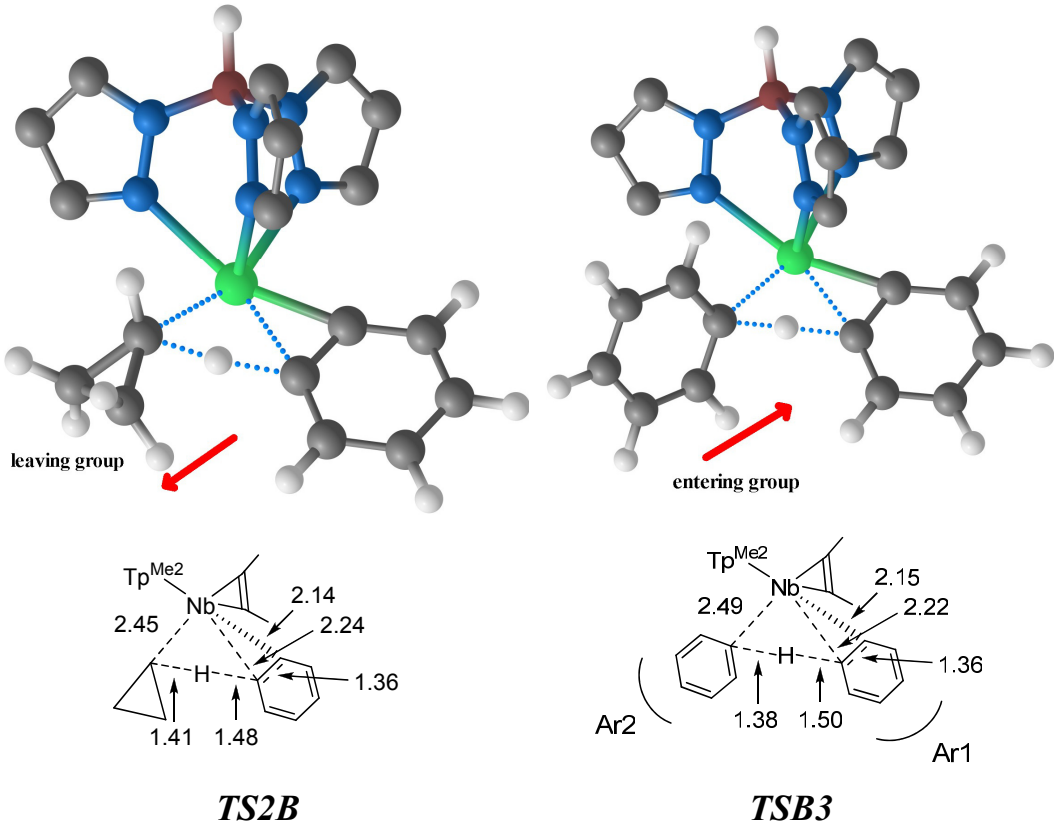

TS2B ***TSB3***

Figure 2.2.8 Computed transition states **TS2B** and **TSB3**.

In **TS2B**, the H-C(Ar) and the C(cyclop)-Nb bonds are cleaved and the C(cyclop)-H and C(Ar)-Nb bonds are formed. In **TSB3**, the Nb-C(Ar2) and the C(Ar1)-H bonds are formed while the C(Ar2)-H and C(Ar1)-Nb bonds are cleaved. The distances between the hydrogen and the leaving/entering groups are very similar to those of the structures of the first activation. In both cases, the aryl group shows an η^2-like geometry, with one of the C(Ar)-Nb distances being 2.14 Å in **TS2B** (2.15 Å in **TSB3**) The other C(Ar)-Nb distance (the one between the carbon where the hydrogen transfer occurs and the metal) is of 2.24 Å in **TS2B** (2.22 Å for **TSB3**).

TS2B is the highest of the transition states computed (29.7 kcal/mol higher than the first complex), and is 3.4 kcal/mol higher than **TSB3**.

2.2.5 Discussion on the energy values

2.2.5.1 Rate constants

Having characterized the mechanism of the reaction, we had a more careful look at the rate constants, in order to assess the reliability of the barriers computed. The profile is depicted again in Figure 1.2.9, this time with only the key intermediates and the nomenclature for the rate constants.

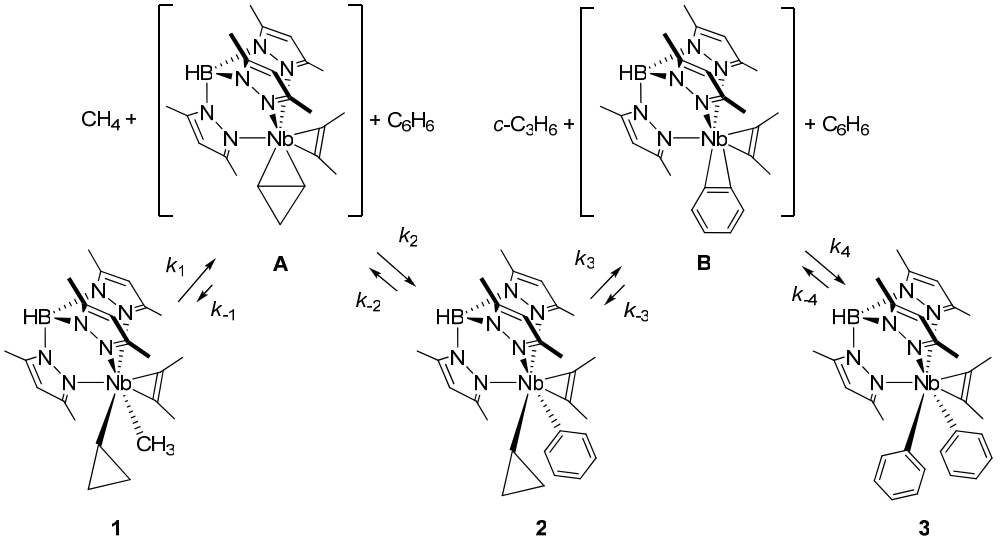

Figure 2.2.9 General profile for benzene activation by complex **1** with inclusion of rate constants.

Table 2.2.1 reports the normalized rate constants obtained experimentally for this reaction. Concentrations of **A** and **B** could not be measured, so absolute values k_{-1}, k_2 and k_{-3}, and k_4 could not be obtained. Therefore, only the ratios k_{-1}/k_2 and k_{-3}/k_4 are reported. The DFT values are also collected in Table 2.2.1.

To calculate the rate constants from our computed energy values, we used the equation (3) developed by Eyring-Polanyi,[207] which is derived from the Arrhenius equation:

$$k = \frac{(k_B T)}{h} e^{\left(-\Delta G / RT\right)} \quad (3)$$

where k is the rate constant, k_B is the Boltzmann's constant, T the temperature in Kelvin, ΔG is the free energy of activation, h is Planck's constant, and R the ideal gas constant (1.985 cal.K^{-1}.mol^{-1}). The pre-exponential factor is considered equal in the reactions, so this term is cancelled for the determination of the relative rate constants. The temperature was set to 298.15 K. In the table we report directly the normalized rates in order to compare them with the experimental values.

Table 2.2.1 Experimental and computed normalized rate constants.

	k_1	k_{-2}	k_3	k_{-4}	k_{-1}/k_2	k_{-3}/k_4
exp. rate constants	$(2.4\pm0.2) \times 10^{-2}$	$(3 \pm 1) \times 10^{-3}$	$(1.53\pm0.06) \times 10^{-3}$	$(8 \pm 2) \times 10^{-4}$	0.3 ± 0.2	1.2 ± 0.4
exp. normalized rate constants	1	0.13	0.06	0.03	0.3	1.2
comp. normalized rate constants	1	0.21	0.0003	0.01	0.5	0.37

Agreement with experimental values is satisfying, with small discrepancies. The rates and the ratios have mainly the same order of magnitude, except for k_3. It should be stressed that a change of only a few kcals in the barriers would lead to a greater variation in the rate constants. Thus the values can be considered reasonably good.

2.2.5.2 Correlation between C-H activation and Bond Dissociation Energies (BDE)

The range of activation barriers in the profile depicted in Figure 2.2.5 is quite narrow, the energy difference between the highest and the lowest transition state being only 3.4 kcal/mol. The difference between **1** and **3** is only 4.8 kcal/mol. **A** and **1** are isoenergetic. The four transition states have very similar energetics and show very similar geometrical features. Along the profile, three species are activated:

- Methane: between **Sig1** and **TS1A** (barrier of 18.6 kcal/mol).
- Benzene: between **Sig2** and **TSA2** and between **Sig4** and **TSB3** (barriers of 18.4 and 19.6 kcal/mol respectively).
- Cyclopropane: between **Sig3** and **TS2B** (barrier of 20.1 kcal/mol).

The activation energies then follow this scale:

$$CH_4 \leq C_6H_6 < c\text{-}(C_3H_5)$$

The barriers for the activation of these small molecules are rather similar. This is rather surprising because the bond dissociation energies (BDE) of these three species (methane, cyclopropane and benzene) are not in the same order, methane having the lowest BDE, benzene the highest, and cyclopropane being in between (see Figure 2.2.10).[15]

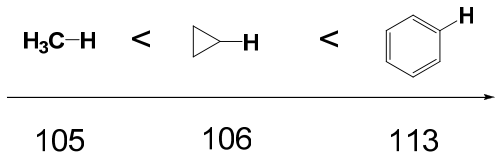

Figure 2.2.10 C-H Bond Dissociation Energies for the three molecules considered in kcal/mol.

There is then a clear discrepancy between the barriers obtained for the activation of these species and their known BDE. For instance, the barrier for the activation of cyclopropane should be lower than the one corresponding to the activation of benzene.

We consider the method used and the level of theory (calculations on the real system with the M06 functional with solvation effects included) reliable. Therefore, we do not believe that the absence of relation between the BDEs and the barriers computed is due to a computational artefact. This apparent contradiction would rather suggest that this niobium complex is insensitive to the bond strength of the C-H bond it activates (the C-H bond being from an aromatic compound, from a sp^3 carbon of a strained ring, or from a simple alkane). In other words, complex **1** does not discriminate too much the molecule activated.

2.2.6 Role of the cyclopropyl ligand

We emphasized at the beginning of this section that η^2-alkene intermediates showing such reactivity are very unusual. Decomposition of this kind of complexes through alkene loss makes their synthesis typically difficult. Similarly, in the $Tp^{Me2}NbMe(R)(MeCCMe)$ family of compounds, no complexes bearing an acyclic alkyl ligand R could be synthetized.

We therefore computed the acyclic complex $Tp^{Me2}NbCH_3(C_2H_4)(MeCCMe)$ (**Aet**), in order to assess the effect of the strain of the alkene ligand on its bonding with the metal center. We calculated the ligand exchange process depicted in equation (4). The reaction is clearly endergonic, with 15.3 kcal/mol needed to undertake the ligand exchange.

If we compare the bond distances of the intermediates represented in Figure 2.2.11, the Nb-C bonds are shorter in **A** than in **Aet**. The cyclopropene ligand is around 0.08 Å closer to the metal than in its acyclic counterpart. The interaction between this ligand and the metal is therefore stronger in **A** than it is **Aet**. The ring strain of the three-membered ring is most probably responsible of this stronger binding. Because of the weaker interaction between the acyclic ligand and the metal center, the alkene loss is likely to be easy with **Aet**, at least easier than in the case of its

cyclic counterpart **A**, where the strong binding of the cyclopropene ligand slows down the alkene loss.

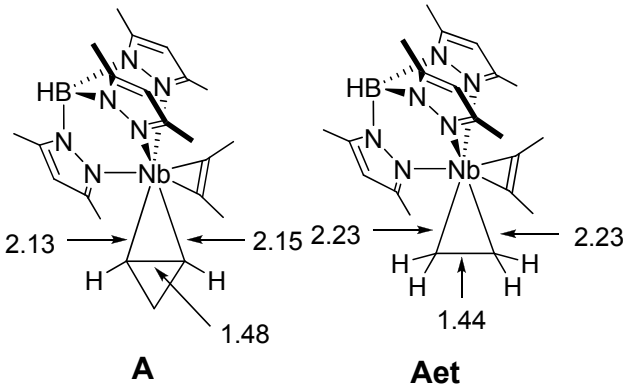

Figure 2.2.11 Comparison of bond lengths in η^2-cyclopopene (**A**) and η^2-ethene (**Aet**) intermediates.

C-H bond activation is then possible with complex **A** because of the ring strain of the cyclopropyl group which prevents further decomposition (due to a strong binding between the cyclopropene ligand and the metal center), and then allows C-H bond activation to be a competitive process.

2.2.7 Concluding remarks

The mechanism of C-H bond activation of benzene by the $Tp^{Me2}NbCH_3(c\text{-}C_3H_5)$(MeCCMe) complex has been rationalized by DFT means. The key intermediate is an unusual η^2-cyclopropene complex. Computed kinetic constants were found to be in reasonable agreement with the experimental values. The complex was found rather insensible to the C-H bond it activates. We found that the unusual reactivity of this cyclopropene complex is due to the ring strain of the cyclopropyl ligand. The strong binding between this ligand and the metal allows C-H activation to compete with the ligand dissociation process.

2.3 Aromatic vs. benzylic C-H activation of dimethylbenzenes

We have discussed in the previous section the mechanism of C-H activation in benzene by the niobium complexes under study. This is a remarkable reaction, but it is simple in the sense that there are no selectivity problems involved. All C-H bonds of benzene are equivalent. Things get more complicated when C-H containing substituents are attached to benzene. The case of methyl substituents is particularly interesting because, while keeping the system quite simple, it introduces the competition between benzylic (methyl C-H) and aromatic (phenyl C-H) activation. This subject has been previously tackled by several research groups.

Scandium derivatives were found to activate toluene, but in a non-selective fashion.[36] Rhodium complexes with scorpionate ligands appeared competent in activating toluene as early as 1989.[33] More recent contributions reported C-H activations of alkylaromatics with molybdenum,[208, 209] tungsten,[183-185] and titanium complexes.[41, 42] In those cases, the C-H activation was found to take place via a 1,2 C-H addition across one metal-carbon multiple bond. Unsaturated alkylidene M=C complexes with molybdenum and tungsten, and an unsaturated alkylidyne M≡C complex in the case of titanium were found the key intermediates in the C-H bond activation process. Regarding the niobium complexes under study in this manuscript, the experimental group of Prof. Michel Etienne and co-workers reported unexpected results which led to our computational study. Having established the mechanism for benzene, we will now focus on the selectivity issues of various alkylaromatics.

Four substrates have been studied:

Three dimethylbenzenes:

- 1,2-dimethylbenzene.
- 1,3-dimethylbenzene.
- 1,4-dimethylbenzene.

One trimethylbenzene:

- 1,3,5-trimethylbenzene or mesitylene.

In all cases, C-H activation has been experimentally observed. The particularity of these substrates is that there are two types of C-H bonds. Two C-H bond activations are possible, at the aromatic position and at the benzylic position. In Figure 2.3.1, the representative example of 1,3-dimethylbenzene is showed. An aromatic activation would lead to the complex $Tp^{Me2}Nb(3,5\text{-}C_6H_3Me_2)(c\text{-}C_3H_5)(MeCCMe)$. Otherwise, a benzylic activation gives the $Tp^{Me2}Nb(CH_2\text{-}3\text{-}C_6H_4Me)(c\text{-}C_3H_5)(MeCCMe)$ complex.

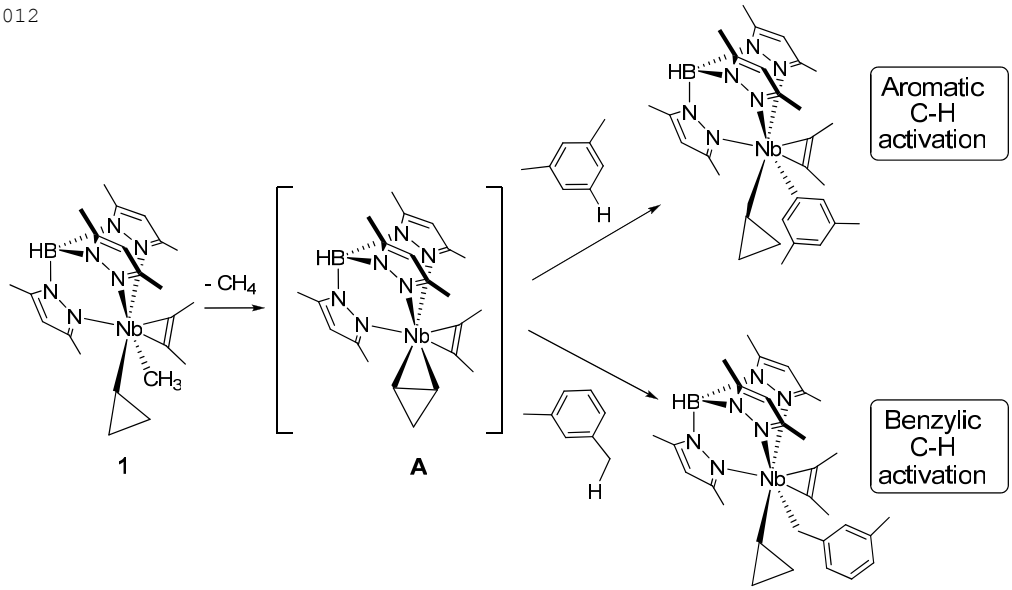

Figure 2.3.1 Two possible C-H activations (aromatic and benzylic) of 1,3-dimethylbenzene by intermediate **A**.

All the compounds discussed in this section have the common η^2-alkene intermediate **A**, which we studied extensively in the previous section. Here we will then only focus on the alkylaromatic activation step, after loss of methane.

2.3.1 Computational methods

In this section, we used the PBE1PBE formalism[130] as implemented in the Gaussian03 package.[163] Nb was described with the LANL2DZ effective core potential for the inner electrons and its associated basis set for the outer ones.[164, 165] A f polarization shell was added (exponent 0.952).[166] All the other atoms were treated with the standard 6-31G(d) basis set.[167, 168] ZPE corrected potential energy and free energy are reported throughout this section, but only the ZPE corrected potential energies will be considered in the discussion. The nature of each optimized minimum was characterized by means of a vibrational analysis. All transition states computed have only one imaginary frequency, and were connected to the corresponding minima by relaxing the transition state geometry towards the reactant and the product. Energy values are all expressed in kcal/mol, and distances in angstroms.

2.3.2 Experimental data

Figure 2.3.2 summarizes the outcome of the reactions between the complex and all the substrates studied in this section.

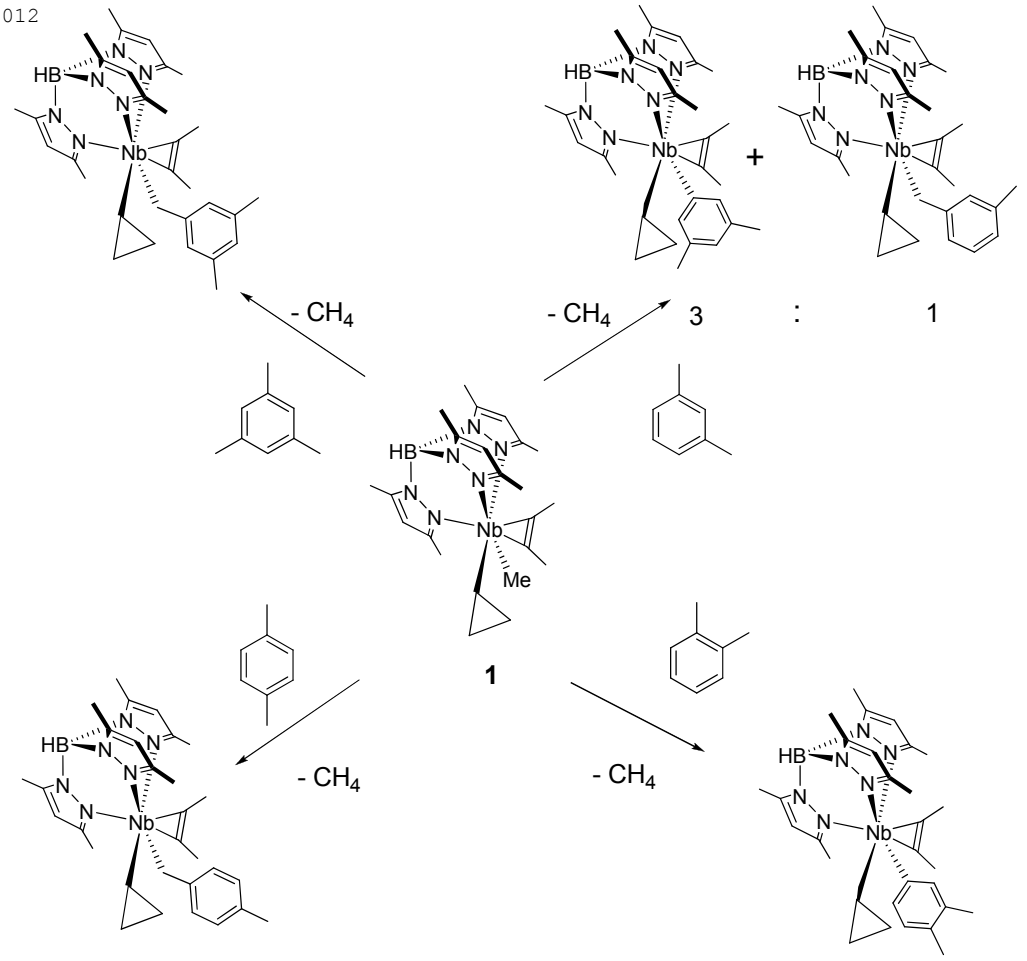

Figure 2.3.2 General reactivity of complex 1 with the methylbenzene substrates considered.

1,3,5-trimethylbenzene (or mesytilene) and 1,4-dimethylbenzene yield selectively the benzylic complexes $Tp^{Me2}Nb(CH_2\text{-}3,5\text{-}C_6H_3Me_2)(c\text{-}C_3H_5)(MeCCMe)$ and $Tp^{Me2}Nb(CH_2\text{-}4\text{-}C_6H_4Me)(c\text{-}C_3H_5)(MeCCMe)$ respectively. No aromatic C-H bond activation is observed. 1,2-dimethylbenzene is also selective, but this time towards the aryl complex $Tp^{Me2}Nb(3,4\text{-}C_6H_3Me_2)(c\text{-}C_3H_5)(MeCCMe)$, resulting from an aromatic C-H activation. In marked contrast, activation of 1,3-dimethylbenzene produces a 3:1 mixture of two products, a benzyl complex and an aryl complex. We will first try to rationalize computationally the selectivities observed. Then, a simple set of rules will be proposed to clarify the outcome.

2.3.3 Computed energy profiles

Figure 2.3.3 presents the two computed profiles for the aromatic and benzylic C-H activation of 1,2-dimethylbenzene. The profiles corresponding to 1,3- and 1,4-

dimethylbenzene are presented in Figure 2.3.4 and 2.3.5, respectively. Finally the activation of 1,3,5-trimethylbenzene is reported (Figure 2.3.6). The case of 1,3-dimethylbenzene is more complicated since two C-H aromatic activation are possible: at position 4 and position 5.

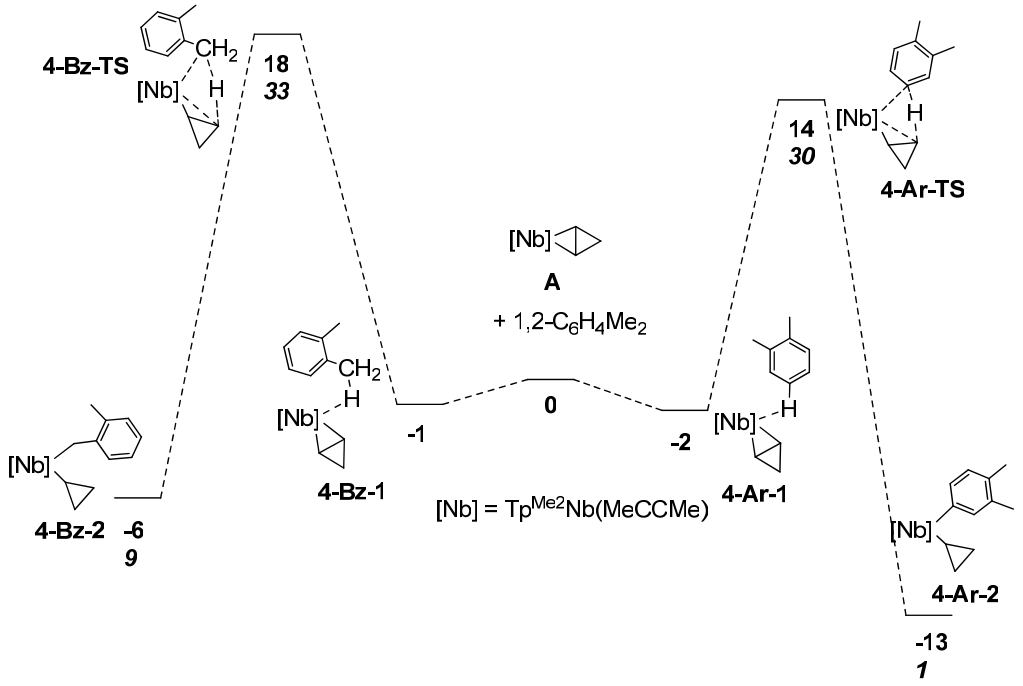

Figure 2.3.3 Benzylic and aromatic activation of 1,2-dimethylbenzene by complex **A**. ZPE corrected energies and free energy (in italics) expressed in kcal/mol.

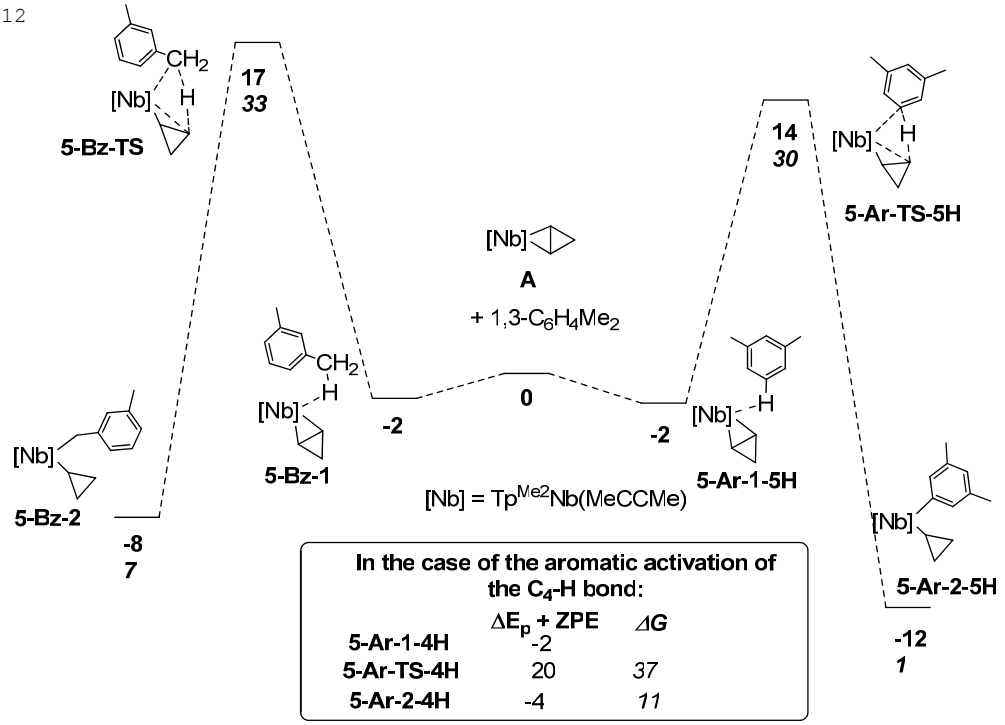

Figure 2.3.4 Benzylic and aromatic activation of 1,3-dimethylbenzene by complex **A**. ZPE corrected energies and free energy (in italics) expressed in kcal/mol.

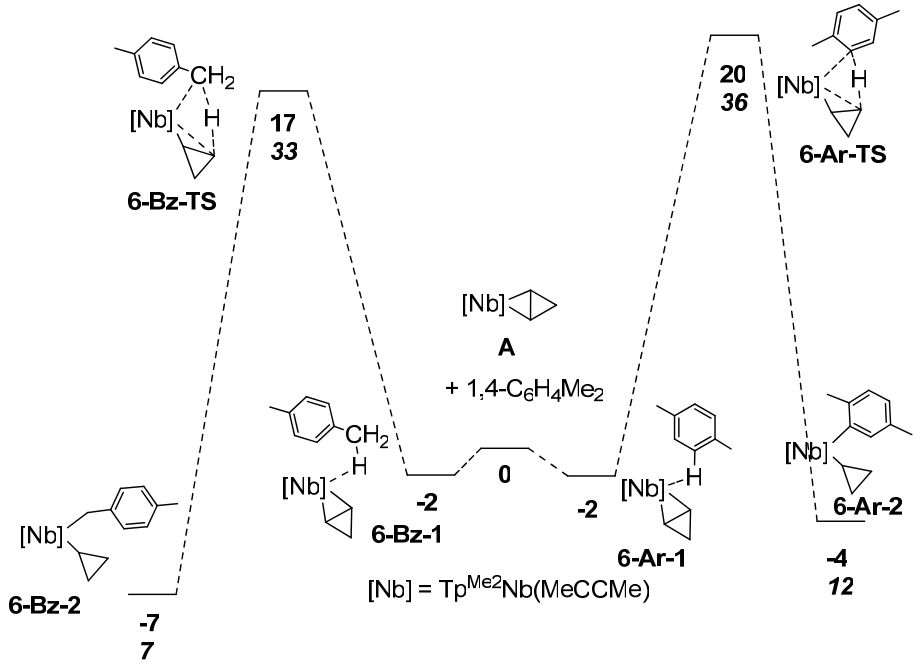

Figure 2.3.5 Benzylic and aromatic activation of 1,4-dimethylbenzene by complex **A**. ZPE corrected energies and free energy (in italics) expressed in kcal/mol.

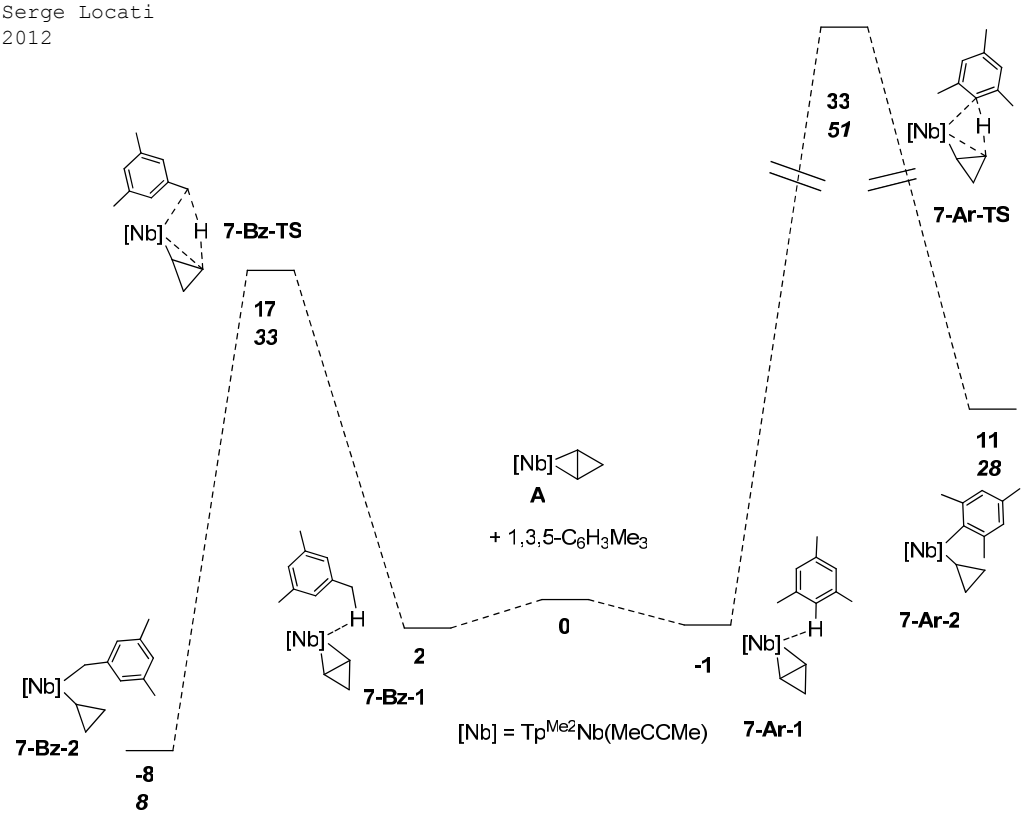

Figure 2.3.6 Benzylic and aromatic activation of 1,3,5-trimethylbenzene by complex **A**. ZPE corrected energies and free energy (in italics) expressed in kcal/mol.

The mechanistic process is the same for all the substrates. In all cases, a sigma-complex was first located (labelled as X-YZ-1 in the figures, with X is an arbitrary number and YZ = Bz or Ar depending if the activation is done at the benzylic or aromatic C-H bond), with a small interaction between the metal and the substrate. Then, a hydrogen transfer from the alkylaromatic to one carbon of the cyclopropene ligand takes place through a transition state X-YZ-TS and provides the final complex (X-YZ-2). The main values of the energy profiles are summarized in Table 2.3.1.

Table 2.3.1 Main energy barriers (ZPE corrected potential energies in kcal/mol) for the C-H activations of the alkylaromatics by complex **A**.

	Benzylic activation		Aromatic activation	
	TS	Product	TS	Product
1,2-dimethylbenzene	18	-6	14	-13
1,3-dimethylbenzene	17	-8	20[a]/14[b]	-4[a]/-12[b]
1,4-dimethylbenzene	17	-7	20	-4
1,3,5-trimethylbenzene	17	-8	33	11

[a] Activation at position 4. [b] Activation at position 5.

The energy values reported in Table 2.3.1 will be first discussed substrate by substrate.

We start with the clear case of 1,3,5-trimethylbenzene (Figure 2.3.6). The aromatic barrier is much higher than the benzylic one (with a ΔΔE of 16 kcal/mol). The aromatic product (**7-Ar-2**) is also considerably destabilized compared to **7-Bz-2**. This is in complete agreement with the exclusive observation of the benzylic product in this case.

For 1,2-dimethylbenzene (Figure 2.3.3), the aromatic activation barrier lies 4 kcal/mol lower than the benzylic activation. Similarly, **4-Ar-2** is 7 kcal/mol more stable than the benzylic complex **4-Bz-2**, which points towards a selective aromatic C-H activation. This is in agreement with the experimental observations which reported a complete selectivity towards the aromatic product.

1,4-dimethylbenzene is selective towards the benzylic compound **6-Bz-2**. The barrier appears 3 kcal/mol lower for this process, and the benzylic product is 3 kcal/mol more stable than that of the aromatic **6-Ar-2** (see Figure 2.3.5). This is also in agreement with the experimental data.

The case of 1,3-dimethylbenzene is experimentally different from the others because it is the only substrate which does not show a complete selective preference for one activation over the other. The first point is that two distinct aromatic activations are possible, in other words two C-H bonds can be activated, at position 4 and position 5 (see Figure 2.3.4). Experimentally, only the later is observed, which means that formation of $Tp^{Me2}Nb(3,5\text{-}C_6H_3Me_2)(c\text{-}C_3H_5)(MeCCMe)$ is favoured over $Tp^{Me2}Nb(2,4\text{-}C_6H_3Me_2)(c\text{-}C_3H_5)(MeCCMe)$. The computed barriers are in agreement with that, since the aromatic activation at position 5 is 6 kcal/mol lower than the activation at position 4. Similarly, the corresponding product obtained is more stable by 8 kcal/mol.

If we omit the aromatic activation at position 4, the computed barriers for 1,3-dimethylbenzene are very similar to those for 1,2-dimethylbenzene. As we indicated before, the reaction is selective towards an aromatic activation in the latter case, and a mixture is obtained in the former. The argumentation we used to

rationalize the outcome obtained with 1,2-dimethylbenzene cannot be applied for 1,3-dimethylbenzene. The computational limitations (functional, basis set, solvent not taken into account) have probably something to do with the discrepancy on the results. Nonetheless, the statistical parameter could also play a role. Indeed, in the case of 1,3-dimethylbenzene, six hydrogen atoms are available for a benzylic activation, while only one aromatic C-H bond can be activated (at position 5). This 6:1 ratio in favour of the benzylic product might counterbalance the energy difference in the barriers, and then explain the mixture obtained. For 1,2-dimethylbenzene, the ratio is reduced to 3:1, and in that case it follows the barriers obtained.

We note that in the cases of 1,4-dimethylbenzene and 1,3,5-trimethylbenzene, this statistical factor goes in the direction of the observed selectivity (benzylic) together with the barriers obtained.

2.3.4 General observations

A first remarkable observation is that the benzylic activation processes have all very similar barriers, between 17 and 18 kcal/mol above the separated reactants. Similarly, the benzylic complexes have all very similar stabilities (between 6 and 8 kcal/mol below the separated reactants). On the other hand, the values for the aromatic activations differ dramatically, depending on the substrate. The variation of the aromatic barriers is then crucial for the selectivity.

We note that the aromatic activation barrier for 1,2-dimethylbenzene and 1,3-dimethylbenzene at position 4 have very similar barriers (14 kcal/mol) and the stability of the products is also very similar (-13 and -12 resp.). In these two cases, there is no methyl in *ortho* from the activated C-H bond. Aromatic activation at position 4 of 1,3-dimethylbenzene and activation of 1,4-dimethylbenzene show very analogous values as well (for both the transition states and the products obtained). The common feature for these two is that they have a methyl group *ortho* from the C-H bond activated. Finally, mesitylene has the highest barrier, at 33 kcal/mol, and the corresponding aromatic product is the least stable complex. This is the only case where there are two *ortho* methyl groups from the activated bond.

Then, the *ortho* methyl has a clear influence on the aromatic activation barrier. When there is no methyl *ortho* from the C-H bond activated, the aromatic activation is favoured over the benzylic one (by 3-4 kcal/mol). At this point, we should note that we computed the activation of benzene at the same level of theory, and we also found a barrier of 14 kcal/mol. When there is one methyl placed in *ortho*, the benzylic activation is then preferred. If two *ortho* methyl groups are present (like in mesitylene), then the barrier increases dramatically.

2.3.5 Steric vs. electronic effect of the ortho methyl group

We established that the presence or absence of a methyl *ortho* from the C-H bond being activated is the key to rationalize the selectivities observed. The next question is then to understand if the influence of this *ortho* methyl is of steric or electronic nature. For this, we undertook a QM/MM hybrid calculation. We chose the ONIOM (PBE1PBE:UFF) procedure.[8, 9] The *o*-methyl is placed in the MM part (UFF force field),[210] and the rest of the molecule stays in the QM part (PBE1PBE functional). The two regions are schematically represented in Figure 2.3.7. The electronic effect of the methyl group treated with molecular mechanics becomes equivalent to the one of an hydrogen atom. On the contrary, the steric effects are kept unchanged compared to a full QM calculation.

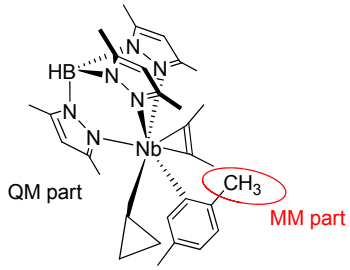

Figure 2.3.7 Schematic representation of the hybrid treatment of the aromatic activation of 1,4-dimethylbenzene.

We chose to model the aromatic activation of 1,4-dimethylbenzene. As reported before, this compound yields only the benzylic product, with no traces of aromatic activation. In the profile depicted in Figure 2.3.5 (full QM), the aromatic barrier was found to be 20 kcal/mol relative to the separated reactants, which is 3 kcal/mol higher than the benzylic activation barrier. We then computed the transition state and the corresponding reactants for this process. The barrier found for the hybrid calculations lies at 21 kcal/mol, which is then very close to the value obtained for the same process in full QM. This is also significantly far from the values obtained when no groups are placed in *ortho* from the C-H bond activated (around 14 kcal/mol, see Table 2.3.1). This result means that the steric effects of the methyl suffice to account for the barriers. We can then consider than the effect of the *ortho* methyl is purely steric, and that the electronic influence of the CH_3 group is negligible in the barriers of these systems.

2.3.6 Concluding remarks

We rationalized the selectivities obtained for the activation of several alkylaromatics by the η^2-cyclopropene niobium complex. The energies computed are in good agreement with the experimental observations.
The benzylic activation has similar barriers for all the substrates considered. This is not the case for the aromatic activation. The aromatic activation is favoured when there is no *ortho* methyl from the C-H bond activated. When present, the *ortho*

methyl operates a switch in the reactivity from the aromatic to the benzylic C-H activation. If a methyl is located at each side of the bond activated (case of mesitylene), steric congestion dramatically increases the barrier for aromatic activation.

Finally, it has been found that the influence of the *o*-methyl is of steric nature.

2.4 Migration processes in niobium complexes

C-H activation is not the only reaction that complexes of the $Tp^{Me2}NbRR'(R''\equiv R''')$ type can undergo. In particular, migration processes involving the alkyne ligand have been experimentally observed. An understanding of the mechanism for this often undesired side reaction is critical for the design of efficient systems for C-H activation.

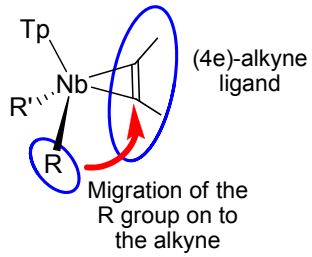

Figure 2.4.1 Schematic representation of the migration process in the niobium complexes.

The particular bonding on the alkyne ligand has been exploited. It is known that the electron donating ability of the alkyne is rather flexible. Apart from being a (2e)-alkyne ligand, its capacity to behave as a four-electron donating ligand has been reported,[198] and computationally studied.[211] A (4e)-donating form is typically characterized by short niobium-alkyne carbon lengths. Previous studies investigated the chemistry of the alkyne ligand in $Tp^{Me2}Nb(Me)(Cl)(MeCCPh)$.[199] Various alkyl groups were found to migrate on to the alkyne (see schematic representation in Figure 2.4.1). In Figure 2.4.2, we show the mechanism which was proposed for this rearrangement.

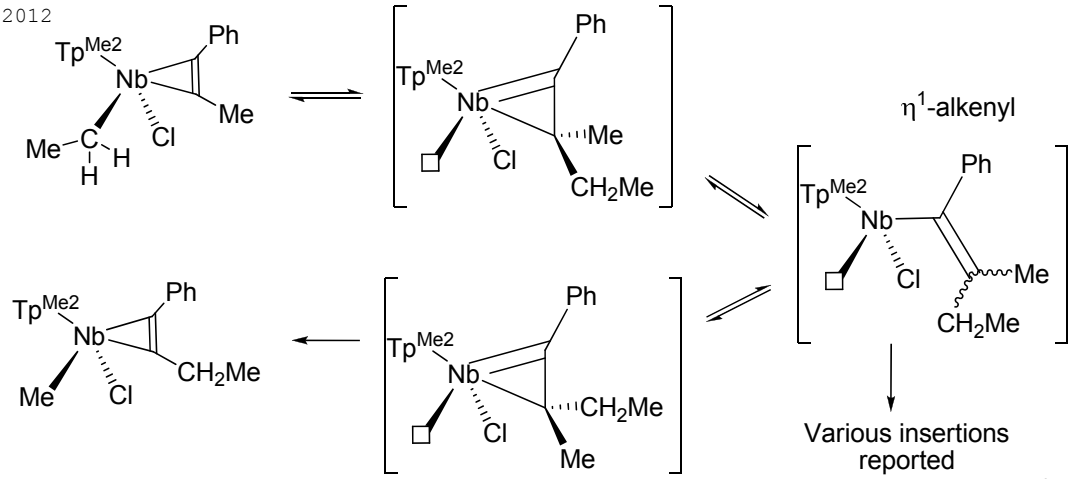

Figure 2.4.2 Proposed mechanism for the migration/insertion in the Tp^{Me2}(R)(Cl)(R'CCPh) family of complexes.

It was proposed that the ethyl group migrates on to the alkyne generating an η^1-(4e)-alkenyl intermediate, which can further react with an entering molecule (insertion). This reaction can also be reversible, and depending of the alkyl group which migrates and the substituent of the alkyne, the outcome of the reaction is different.

In the case of complexes $Tp^{Me2}NbCH_3(c\text{-}C_3H_5)$(MeCCMe) (labelled as **1** in the previous sections) and $Tp^{Me2}NbC_6H_5(c\text{-}C_3H_5)$(MeCCMe) (labelled as **2** in the previous sections), such migrations are not observed. On the opposite, C-H activations of benzene and dimethylbenzenes have been established (as reported in sections 2.2 and 2.3). This points out to the key role of the cyclopropyl group in the particular reactivity of $Tp^{Me2}NbMe(c\text{-}C_3H_5)$(MeCCMe).

Interestingly, it has been experimentally observed that substitution of the C_6H_5-group in the niobium complex **2** by a C_6F_5- group changes dramatically the reactivity.

We will first report a few calculations on the methyl migration in Tp^{Me2}Nb(Me)(Cl)(MeCCR) (with R = Me, Ph) complexes. Then we will study in more detail the complexes bearing a cyclopropyl group and propose a mechanism for the thermal rearrangement of $Tp^{Me2}NbC_6\mathbf{F}_5(c\text{-}C_3H_5)$(MeCCMe). The comparison of reactivity between $Tp^{Me2}NbC_6\mathbf{F}_5(c\text{-}C_3H_5)$-(MeCCMe) and $Tp^{Me2}NbC_6\mathbf{H}_5(c\text{-}C_3H_5)$(MeCCMe) will be discussed.

2.4.1 Computational methods

In this section, we used the M06 functional[135, 140] with the SDD pseudo-potential and its associated basis set for niobium,[179] and the 6-31(d) basis set[167, 168] for all other atoms. All calculations were run using the Gaussian09[178] suite of programs. Unless otherwise stated, the values reported in this section are gas phase free energies in kcal/mol, and distances are expressed in Angstroms. Additional

calculations were performed for one particular problem using the B97D formalism,[141, 212] and solvation tests were carried out using the SMD method for both M06 and B97D.[180] The nature of each optimized minimum was verified by means of a vibrational analysis. The transition states computed have one and only one imaginary frequency, and were connected to the corresponding minima by collapsing the transition state geometry towards the reactant and the product.

2.4.2 Methyl migration in TpNb(Me)(Cl)(MeCCR) complexes, with R=Ph, Me

Figures 2.4.3 and 2.4.4 depict the migration processes of the methyl group, respectively in the Tp^{Me2}Nb(Me)(Cl)(MeCCMe) and in the Tp^{Me2}Nb(Me)(Cl)(MeCCPh) complexes.

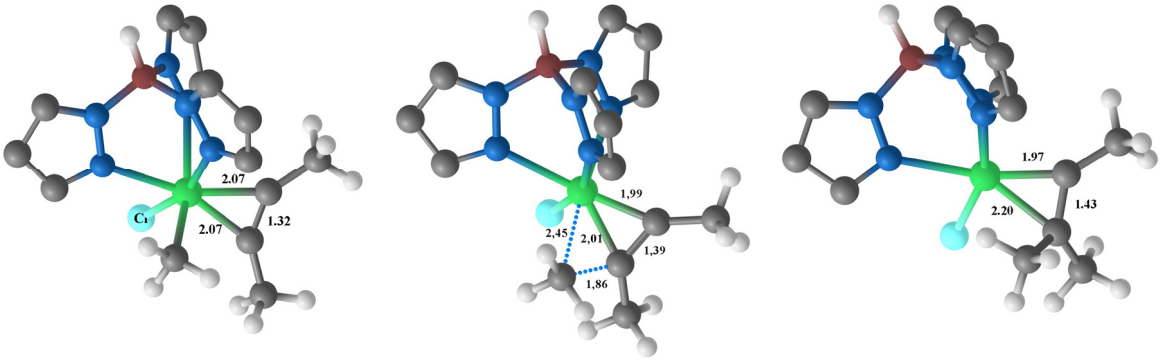

0.0 ***30.5*** ***17.8***

Mig_Cl_Me_R ***Mig_Cl_Me_TS*** ***Mig_Cl_Me_P***

Figure 2.4.3 Reactant, transition state, and product for the migration of the methyl group to the alkyne in Tp^{Me2}Nb(Me)(Cl)(MeCCMe). Energies reported below are free energy values in kcal/mol.

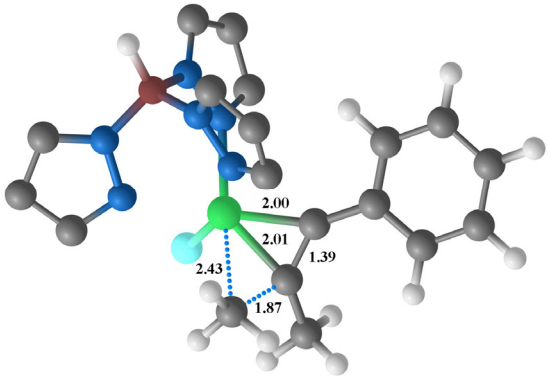

Mig_Cl_Ph_TS
26.9

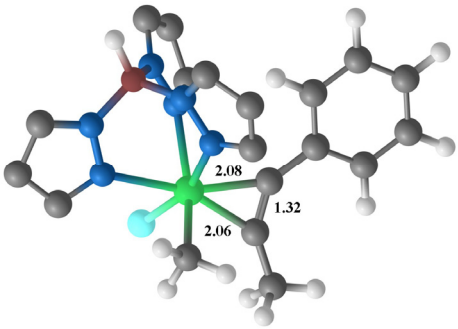

Mig_Cl_Ph_R
0.0

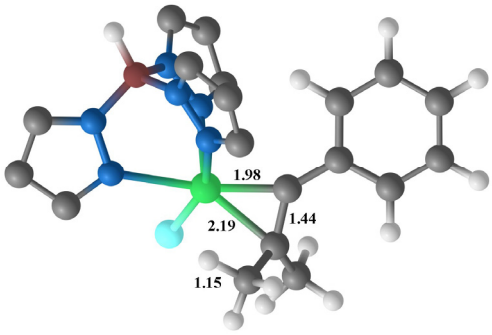

Mig_Cl_Ph_P
14.2

Figure 2.4.4 Reactant, transition state, and product for the migration of the methyl group to the alkyne in $Tp^{Me2}Nb(Me)(Cl)(MeCCPh)$. Energies reported below are free energy values in kcal/mol.

The structural features are similar in both cases. The C≡C distance of the alkyne group is 1.32 Å for both starting complexes (**Mig_Cl_Me_R** and **Mig_Cl_Ph_R**), and the C(alkyne)-Nb distances are all around 2.07 Å. In the transition states, the C≡C distances are slightly elongated (1.39 Å) while the C(alkyne)-Nb bonds are reduced by around 0.8 Å, at 1.99 and 2.01 Å respectively in **Mig_Cl_Me_TS**. The barrier for the migration in $Tp^{Me2}Nb(Me)(Cl)(MeCCPh)$ is 3.6 kcal/mol lower than in the case of $Tp^{Me2}Nb(Me)(Cl)(MeCCMe)$. This is consistent with the experimental observations. The migration process has indeed been reported to be facilitated when a bulky group is present on the alkyne ligand. After migration of the alkyl group to the alkyne, rotation of the alkenyl unit is likely, and then insertion to the metal or reversibility of the process is possible.
We did not enter in more detail in the study of these complexes. After these preliminary calculations, we moved back to the study of the $Tp^{Me2}NbR(c\text{-}C_3H_5)(MeCCMe)$ complexes, where similar phenomena have been reported.

2.4.3 Mechanism of the thermal rearrangement of $Tp^{Me2}NbC_6F_5(c\text{-}C_3H_5)(MeCCMe)$

An intriguing fact is the rearrangement of $Tp^{Me2}NbC_6F_5(c\text{-}C_3H_5)(MeCCMe)$ (labelled as **1_F)**, which is very similar to complex **2**, but with a C_6F_5- group instead of C_6H_5-. It has been experimentally observed that substitution of the C_6H_5- group in the niobium complex by a C_6F_5- group changes dramatically the reactivity of the complex. When the aromatic ring is enriched with fluorine atoms, no loss of cyclopropane is observed, and no subsequent C-H activation of benzene is reported. Instead, after several days of mild heating, two products are observed, labelled as **Prod_1_F** and **Prod_2_F** in Figure 2.4.5, with **Prod_1_F** being the major product by 95 %. The configuration of the stereocenter could not be unambiguously established.
A migration of the cyclopropyl group similar to the one described with the methyl in $Tp^{Me2}Nb(Me)(Cl)(MeCCPh)$ is envisioned. The putative intermediate **Int_F** (showed in Figure 2.4.5) was thus proposed.

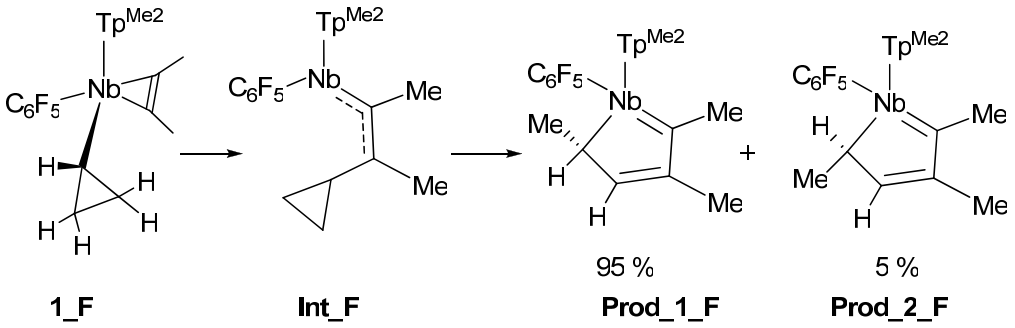

Figure 2.4.5 Thermal rearrangement of $Tp^{Me2}NbC_6F_5(c\text{-}C_3H_5)(MeCCMe)$.

2.4.3.1 General profile

We undertook theoretical calculations to unravel the mechanism of the transformation from **1_F** to **Prod_1_F**. We report in Figure 2.4.6 the four step process that we characterized. We start with complex **1_F**, with a structure very similar to that of complex **2** (they differ only in the presence of four fluorine atoms in the phenyl group in **1_F**). The migration of the cyclopropyl group to the alkyne goes through the transition state **TS12_F**. This is a costly process (barrier of 32.1 kcal/mol), with a barrier higher than the migration of the methyl group in the related complex $Tp^{Me2}Nb(Me)(Cl)(MeCCMe)$. After the migration, the three-membered ring opens (from **2_F** to **3_F**). It is worth mentioning that we could not locate a similar ring-opening when the cyclopropyl group is still bound to the metal. Once the ring is open, a hydrogen transfer takes place from C2

(nomenclature showed on **1_F** in Figure 2.4.6) to Nb through the transition state **TS34_F**. A niobium hydride species is then formed (**4_F**). This complex is rather unstable (22.3 kcal/mol higher in energy than **1_F**) but another hydrogen transfer, this time from the metal to C3 is feasible (**TS45_F** 30.6 kcal/mol higher than the starting complex), to obtain the final product. Between **3_F** and **Prod_1_F**, one of the hydrogen atoms bound to C2 is transferred to C3, giving **Prod_1_F**.

The free energy profile reported can then be summarized as a four step process, consisting of the migration, the opening of the cyclopropyl ring, and two hydrogen transfers.

The overall process is feasible, the highest barrier being the migration of the cyclopropyl group to the alkyne. The reaction is also thermodynamically favoured, with the final product (**Prod_1_F**) being 15.8 kcal/mol lower than the starting complex. **Prod_2_F** has been found 7.1 kcal/mol below the same starting complex. A difference of more than 8 kcal/mol is not consistent with the 95:5 ratio obtained experimentally. These energy values suggest instead that the equilibrium is fully directed towards **Prod_1_F**. No transition state connecting **Prod_1_F** with **Prod_2_F** could be located.

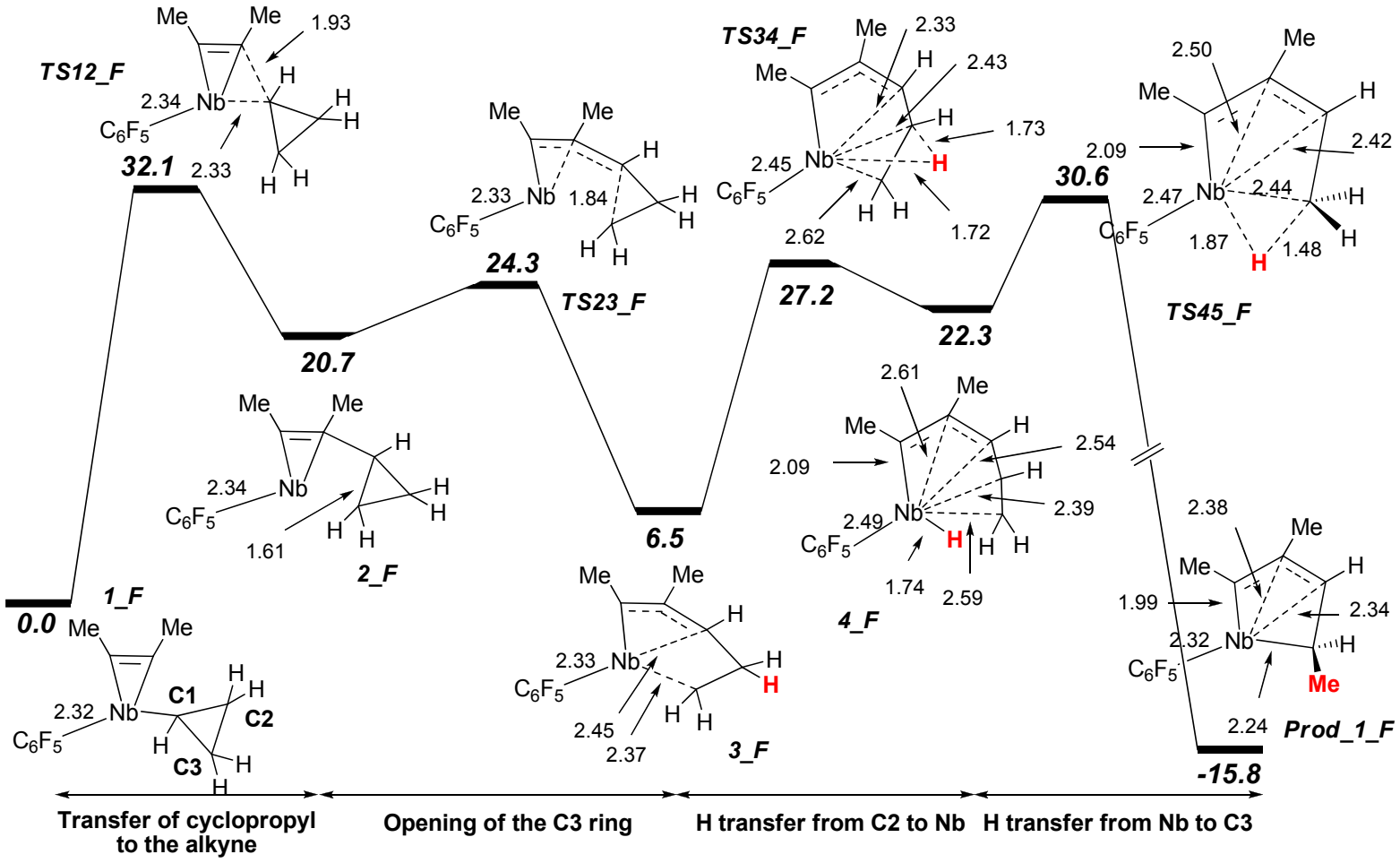

Figure 2.4.6 Computed profile for the rearrangement of **1_F**. Gas phase free energies in kcal/mol. Tp^{Me2} ligand omitted for clarity

2.4.3.2 Direct hydrogen transfer

To check the possibility of a direct transfer from C2 to C3, we computed three transition states where no niobium hydride intermediates are formed during the process. The structures are collected in Figure 2.4.7. **TS_htran_1_F** shows a hydrogen transfer with C2 and C3 interacting with the metal centre (Nb-C2 distance is 2.18 Å, and Nb-C3 lies slightly longer, at 2.26 Å). In **TS_htran_2_F** the hydrogen transferred is only 1.82 Å from the niobium centre, but no hydride intermediate is found. In that case, C3 is clearly away from the metal, at 2.67 Å. In **TS_htran_3_F**, no interactions between the metal and C2, C3, or the hydrogen transferred are apparent (*d*(Nb-C2): 3.03 Å, *d*(Nb-C3): 2.65 Å).

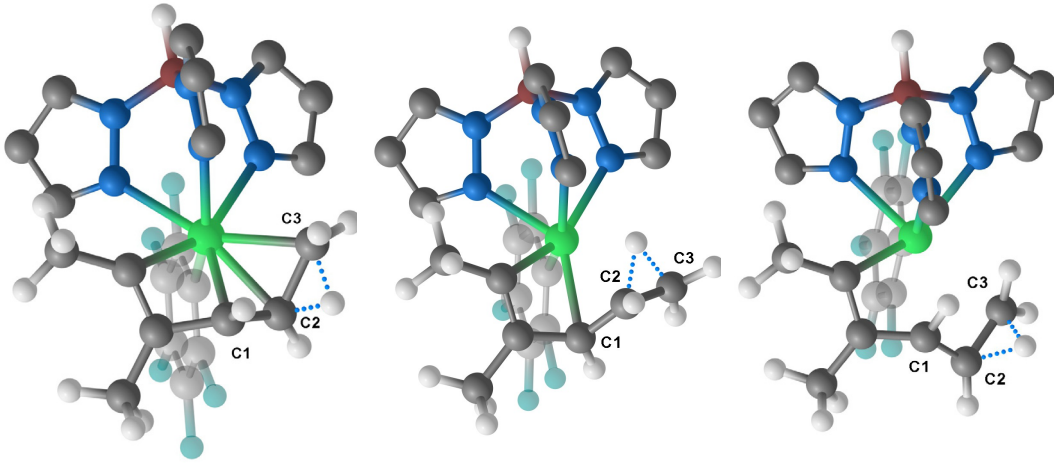

TS_htran_1_F ***TS_htran_2_F*** ***TS_htran_3_F***

Figure 2.4.7 Structures of three transition states showing a direct hydrogen transfer from C2 to C3 in $Tp^{Me2}NbC_6F_5(c\text{-}C_3H_5)$(MeCCMe).

These three transition states are respectively 48.9, 52.5, and 87.4 kcal/mol higher in energy than **1_F**, which places the most stable (**TS_htran_1_F**) around 18 kcal/mol higher than **TS45_F**. A two-step hydrogen transfer (with a niobium hydride intermediate) is thus much more accessible than a direct transfer between C2 and C3.

2.4.3.3 Cyclopropyl transfer and conformational issues

Having established the whole pathway for the rearrangement, we then considered in more detail the rate determining step for this transformation, which is the cyclopropyl migration (from **1_F** to **2_F**).
Figure 2.4.8 depicts the structures of the three possible transition states corresponding to the cyclopropyl migration. Two views are shown for each of them. **TS12_F** is the transition state whose energy value has been used in the full profile of Figure 2.4.6. The CH_2 of the three-membered ring is directed toward the

wedge formed by two of the pyrazolyl arms. We can observe a weak interaction between one hydrogen atom of one of the β carbons of the cyclopropyl group and one fluorine atom of the C_6F_5- group placed in *ortho*. In **TS12_F_2**, the CH_2 group points towards the other direction. Its free energy value compared to **1_F** is 35.6 kcal/mol, which is 3.5 kcal/mol higher than **TS12_F**. In this transition state, two hydrogen-fluorine interactions are observed between the cyclopropyl- and the C_6F_5- group. Finally, **TS12_F_3** lies 34.4 kcal/mol higher than **1_F**.

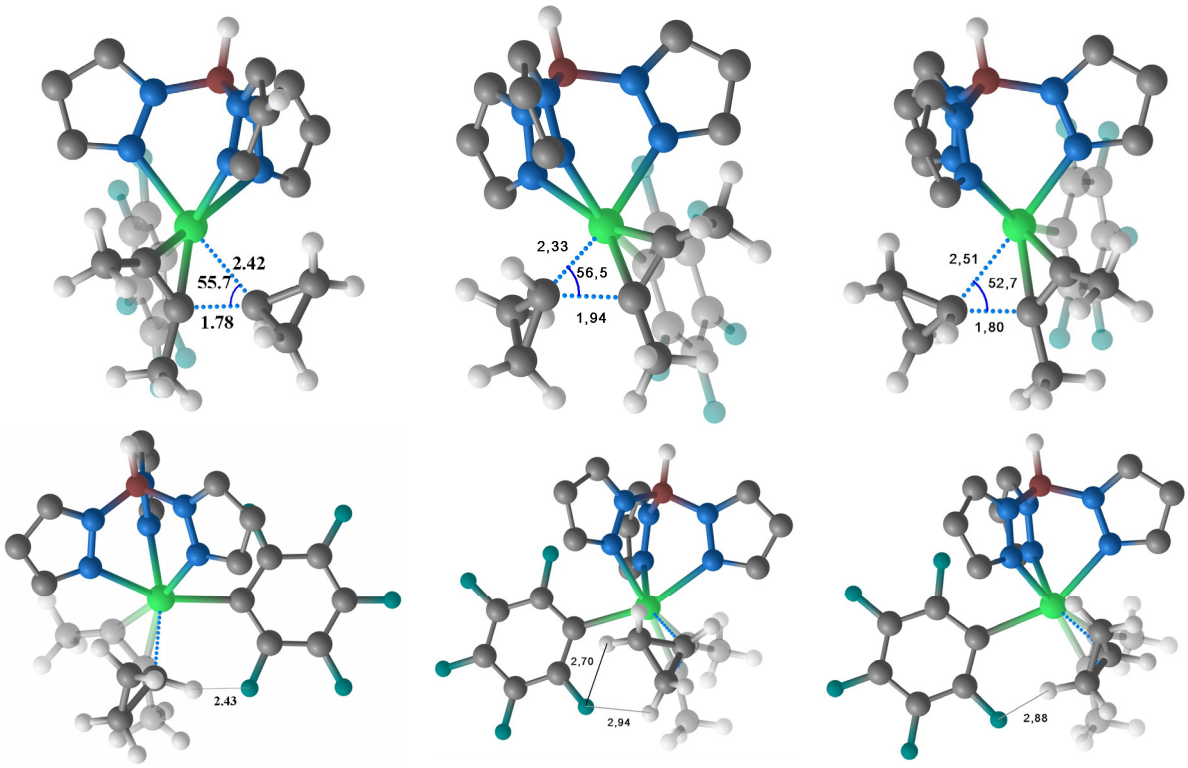

TS12_F ***TS12_F_2*** ***TS12_F_3***

Figure 2.4.8 Two views of the transition states computed for the migration of the cyclopropyl group in $Tp^{Me2}NbC_6F_5(c\text{-}C_3H_5)$(MeCCMe).

The orientation of the various ligands around the metal center appears to be critical.

2.4.3.4 C-F bond activation

Even if not observed experimentally, we computed the process corresponding to the activation of a C-F bond in $Tp^{Me2}NbC_6F_5(c\text{-}C_3H_5)$(MeCCMe). Figure 2.4.9 depicts the geometries of the transition state and that of the corresponding reactant and product.

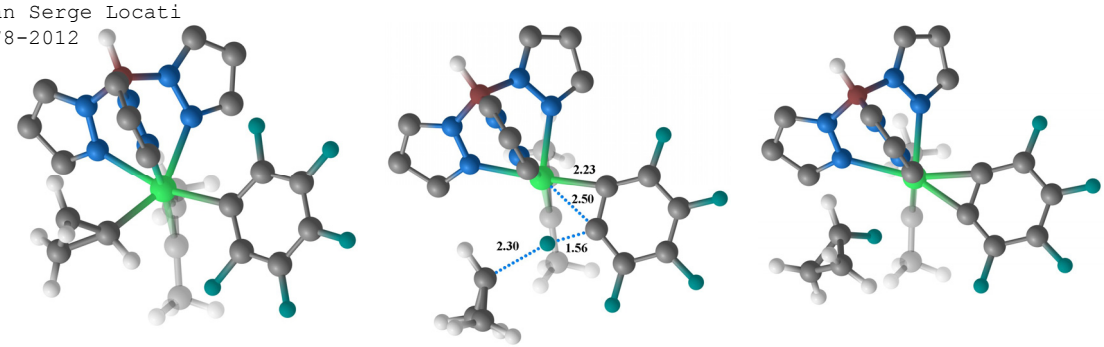

0.9 ***94.6*** ***4.5***

C_F_R ***C_F_TS*** ***C_F_P***

Figure 2.4.9 Reactant, transition state, and product for the C-F activation in $Tp^{Me2}NbC_6F_5(c\text{-}C_3H_5)(MeCCMe)$.

The transition state (**C_F_TS**) is early, with a C(Aryl)-F distance of only 1.56 Å, and a F-C(cyclopropyl) distance of 2.30 Å. The energy barrier of this process is prohibitively high, with the transition state lying 94.6 kcal/mol higher than **C_F_R** (which is structurally and energetically very close to **1_F**). This is in agreement with the experimental data, which do not observe any C-F bond activation.

2.4.4 Comparison between $Tp^{Me2}NbC_6F_5(c\text{-}C_3H_5)(MeCCMe)$ and $Tp^{Me2}NbC_6H_5(c\text{-}C_3H_5)(MeCCMe)$

Having determined the mechanism of the rearrangement for $Tp^{Me2}NbC_6\mathbf{F}_5(c\text{-}C_3H_5)(MeCCMe)$, we focused on the related $Tp^{Me2}NbC_6\mathbf{H}_5(c\text{-}C_3H_5)(MeCCMe)$ complex, in order to explain why no such process is observed in that case.
To check if the profile depicted in Figure 2.4.6 is applicable to both complexes, we computed the same pathway, but using complex $Tp^{Me2}NbC_6\mathbf{H}_5(c\text{-}C_3H_5)(MeCCMe)$ instead of $Tp^{Me2}NbC_6\mathbf{F}_5(c\text{-}C_3H_5)(MeCCMe)$. The results are shown in Figure 2.4.10, together with the barriers obtained with the fluorine-enriched compound for the sake of comparison.

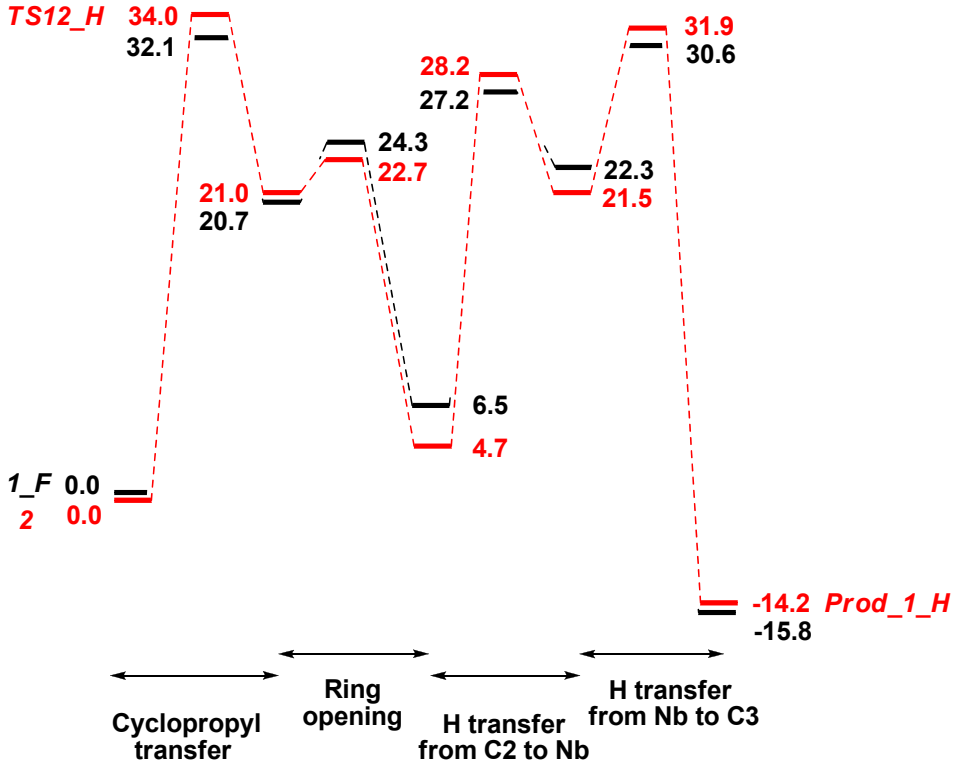

Figure 2.4.10 Comparison of the thermal rearrangement mechanisms for $Tp^{Me2}NbC_6\mathbf{F}_5(c\text{-}C_3H_5)$(MeCCMe) (in black) and $Tp^{Me2}NbC_6\mathbf{H}_5(c\text{-}C_3H_5)$(MeCCMe) (in red). Free energy values in kcal/mol. Nomenclature of the complexes discussed in the following are shown next to their corresponding energy values.

The general picture of the profile is broadly the same for both complexes. The energy values are slightly higher, or slightly lower depending on the step considered. The migration of the cyclopropyl group corresponds to the highest barrier. In the case of $Tp^{Me2}NbC_6\mathbf{H}_5(c\text{-}C_3H_5)$(MeCCMe), the barrier is slightly higher (by 1.9 kcal/mol) than in the case of the complex enriched with fluorine. This confirms the importance of this step in the reactivity.
Note that we computed several transition states for the migration of the $c\text{-}C_3H_5$ group (see Figure 2.4.11) in order to tackle the conformational issues. The lowest one (**TS12_H**) lies 34.0 kcal/mol higher than **2** (as shown in Figure 2.4.10). Two other transition states are depicted in Figure 2.4.11, namely **TS12_H_2**, which has the CH_2 directed to the wedge formed by two of the pyrazolyl arms, and **TS12_H_3** whose CH_2 of the cyclopropyl group is directed to the opposite direction. Both of them have high energies, **TS12_H_2** is 38.9 kcal/mol higher than complex **2**, and **TS12_H_3** lies slightly lower, at 35.1 kcal/mol. The energy barrier for the cyclopropyl migration is then rather high. However, it appears very close to the barrier found for the activation of benzene (see Figure 2.2.5 in subsection 2.2.2 of this chapter).

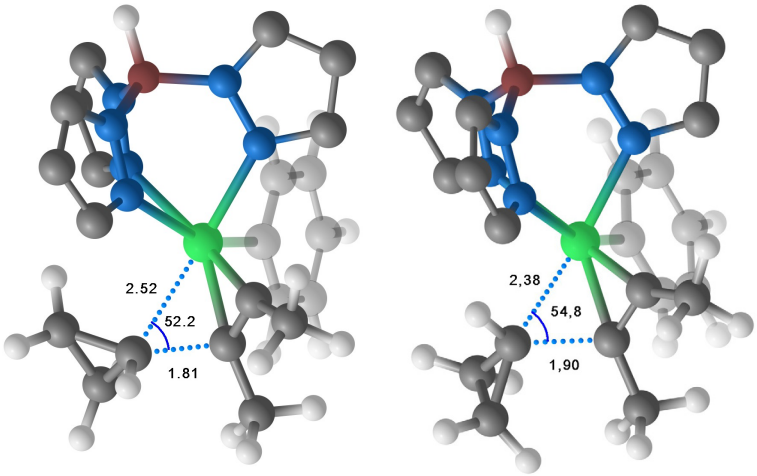

TS12_H_2 ***TS12_H_3***

Figure 2.4.11 Two transition states computed for the migration of the cyclopropyl group in $Tp^{Me2}NbC_6H_5(c\text{-}C_3H_5)$(MeCCMe).

Finally we can compare the reactivities of **2** and **1_F**. Figure 2.4.12 summarizes the reactivity of $Tp^{Me2}NbC_6\mathbf{H}_5(c\text{-}C_3H_5)$(MeCCMe), and Figure 2.4.13 that of $Tp^{Me2}NbC_6\mathbf{F}_5(c\text{-}C_3H_5)$(MeCCMe).

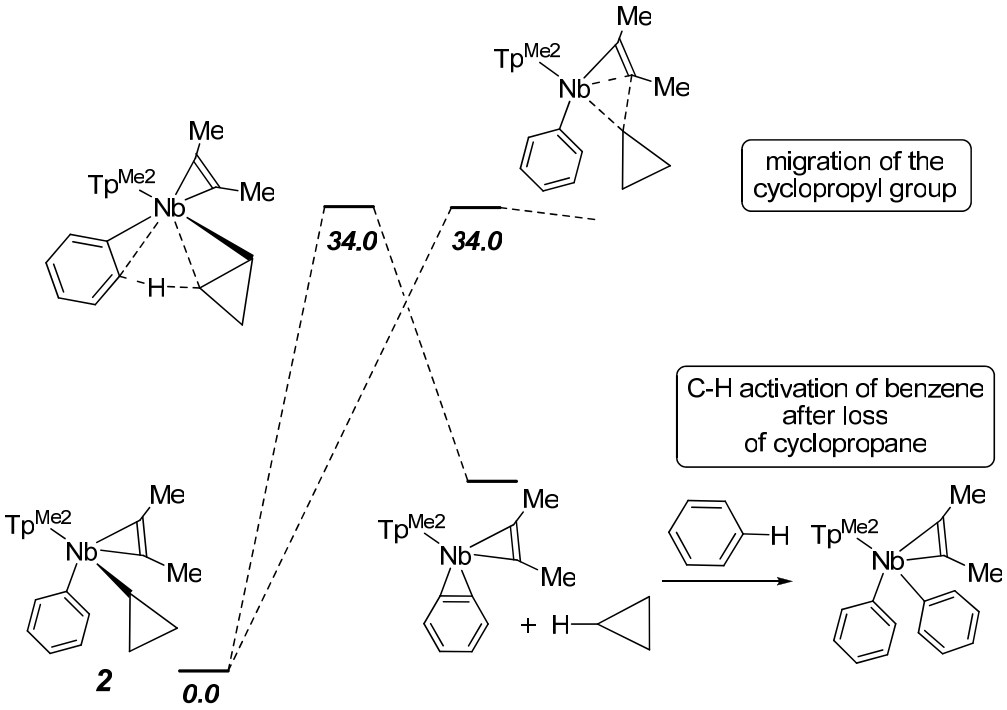

Figure 2.4.12 Reactivity of **2**. Free energy values in gas phase in kcal/mol, obtained with the M06 functional.

In the case of complex **2**, the reactivity is characterized by the competition of two distinct processes. C-H activation and migration of the cyclopropyl group have similar barriers, and both should be observed. This disagrees with the experimental observations, which reported the exclusive presence of the C-H activation product (complex **3**) with this complex.

Complex **1_F** shows a very different picture. C-F activation appears impossible (barrier of 94.6 kcal/mol), leaving the migration process the only transformation energetically feasible. In that case, subsequent rearrangement of the $Tp^{Me2}NbC_6\mathbf{F}_5(c\text{-}C_3H_5)$(MeCCMe) complex is likely, since there is no other competitive process.

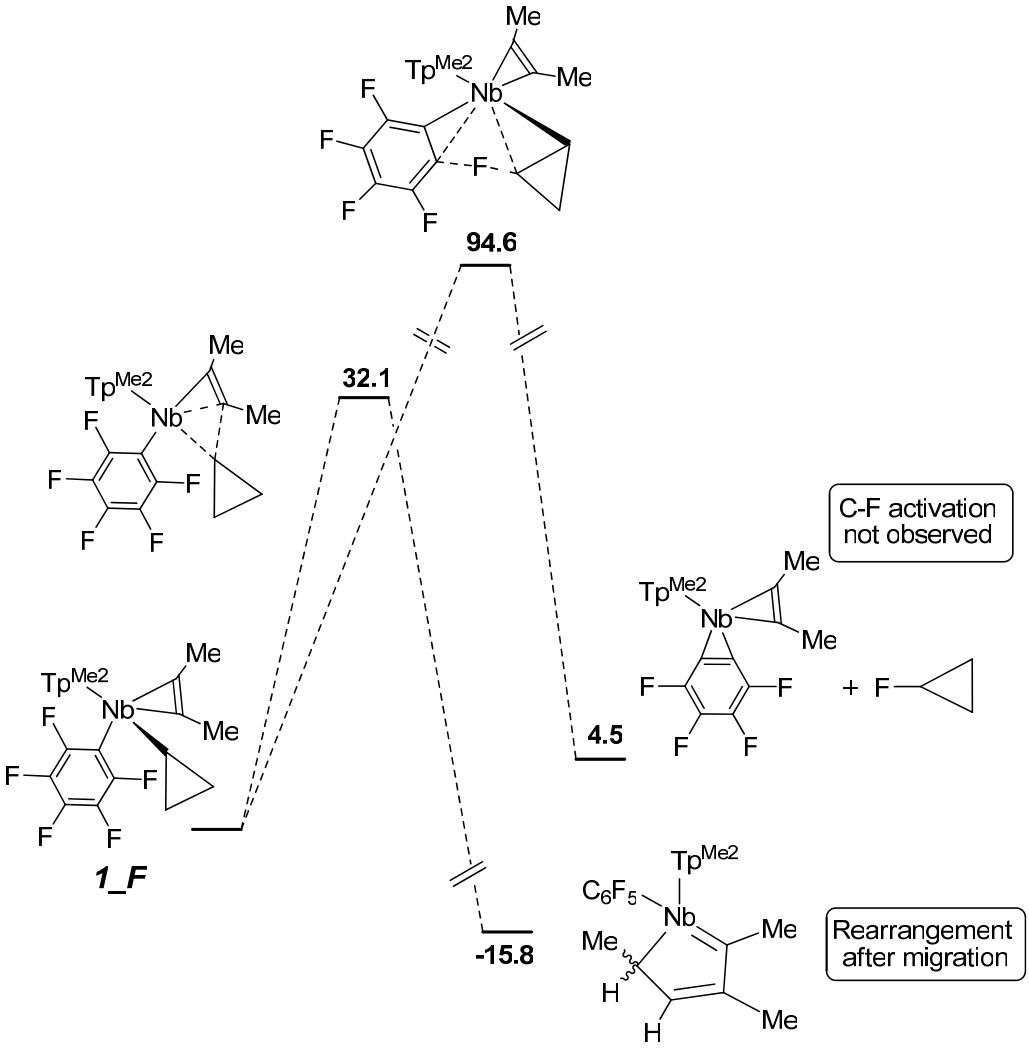

Figure 2.4.13 Reactivity of **1_F**. Free energy values in gas phase in kcal/mol, obtained with the M06 functional.

2.4.4.1 Influence of the computational method

Because of the small energy differences involved, we decided to assess the influence of the computational methodology through some additional calculations on some of the structures depicted in Figures 2.4.12 and 2.4.13. We first expanded the basis set with the use of 6-31++G(d,p) for hydrogen and fluorine, keeping 6-31G(d) for the remaining atoms (carbon, nitrogen and boron). For this, we performed single point calculations on the structures obtained with the simpler 6-31G(d). We also performed calculations with the B97D functional as implemented in Gaussian09, considering that the dispersion corrections included in this method could better capture the weak interactions between the fluorine and hydrogen atoms in our systems. In that case, complete optimization were carried out, and we then optimized in solvent (through the SMD method) the structures obtained. The C-F activation was deemed too unlikely (due to its very high barrier) to deserve this detailed analysis. We thus only computed the processes likely to be sensitive to the computational method, namely the rearrangement of $Tp^{Me2}NbC_6\mathbf{H}_5$(*c*-$C_3H_5$)(MeCCMe) and $Tp^{Me2}NbC_6\mathbf{F}_5$(*c*-$C_3H_5$)(MeCCMe), and the C-H activation occurring with $Tp^{Me2}NbC_6\mathbf{H}_5$(*c*-$C_3H_5$)(MeCCMe), which all have similar barriers. The results are collected in Table 2.4.1.

Table 2.4.1 Influence of the computational methodology on the energy barriers for the migration process in **1_F** and **2**, and the C-H activation in **2**.

	migration process complex **1_F**	migration process complex **2**	C-H activation complex **2**
M06/ 6-31G(d)	32.1	34.0	34.0
M06/ 6-31++G(d,p)	30.7	33.1	32.4
B97D/6-31G(d)	32.9	35.0	34.0
B97D/6-31G(d)/SMD	31.1	32.7	32.7

Regardless of the method used, we get similar trends. First, the rearrangement of the fluorine-enriched complex (**1_F**) has a barrier slightly higher than 30 kcal/mol (between 30.7 and 32.9 kcal/mol depending on the method). The corresponding transition states for the mirrored mechanism for the all-hydrogen cyclopropyl complex (**2**) lie around 2 kcal/mol higher (between 32.7 and 35.0 kcal/mol), confirming the determining role of the fluorine atoms in lowering the barrier of the rearrangement. Secondly, the C-H activation of benzene by $Tp^{Me2}NbC_6\mathbf{H}_5$(*c*-$C_3H_5$)(MeCCMe) is as easy as the rearrangement process for this complex. Two of the methods used (M06/ 6-31++G(d,p) and B97D/6-31G(d)) show a preference of 1 kcal/mol for the former reaction, and the two others (M06/6-31G(d) and B97D/6-31G(d)/SMD) produce similar barriers for both processes. The very low energy difference between these two barriers (if any) cannot be considered as significant enough to clearly rationalize the experimental outcome. A difference of 1 kcal/mol should translate into a mixture of the product of C-H activation (labelled as **3** in section 2.2) and the product of the rearrangement (the niobium metallacycle

Prod_1_H). We also note that the product of rearrangement is much favoured thermodynamically (**Prod_1_H** more stable by 15 kcal/mol relative to **2**), than the product of C-H activation (**3** more stable only by 1.5 kcal/mol relative to **2**).
Since the results obtained with various methods are rather similar, we can reasonably conclude that these systems (or at least their reactivity) are fairly insensitive to the functional, basis set or solvation. The origin of the lack of full agreement with experiment must be somewhere else.

2.4.5 Concluding remarks

The methyl migrations in the $Tp^{Me2}Nb(Me)(Cl)(MeCCR)$ (with R = Me, Ph) complexes have been rationalized. The phenyl group on the alkyne ligand lowers the barrier of this process.
A mechanism for the thermal rearrangement of $Tp^{Me2}NbC_6F_5(c\text{-}C_3H_5)(MeCCMe)$ has been proposed. A prohibitively high energy barrier for the C-F activation has been computed, in agreement with the non observation of fluorine enriched cyclopropane. The occurrence of a rearrangement process in $Tp^{Me2}NbC_6F_5(c\text{-}C_3H_5)(MeCCMe)$ seems to be mainly due to the high energy barrier of C-F activation which allows the rearrangement as the only alternative. The configuration of the final product still has to be determined.
Regarding the $Tp^{Me2}NbC_6H_5(c\text{-}C_3H_5)(MeCCMe)$ complex, C-H activation and migration of the cyclopropyl group have very similar computed barriers, which is not fully consistent with the experiments. An exclusive C-H activation process is indeed observed.

UNIVERSITAT ROVIRA I VIRGILI
COMPUTATIONAL STUDY OF C-H BOND CLEAVAGE AND C-C BOND FORMATION PROCESSES CATALYZED BY TRANSITION METAL COMPLEXES
Abel Jean Serge Locati
DL:T. 278-2012

Chapter 3

Palladium-catalyzed cross-coupling of silanolates

UNIVERSITAT ROVIRA I VIRGILI
COMPUTATIONAL STUDY OF C-H BOND CLEAVAGE AND C-C BOND FORMATION PROCESSES CATALYZED BY TRANSITION METAL COMPLEXES
Abel Jean Serge Locati
DL:T. 278-2012

In the introduction, we described the cross-coupling of silanolates, first developed by Hiyama, at the end of the 1980's.[87] Over the last decade, the group of Denmark significantly improved this coupling by elaborating a fluoride-free process.[213] This has been made possible by considerable improvements in the storage, the isolation and the synthesis of the silanolate compounds.[88] This cross-coupling consists of a palladium-catalyzed carbon-carbon bond formation between an organic halide agent and a silanolate salt. Heterocyclic-, aromatic-, alkenyl-, and allyl- silanolates are among the silicon reagents found to be competent for this reaction. Various mechanistic studies (mainly through kinetic experiments) were undertaken,[214] and the main mechanistic features could be unravelled.[215] Figure 3.1.1 depicts the proposed catalytic cycle.

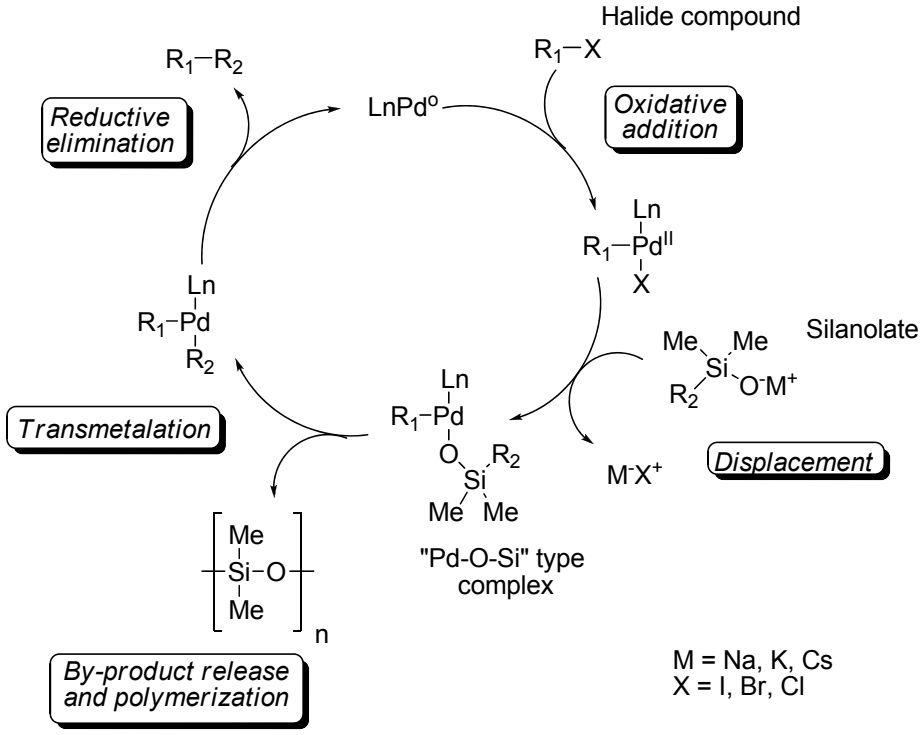

Figure 3.1.1 Proposed catalytic cycle for the fluoride-free cross-coupling of silanolates.

The Pd(0) catalyst first reacts with an aryl halide through an oxidative addition process, forming a Pd(II) species. Then the silanolate salt reacts with the Pd(II) intermediate to form a "Pd-O-Si" type complex. This Pd-O-Si linkage containing complex undertakes the transmetalation, with release of a siloxane by-product

which polymerizes. Finally a reductive elimination step closes the cycle and regenerates the Pd(0) species. This mechanistic picture presents different features compared to the catalytic cycle proposed by Hiyama. An important point is that the "Pd-O-Si" type complex is competent for the transmetalation process, and that the silicon atom does not need to be hypervalent (it was considered a prerequisite by Hiyama for the fluoride promoted cross-coupling) for the reaction to occur.[216] This has been suggested by a zeroth-order dependence for the phosphine ligand.

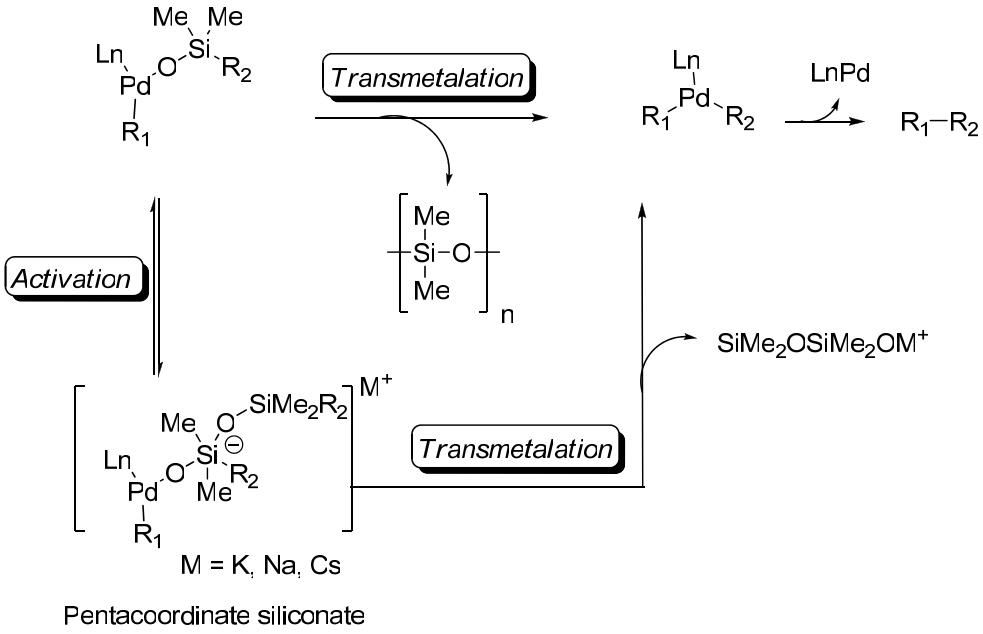

Figure 3.1.2 Activated and non-activated pathways for the cross-coupling of silanolates.

Regarding the transmetalation, the mechanism has been refined through the most recent developments, and two general mechanistic pathways appear then possible.[215] The first, which is analogous to that proposed by Hiyama, consists of an activation of the "Pd-O-Si" type complex by another silanolate and is depicted in the lower portion of Figure 3.1.2. This proceeds via a complex bearing a hypervalent silicon, which is believed to undertake the transmetalation with concomitant loss of the siloxane moieties. This pathway was found operative for the fluoride promoted cross-coupling,[217] but could also be favoured in some fluoride-free couplings, depending on the silanolate used, the ligands on the catalyst, and the organic halide type.[215, 218] Recent kinetic studies showed a dramatic increase in the rate constant when the Pd-O-Si type complex was treated with an excess of silanolate (which corresponds to the catalytic conditions). However, other results suggest that the "Pd-O-Si" type complex is *also* operative for the transmetalation process, and that the silicon atom does not need to be pentacoordinated to afford the expected outcome of the reaction (top of Figure 3.1.2). Furthermore, the "Pd-O-Si" type complex was detected in various occasions

in the reaction media (by ^{31}P NMR spectroscopy).[88, 213, 215] Finally, a key experiment corroborated the importance of this intermediate. The complex depicted in Figure 3.1.3 was independently synthetized, and a simple heating allowed the desired biaryl product in quantitative yields. No activator was present in that case. It is worth noting that the temperature needed in that case (100 °C) is slightly higher than those described in the general cross-coupling reactions performed.[219]

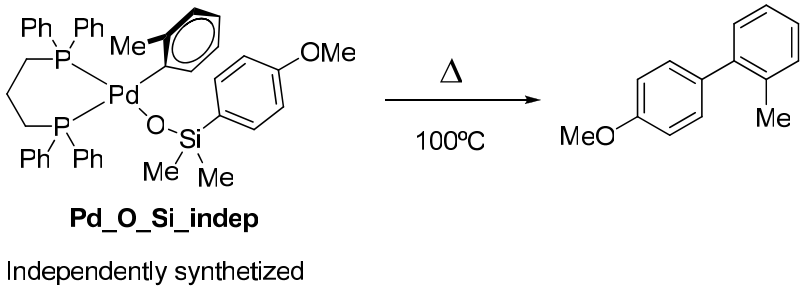

Pd_O_Si_indep

Independently synthetized

Figure 3.1.3 Biaryl formation from an independently synthetized "Pd-O-Si" type complex.

The mechanistic picture appears thus particularly complex. Two main pathways seem to be operative: the "non-activated" process which relies on the ability of the Pd-O-Si linkage containing complex to undergo the transmetalation through simple thermal activation, and the "activated" process which proceeds via a pentacoordinate silicon. The first section will deal with the first pathway, and we will focus on the feasibility of the non-activated mechanism. In the second section, the role of activating molecules (which generate a hypervalent silicon) will be studied. The key role of dba (dibenzylidene acetone) will be highlighted, the effect of an additional silanolate and the siloxane by-product will be studied.

3.1 Non-activated mechanism

This section will be centred on the feasibility of the non activated mechanism. For this study, we will focus on the cross-coupling of aromatic halides with aromatic silanolates.[219, 220] Among the numerous reagents described for the cross-coupling of silanolates, the reaction of aryl halides with aryl silanolates is generally used for the experimental kinetic studies. The reason for this is the slower reaction times of these reagents compared to other silanolates (such as alkenyl or allyl silanolates), which allow easier experimental characterizations. Figure 3.1.4 a) shows the general conditions of the aromatic silanolates coupling with aromatic halides. A bromide halide is used, together with a palladium catalyst bearing a phosphine ligand. The phosphine employed is (t-Bu_3)P,[221] and its main characteristic is that it is very bulky. It has been used successfully in various cross-coupling reactions.[222] Its ability to generate T-shaped palladium species is well documented,[223] and X-ray characterizations determined the monomeric character of this active form of the catalyst. The reaction is usually done in toluene (but some other solvents are also

found competent), and a heating of around 70-90°C is necessary to obtain the biaryl product.

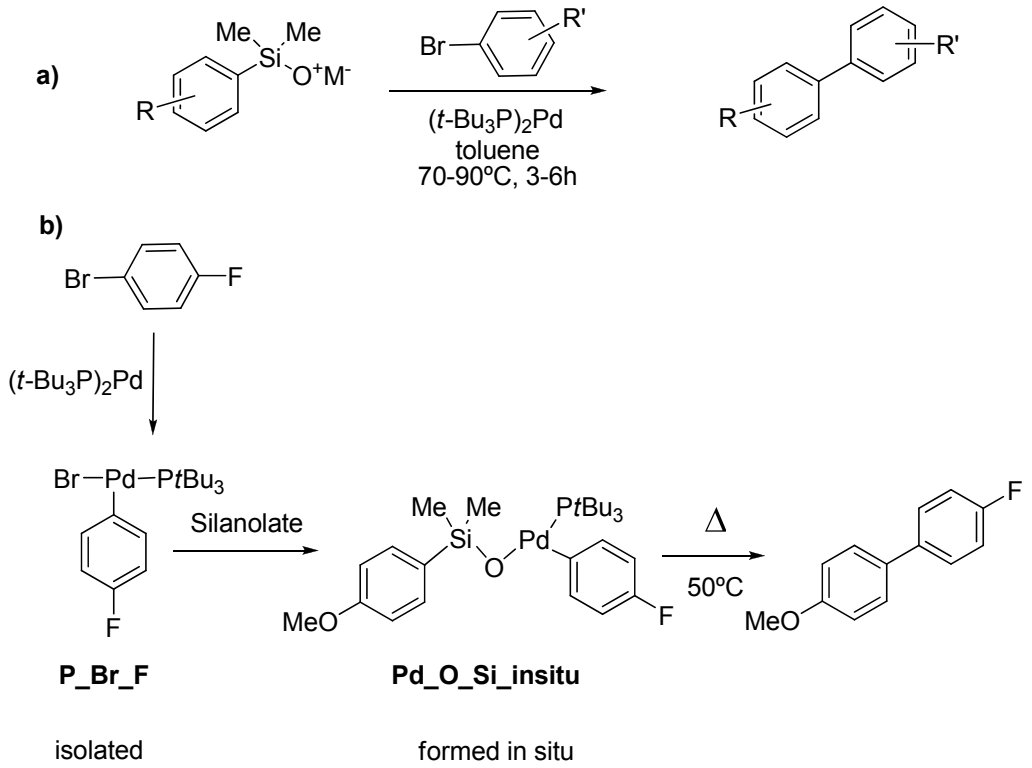

Figure 3.1.4 General conditions for the cross-coupling of aryl halides with aryl silanolates.

A few facts have been determined thanks to the experimental mechanistic studies undertaken. These are collected in Figure 3.1.4 b). Complex **P_Br_F** could be isolated and further reacted with a silanolate to afford the biaryl product.

The "Pd-O-Si" type complex was detected in the reaction media. The complex **Pd_O_Si_insitu** was then isolated and characterized. An X-Ray structure could be obtained, which confirmed again the presence of this complex in the reaction media. A simple heating (50°C) of **Pd_O_Si_insitu** results in the biaryl formation.

After presentation of the computational methods, we will report the mechanisms considered to rationalize the biaryl formation starting from the T-shaped palladium catalyst, using both a model and a real system. Formation of the "Pd-O-Si" type complex will be computed. Then, we will look at the feasibility of the conversion of the "Pd-O-Si" type complex into the biaryl product.

3.1.1 Computational methods

In this section, two systems will be employed: the real system and a model system. The first corresponds to all the reagents experimentally used and to the bulky phosphine (t-Bu_3)P, and will be referred as "the real system" or "the real phosphine", or "the bulky phosphine". Some of the calculations were done using Me_3P as a model phosphine. This will be referred as "the model system" or "the model phosphine".

The whole study was performed by means of DFT methods implemented in the Gaussian03[163] and Gaussian09[178] suites of program. We used the B3LYP functional[127, 132] and the SDD effective core potential together with its associated basis set[179] for palladium and the 6-31G(d) basis[167, 168] for all the other atoms (BS1). In the cases which the molecule is anionic (added silanolate or bromide on the metal center), a diffuse function was added (e.g. atoms were described with 6-31+G(d)[224]) (BS2). Direct comparison of energy values obtained with BS1 and BS2 is not strictly correct, but is indicative of the pathways followed. We also performed test calculations using the M06 [135, 140] and B97D[141] functionals, which introduce a better description of dispersion[141, 212] and long range interactions. The SMD method was used for solvation.[180] The nature of each optimized minimum was characterized by means of a vibrational analysis. All transition states computed have only one imaginary frequency, and were connected to the corresponding minima by relaxing the transition state geometry towards the reactant and the product. All reported values are free energy values in gas phase, except otherwise stated in the text. Energy values are all expressed in kcal/mol, and distances in angstroms. Charged complexes are represented between brackets.

3.1.2 Transmetalation from the (Ph)(R_3P)Pd(Br) catalyst and formation of the "Pd-O-Si" type complex

In the following subsection, we consider the starting elements of the reaction, after oxidative addition. The oxidative addition did not appear fundamental in this study, since the reaction can be equally performed if started from the previously formed (Ph)($t$$Bu_3P$)Pd(Br) and the silanolate.

As showed in Figure 3.1.4, the reaction starts when mixing the silanolate and the Pd(II) catalyst. This is done in presence of solvent, mostly in toluene in the case of the cross-coupling of aryl silanolates. The palladium catalyst is ($t$$Bu_3P$)$_2$Pd which is widely used in organic synthesis. The active species is admittedly (Ph)($t$$Bu_3P$)Pd(Br) which is obtained after oxidative addition with the phenyl bromide. As stated in the introductory paragraph of the section, a family of these complexes have been isolated by Hartwig and coworkers,[223] and X-Ray characterization has been obtained.

3.1.2.1 Isomerization of the Pd(II) catalyst

The *t*Bu$_3$Pgroup being very bulky, it is common, when modelizing reactions using this species, to reduce the size of the phosphine. Then many computational studies compute (Ph)(Me$_3$P)Pd(Br) as the catalyst. Three isomers are possible, depending of which of the ligands is located *trans* to the vacant site. Figure 3.1.5 shows these different possibilities. In the first case, the phenyl group is *trans* to the vacant site, and the phosphine *trans* to the halide (labelled as **P_Br_1_Met**). This is the most stable isomer (the relative free energies are reported below each structure). A second conformation (**P_Br_1_bis_Met**) with the phosphine *trans* to the vacant site has a very similar energy. Finally, a third structure with the bromide *trans* to the vacant site is 14.6 kcal/mol higher in energy compared to the other two. **P_Br_1_Met** is then the most stable which is consistent with the experimental characterizations obtained. In the X-Ray structure, the phenyl is indeed always *trans* to the vacant site, whatever the phosphine ligand or the halide. This is also consistent with the well-accepted *trans* influence trend.[16] The phenyl group having a stronger *trans* influence than the other ligands, the conformation with this group *trans* to the vacant site is adopted.

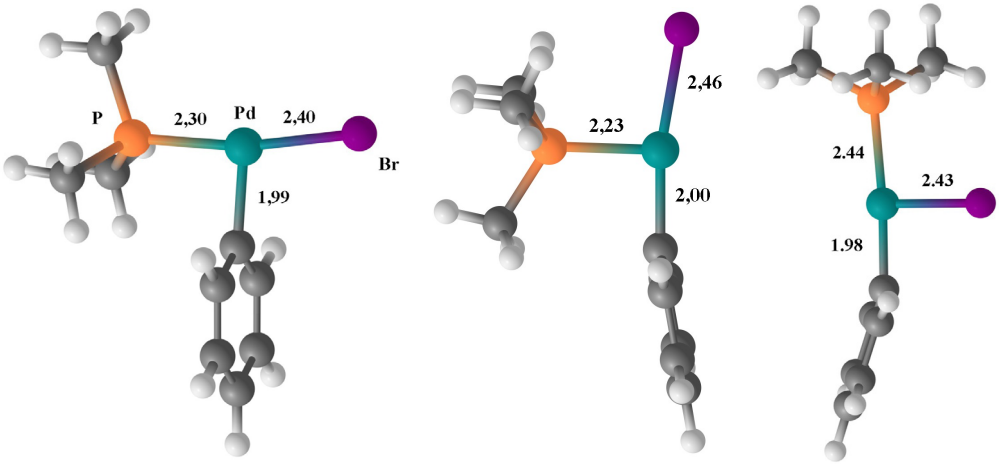

P_Br_1_Met ***P_Br_1_bis_Met*** ***P_Br_2_Met***

0.0 ***0.9*** ***14.6***

Figure 3.1.5 Computed isomers of the (Ph)(Me$_3$P)Pd(Br) catalyst. Free energy below each structures.

If we compute the real system, with a bulky phosphine, only two minima are obtained (collected in Figure 3.1.6). The most stable one is the same isomer that the one adopted in the model system. In the case of **P_Br_1_Bulk**, the Pd-P distance is slightly longer (2.37 Å instead of 2.30 Å with the model phosphine), most probably due to the very bulky group on the phosphine. No structure similar to **P_Br_1_bis_Met** could be located. Whatever the starting structure, the calculation

always converged to geometries such as that of **P_Br_1_Bulk** or **P_Br_2_Bulk**. This can be easily explained by the steric hindrance of the phosphine. This very bulky group prevents the possibility to have two neighbouring ligands in the *cis* position. In the literature, some computational studies use this conformation as the starting complex,[225] which is not energetically wrong (since **P_Br_1_Met** and **P_Br_1_bis_Met** are almost degenerate in energy), but could be misleading regarding the geometry adopted by the complexes. **P_Br_2_Bulk** is only 8.5 kcal/mol higher than the experimentally isolated complex, which is 6.1 kcal/mol more stable than the corresponding complex with a model phosphine. The bulky group thus stabilizes significantly the least stable isomer of the complex.

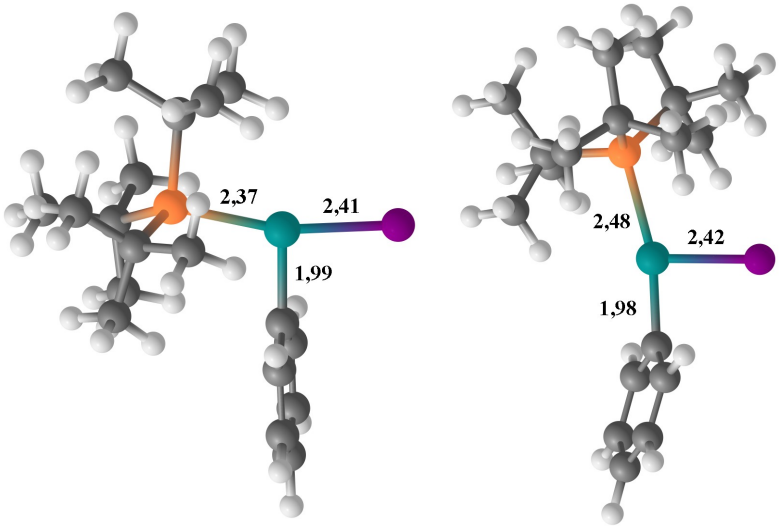

Figure 3.1.6 Computed isomers of the (Ph)(tBu$_3$P)Pd(Br) catalyst.

3.1.2.2 Reaction profile for the model phosphine

We first computed the formation of the Pd-O-Si linkage containing complex starting with the Pd(II) catalyst (**P_Br_1_Met**) and the anionic silanolate. Figure 3.1.7 reports the profile computed for this model system. We first observe an isomeric change of the catalyst. Starting from **P_Br_1_Met**, the structure evolves to **P_Br_2_Met** through the transition state **P_Br_TS12_Met**. The energy barrier is about 18.0 kcal/mol, and the process is endothermic. Following this, a complex is formed with the silanolate, with weak interactions between two carbons of the phenyl ring of the silanolate and the metal center. This complex (**Trans_1_Met**) is 6.2 kcal/mol higher than the starting reactants. From **Trans_1_Met**, we found a transition state only 0.7 kcal/mol higher which corresponds to the formation of **PdO_form_2_Met**, which is the Pd-O-Si linkage containing complex. Formation of **PdO_form_2_Met** appears very exothermic and is -22.3 kcal/mol lower than

the separate reactants. This is the most stable complex of the whole profile. From this, we found a transmetalation process with a very high barrier (more than 41 kcal/mol). The resulting complex, **PdO_form_3_Met** is the complex immediately prior to reductive elimination. We also found a transmetalation process starting from **Trans_1_Met**. In that case the barrier is about 11.7 kcal/mol and leads to complex **Trans_2_Met**. This complex is energetically degenerate with **PdO_form_3_Met**, its structure is very similar, but the orientation adopted by some of the ligands is slightly different.

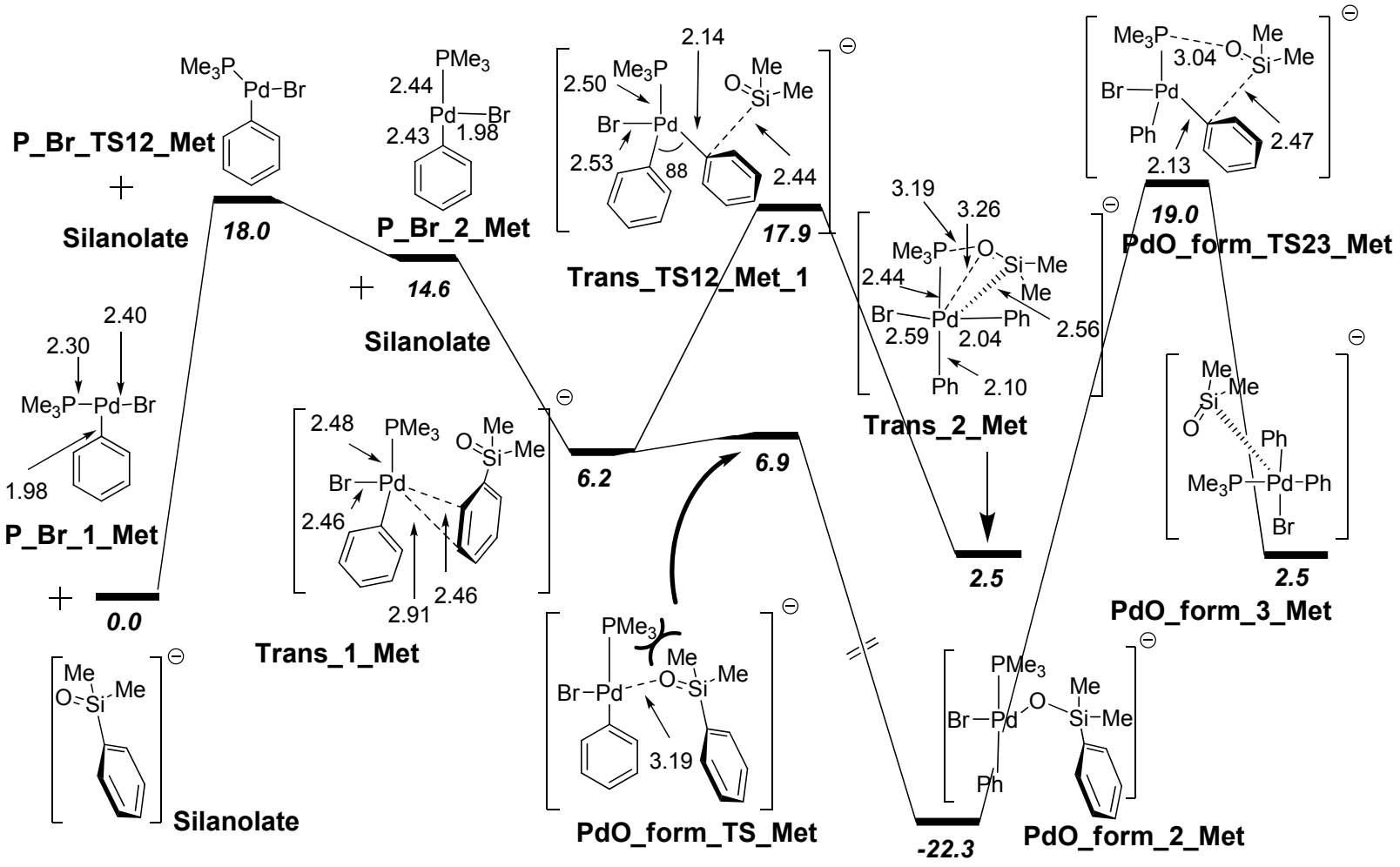

Figure 3.1.7 Free energy profile of the transmetalation process and the Pd-O bond formation, in the case of the model phosphine.

We would like to emphasize the importance of the ligand distribution around the metal center on the reactivity of the complex. To address this issue, we computed four different transition states for the transmetalation step before Pd-O bond formation (corresponding to **Trans_TS12_Met_1**). Their schematic drawings are depicted in the upper part of Figure 3.1.8.

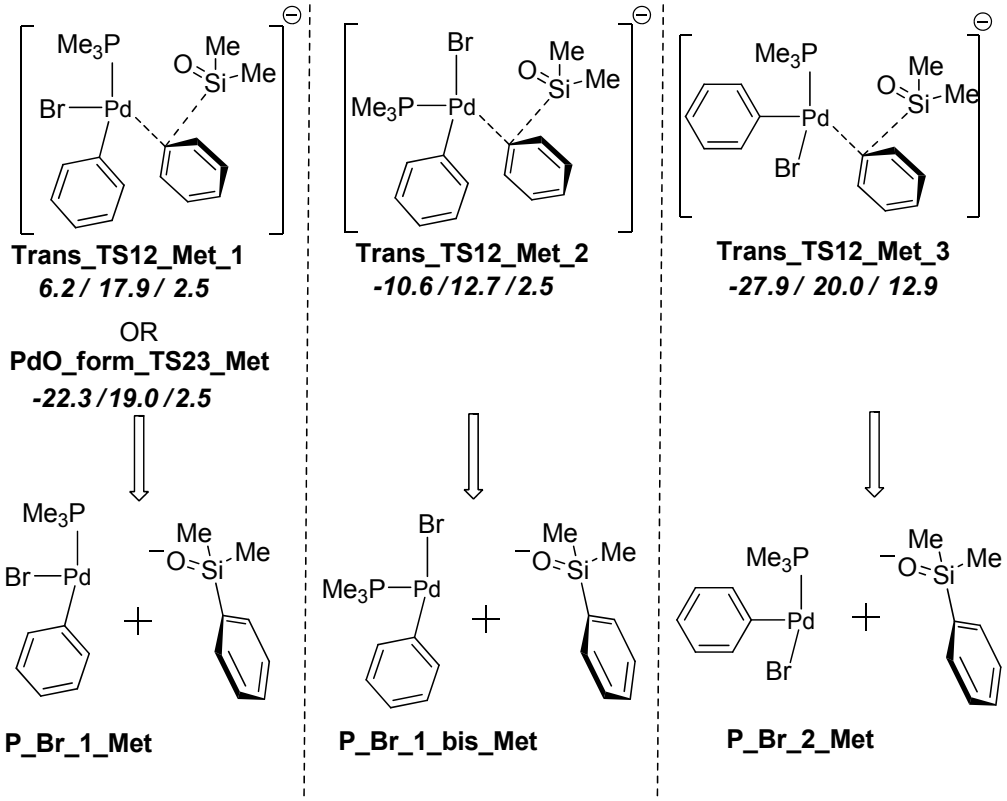

Figure 3.1.8 Transmetalation process for the three possible isomers of (Ph)(Me_3P)Pd(Br). The transition states are schematically represented in the upper portion of the figure, together with the energetics. Energy of the transition states (middle values), together with their corresponding reactants (left values), and products (right values) are reported below each structures. Their corresponding separated reactants are depicted in the lower part of the figure. All energy values are free energies relative to the separated reactants depicted in Figure 3.1.7 (**P_Br_1_Met** and **Silanolate**).

When relaxing the geometries of **PdO_form_TS23_Met** and **Trans_TS12_Met_3** towards the reactant side, the structures go to the Pd-O-Si linkage containing complex (see **PdO_form_2_Met**), which is reflected by very low energy values for the reactants. It should be stressed that in both cases, the barrier for the transmetalation is around 40 kcal/mol. In contrast, **Trans_TS12_Met_1** (depicted in the full profile of Figure 3.1.7) and **Trans_TS12_Met_2** collapse to an adduct between the silanolate and the Pd(II) species with weak interactions between the

aryl ring and the metal. These complexes are less stable than the Pd-O-Si linkage containing complexes obtained when connecting **PdO_form_TS23_Met** and **Trans_TS12_Met_3**. The adduct obtained from **Trans_TS12_Met_2** is more stable (-10.6 kcal/mol) than the adduct obtained from **Trans_TS12_Met_1** because, as mentioned previously, the arrangement adopted in this case is less stable (see Figure 3.1.5). **Trans_TS12_Met_2** is then a transition state with a reasonable barrier (23.3 kcal/mol) for the transmetalation, but, importantly, the conformation adopted in that case by the Pd(II) catalyst corresponds to **P_Br_1_bis_Met**, which is not a realistic structure for the real system (due to steric hindrance). This is why we did not discuss this transition state in the full profile of Figure 3.1.7.

Thus, depending on the arrangement of the ligands in the transition state, it could be connected to either a van der Waals complex (such as **Trans_1_Met**), or a complex containing a Pd-O-Si linkage (such as **PdO_form_2_Met**). This is directly related to the fact that the barrier for the Pd-O bond formation is very low (around 0.7 kcal/mol in the case of the structures showed in Figure 3.1.7). Then, slightly changing the orientation of the silanolate, or varying the position of the ligands around the metal center, makes these two starting complexes both possible for this transition state. In our case, each transition state computed is connected to a particular intermediate, but the very low barrier of the Pd-O bond formation makes that the weak van der Waals complexes such as **Trans_1_Met** are not obtained in each cases. A number of points are of interest in the full profile depicted in Figure 3.1.7. First, two different processes can be initiated with **Trans_1_Met**: the Pd-O bond formation and the transmetalation. The former is much easier, both thermodynamically and kinetically. This would mean that the reaction is completely favoured towards this process, and no transmetalation through **Trans_TS12_Met_1** would be possible. Furthermore, transmetalation starting from **PdO_form_2_Met** is found too high in energy (41 kcal/mol is not a reasonable value for the experimental conditions). Finally, Pd-O bond formation taken apart, the transmetalation process through **Trans_TS12_Met_1** has a rather low barrier (around 18 kcal/mol), which is rather low for a reaction occurring at 70°C. All these facts are inconsistent with the experimental data.

Nonetheless, an important point is that the methyl substituents of the phosphine ligand in **PdO_form_TS_Met** are very close to the oxygen atom. On the contrary, no steric interactions seem to apply in **Trans_TS12_Met_1**. We thought than the barrier for the Pd-O bond formation could be artificially low in the absence of the steric bulk of the phosphine ligand. The bulky group on the phosphine could then inhibit, or at least slow down, the formation of the Pd-O-Si linkage containing complex. This phosphine would not interfere too much in the transmetalation process, since in **Trans_TS12_Met_1**, the methyl substituents of the phosphine appear far from the phenyl transfer. To check if the order of the barriers would be changed using a bulky phosphine, we then decided to compute the same pathways with the real system.

3.1.2.3 Reaction profile for the real phosphine

We report the full profile using the real phosphine in Figure 3.1.9. The process starts with an isomerization of the catalyst. The phosphine ligand goes from being *trans* to the bromide (most stable isomer), to *trans* to the phenyl. The barrier decreases slightly compared to the corresponding process depicted in Figure 3.1.7 (transition state labelled as **P_Br_TS_12_Bulk**). The next species in the profile is a weak complex between the anionic silanolate and the Pd(II) catalyst. It is labelled as **PdO_form_1_Bulk** and shows an interaction between the oxygen atom of the silanolate and two of the hydrogen atoms of one of the *t*Bu groups. The oxygen is 5.80 Å away from the metal centre, and the phosphine is bound to the palladium (the key distances are collected in Table 3.1.1). We found that **PdO_form_1_Bulk** leads to the formation of the Pd-O-Si linkage containing complex (**PdO_form_2_Bulk**). This process is indeed more costly than in the case of a model phosphine. Now the energy of the transition state is around 9.6 kcal/mol higher than the separated reactants. The formation of the Pd-O bond is then clearly made difficult by the presence of the methyl groups. It should be noted that the phosphine ligand stays bound to the metal center (Pd-P distance of 2.46 Å in the transition state and 2.72 Å in the product) along the Pd-O bond formation. Then we found a transmetalation process which starts with **Trans_1_Bulk** which shows the same kind of η^2 interaction between the phenyl ring of the silanolate and the palladium that with the model system.
The step from **PdO_form_2_Bulk** to **Trans_1_Bulk** consists of the phosphine dissociation from the palladium. The main difference between the complexes **Trans_TS12_Met_1** and **Trans_TS_Bulk** is that the phosphine atom is not bound anymore to the metal center (Pd-P distance of 4.81 Å in the latter), but we do have an interaction between the oxygen and one of the hydrogen atom of the tBu$_3$P group (O···H distance of 2.25 Å). Importantly, the phosphine dissociation is clear during the whole step (Pd-P distance of 4.94 Å in the transition state and 5.21 Å in **Trans_2_Bulk**). We note that the hydrogen interaction observed in **Trans_1_Bulk** is also observed in the transition state and the product. We computed the same process (from **Trans_1_Bulk** to **Trans_2_Bulk**) without phosphine, and we found virtually the same barrier. The phosphine ligand (through the weak hydrogen bonds) has then no effect on the transmetalation step after dissociation.
The barrier for the Pd-O bond formation increases then significantly when computing the real system. On the other hand, the barrier for the transmetalation would stay almost unchanged, if not for the required phosphine dissociation process. The energy difference between **PdO_form_2_Bulk** (the Pd-O-Si linkage containing complex) and **Trans_TS_Bulk** is around 27.5 kcal/mol which is a value consistent with the experimental conditions. The transition state for phosphine dissociation has not been computed, but it is not believed that the corresponding barrier would be much higher than 27.5 kcal/mol.

Finally, note that we cannot discard that the transmetalation could occur directly from the **P_Br_1_Bulk** form of the catalyst, but we wanted to show that both forms (**P_Br_1_Bulk** and **P_Br_2_Bulk**) could be operative in the process. In the transmetalation depicted in Figure 3.1.9, the phosphine ligand is dissociated anyway, but the possible isomerization of the starting complex through the low energy transition state **P_Br_TS_12_Bulk** indicates that both substituents on the palladium (Ph- or Br-) can be brought *trans* to the migrating phenyl group very easily, whichever the starting structure of the catalyst is.

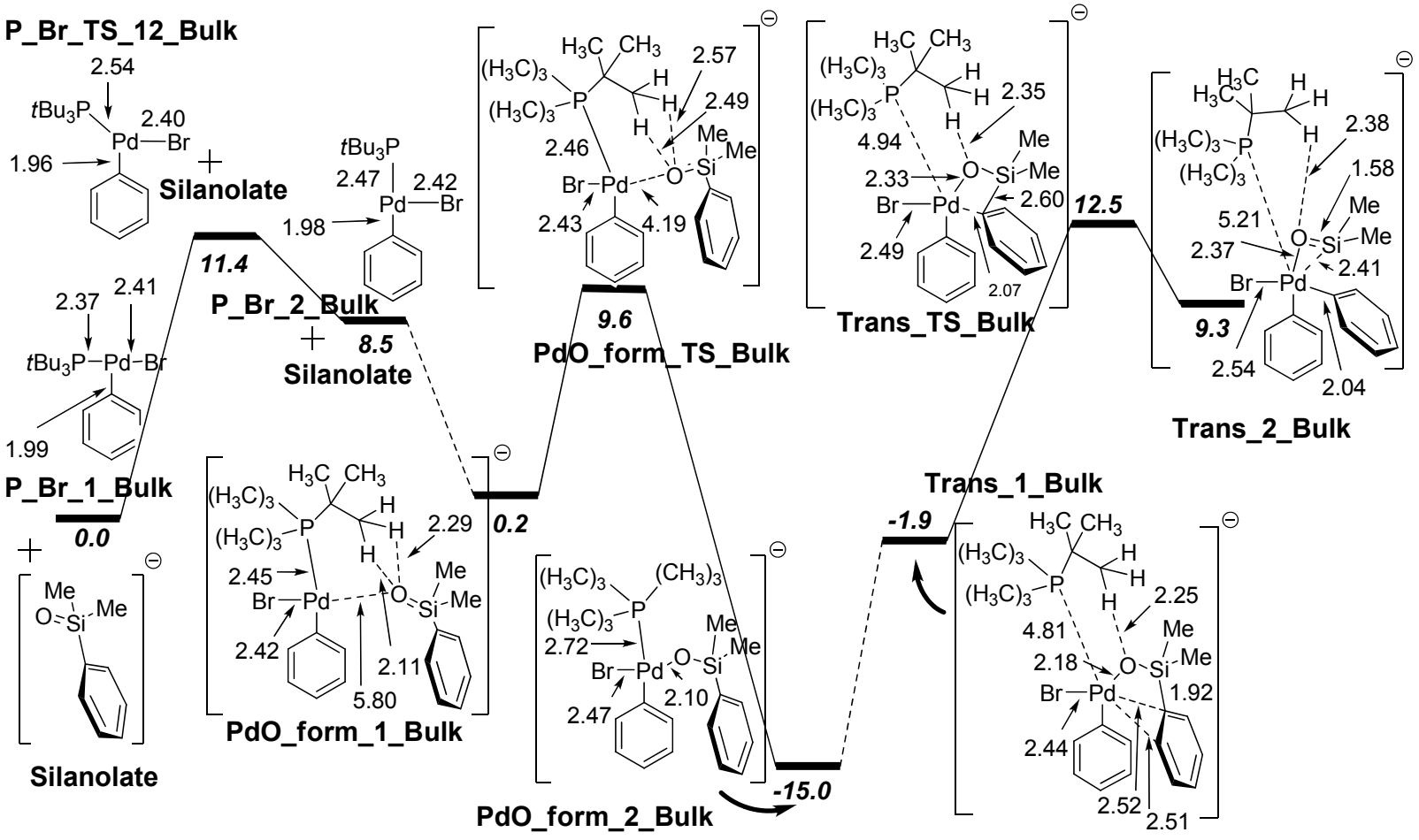

Figure 3.1.9 Free energy profile of the Pd-O bond formation and the transmetalation process, in the case of the bulky phosphine.

Table 3.1.1 Key distances of the energy profile computed with the real catalyst.

	Pd-P	P-Cα(Si)	Pd-O	Pd-Br
P_Br_1_Bulk	2.37			2.41
P_Br_TS_12_Bulk	2.54			2.40
P_Br_2_Bulk	2.47			2.42
Pd_O_form_1_Bulk	2.45		5.80	2.42
Pd_O_form_TS_Bulk	2.46		4.19	2.43
Pd_O_form_2_Bulk	2.72		2.10	2.47
Trans_1_Bulk	4.81	2.51	2.18	2.44
Trans_TS_Bulk	4.94	2.07	2.33	2.49
Trans_2_Bulk	5.21	2.04	2.37	2.54

3.1.3 Feasibility of biaryl formation from a (Ph)(R_3P)PdOSi(Me_2)Ph complex

In the previous subsection, all the complexes studied had a bromide ligand bound to the palladium, and we concluded that for the real system the transmetalation occurred after phosphine dissociation. This does not explain all available experimental reports, which point to the ability of a Pd-O-Si type complex without any bromide to undertake the transmetalation (see experiment depicted in Figure 3.1.3). In that case, no phosphine dissociation is required.[215] In the following, we will then look at the biaryl formation in systems which do not bear any bromide ligand.

3.1.3.1 Computed conformations of the (Ph)(Me_3P)PdOSi(Me_2)Ph complex

We obtained several isomers of the (Ph)(Me_3P)PdOSi(Me_2)Ph complex, whose structures are collected in Figure 3.1.10. The most stable (**Conf_1**) has the phenyl ring *trans* to the oxygen atom. There is also an η^2 interaction between the phenyl ring of the silanolate and the palladium (C-Pd distances of 2.54 Å and 2.70 Å). The phosphine group is then *trans* to the phenyl ring which has to be transferred. **Conf_2** has the silanolate group *trans* to the phosphine ligand, and the phenyl *trans* to the vacant site. It is slightly less stable, being 2.6 kcal/mol higher than **Conf_1**. In **Conf_3**, the ligands are similarly distributed around the metal center, with the exception of an η^2 interaction between the phenyl ring of the silanolate group and the palladium. **Conf_2** and **Conf_3** have very similar energies (difference of 0.8 kcal/mol). Structure **Conf_4** can be compared with **Conf_1**, but without the η^2

interaction. This interaction seems to stabilize more the complex in that case, since **Conf_4** is destabilized by 2.9 kcal/mol compared to **Conf_1**. Finally, a complex with the phenyl ring *trans* to the phosphine has been computed (**Conf_5**), and its energy is significantly higher than the others (21.1 kcal/mol higher than **Conf_1**).

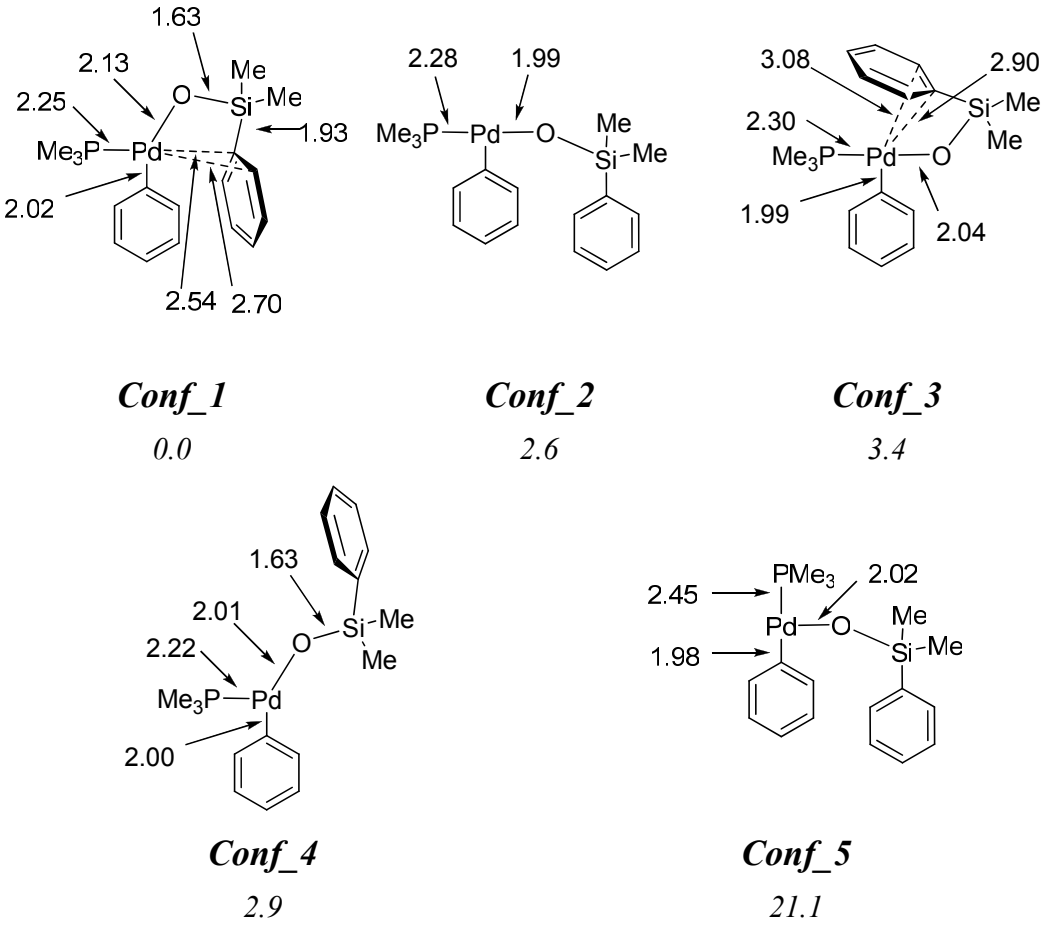

Figure 3.1.10 Computed isomers of the (Ph)(Me_3P)PdOSi(Me_2)Ph complex. Relative free energies are indicated below each structure.

In the following, we will use **Conf_1** as a starting point for the computed profiles (for the model system) and, when applicable, the energies reported will be relative to this complex.

3.1.3.2 Transmetalation mechanism

We then carried out calculations on the transmetalation step. **Conf_1** is the most stable structure and has the phosphine *trans* to the phenyl ring of the silanolate, which shows an η^2 interaction between the metal center and the ring. Logically, we first tried to compute the transmetalation process with the phenyl ring of the silanolate *trans* to the phosphine. However, no transition state could be located with **Conf_1** as a starting point, and all attempts failed to account for a phenyl

transfer from the silicon atom to the palladium. In the same lines, we did not find any minimum with the two phenyl groups in *cis* from each other. All calculations started with such structure end up to minima with similar geometries as **Conf_1**. In contrast, we obtained a transition state (depicted in the left of Figure 3.1.11) with the two phenyl groups *trans* to each other and the phosphine *trans* to the oxygen atom. Generally speaking, the transmetalation process of a cross-coupling reaction can take place from the *trans* and/or the *cis* species.[73, 226] More recently, it has been reported that no transition state for the transmetalation step could be located in a palladium catalyzed ene-yne coupling reaction, when the phosphine ligand is *trans* to the transferred group.[227]

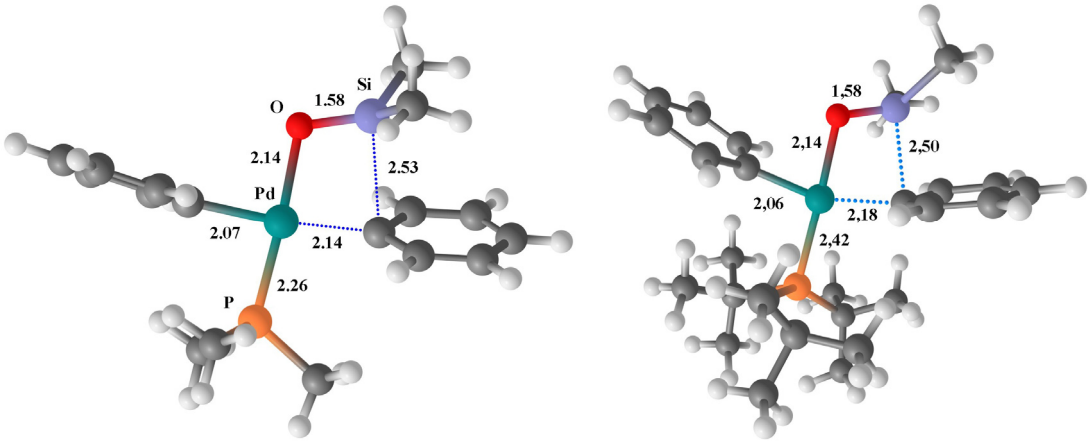

TS_trans_trans ***TS_trans_trans_bulk***

Figure 3.1.11 Transition states computed with the model (left) and the real system (right) for the transmetalation step.

The transition state **TS_trans_trans** is connected to **Conf_3** on the reactant side. The corresponding product is similar to the transition state, geometrically and energetically. In other words, **TS_trans_trans** is a very late transition state. The transition state is 31.7 kcal/mol higher than **Conf_1**. The values are collected in Table 3.1.2.

Table 3.1.2 Energetics of the transmetalation step depending on the ligand (model and real phosphine)

Ligand	TS	Product
Me_3P	31.7 [a, c]	30.6 [a, c]
tBu$_3$P	46.0 [b,c]	46.5 [b,c]
tBu$_3$P	38.8 [b,d]	37.1 [b,d]
tBu$_3$P	37.5 [b,e]	35.9 [b,e]
tBu$_3$P	40.5 [b,f]	39.0 [b,f]
tBu$_3$P	41.9 [b,g]	40.4 [b,g]

[a] Free energy relative to **Conf_1**. [b] Free energy relative to the corresponding reactant (structure similar to **Conf_4**). [c] Values obtained using the B3LYP functional (BS1), gas phase free energy. [d] Values obtained using the M06 functional (BS1), gas phase free energy. [e] Values obtained using the M06 functional (BS1), solvation free energy (SMD method). [f] Values obtained using the B97D functional (BS1), gas phase free energy. [g] Values obtained using the B97D functional (BS1), solvation free energy (SMD method).

The fact that a transition state for the transmetalation step with a phosphine ligand bound to the metal has been located is consistent with the experimental data reported regarding the zeroth-order concentration dependence for this ligand.[215] This agrees with the idea that phosphine dissociation is not required for the phenyl transfer from the silicon to the palladium. However, when computing the transmetalation with the real phosphine, the barrier increased significantly, up to 46.0 kcal/mol. In this case, the reactant resembles the structure of **Conf_4**, meaning a structure without η^2 interaction between the phenyl ring bound to the silicon and the metal center (due to steric hindrance of the phosphine), and the phenyl group bound to palladium *trans* to the vacant site. We note that the corresponding product is slightly higher than the transition state in free energy. Even if this looks counterintuitive, this can be considered as a computational artefact due to the very flat energy surface at that point, the transition state being very late, and structurally very close to the product of transmetalation. In potential energy (values not reported here), **TS_trans_trans_bulk** appears indeed around 1 kcal/mol higher than its corresponding product.

Nevertheless, the main point here is the very high energy barrier needed to reach the transition state with the real phosphine. A difference of more than 14 kcal/mol between the two systems is rather surprising. The distances around the metal center in the two transition states are pretty similar, except the Pd-P distance which is elongated by almost 0.2 Å in the case of the bulky phosphine. However, the plane formed between the palladium and the two phenyl rings is more flat in **TS_trans_trans** than in **TS_trans_trans_bulk**. The angle formed between the carbon in *para* position in the phenyl group bound to the metal (carbon at the far

left of each structures in Figure 3.1.11), the palladium, and the carbon in *para* position in the migrating phenyl group (carbon at the far right of each structures in Figure 3.1.11) is not the same in the two transition states. In the case of the model system, this angle is around 168°, when in **TS_trans_trans_bulk**, it is close to 145°. The structure in the former case is then significantly more flat than in the latter. The steric crowding induced by the methyl groups on the phosphine are most probably responsible of the distortion observed in the real system.

Regarding the energy barrier, the very high value obtained with the real system is not consistent with the experimental data indicating a transmetalation process at 100°C without requiring phosphine dissociation.[215] This discrepancy, together with the surprising difference between model and real systems led us to compute the same transition state with other DFT functionals. We thought that the weak interactions between the substituents of the bulky phosphine and the metal, but also between the substituents and the migrating phenyl, might not be properly described with the B3LYP functional. Some recent examples showed the importance of dispersion in the case of large molecules with bulky substituents.[228] For this test we used the M06 and B97D functionals which are known to account better for such weak interactions.[229] The results are also reported in Table 3.1.2, and the barriers are significantly lowered compared to the one obtained with the B3LYP functional. The barrier is reduced by almost 8 kcal/mol, at 38.8 kcal/mol in free energy relative to the corresponding Pd-O-Si type complex with M06, and at 40.5 with B97D (both free energies in gas phase). The barrier stays significantly high, but this time the value is a bit more consistent with the experimental data. The solvation calculations (SMD method) are in the same lines, and they do not significantly alter the energy barrier.

All in all, this result rather supports the ability of the Pd-O-Si type complex to undertake the transmetalation without prior phosphine dissociation. However, this process is considerably more costly (by 11 kcal/mol) than that of the process depicted in Figure 3.1.9, which describes a transmetalation with a bromide-ligated palladium after phosphine dissociation. This also suggests that bromide dissociation is required before the transmetalation from the phosphine-containing complex can take place. We recall that a transition state bearing a bulky phosphine ligand *and* a bromide could not be located in the previous subsection. In that case, the bromide was bound to the metal, and transmetalation occurred after phosphine dissociation. These results suggest that two Pd-O-Si type complexes are in equilibrium in solution. A complex with a bromide ligand obtained after phosphine dissociation such as **Trans_1_Bulk**, and a similar complex without the bromide, but with a phosphine such as **Conf_1**. Both are competent to undertake the transmetalation. The former has a rather low barrier (14.4 kcal/mol between **Trans_1_Bulk** and **Trans_TS_Bulk**) if we do not take into account the phosphine dissociation (and around 27.5 kcal/mol if we do take into account the dissociation). The latter has a barrier of more than 38 kcal/mol (more than 45 kcal/mol with B3LYP) and does not require phosphine dissociation for the transmetalation to occur.

In summary, a complex bearing both ligands (such as **Pd_O_form_2_Bulk)** is very stable. Bromide or phosphine dissociation can occur from this complex, and only after one of these dissociations the transmetalation can take place. Calculations suggest that a transmetalation starting with a bromide ligated complex is much easier than starting with a phosphine ligated complex. The barrier of the former is about 27.5 kcal/mol, when the latter is greater than 38 kcal/mol . We note that we also computed (with B3LYP, BS1) the transmetalation without any ligand on the metal center (after dissociation of the phosphine *and* the bromide, see Figure 3.1.12). The barrier between the Pd-O-Si type complex without any ligand and the corresponding transition state is as low as 5 kcal/mol. The possibility of having a "naked" palladium complex in solution in presence of many coordinating species (such as the phosphine, the halide, the solvent) is pretty low, not to say unrealistic, but this indicates that the phenyl transfer itself from the silicon atom to the palladium is a very easy process which is actually hampered by the presence of ligands on the metal center.

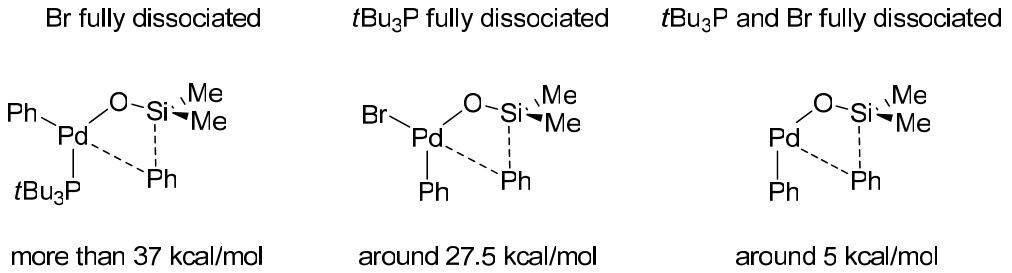

Figure 3.1.12. Comparison of the transmetalation barriers depending on the ligand located on the metal center.

In spite of the discrepancies between B3LYP and the more sophisticated functionals in this critical case, we decided to continue our study using this functional. Since we focus on the feasibility of mechanisms, and the relative barriers obtained between each others, we will stick with B3LYP. Moreover, we do not expect the dispersion interactions to be too critical in the majority of our mechanisms.

The barrier for the transmetalation step through **TS_trans_trans_bulk** is broadly consistent with a reaction requiring high temperatures (100°C when heating the independently synthetized "Pd-O-Si" type complex). However, a barrier of 38.8 kcal/mol (46.0 with B3LYP) is likely too high to account for the great majority of the reactions experimentally described. Indeed, getting the biaryl product does not require very harsh conditions especially not when the reaction is performed in a classical way, meaning starting from the palladium catalyst, the silanolate and the aryl halide. In such cases (aromatic silanolates cross-coupling with aromatic halide), typical reaction temperatures are around 70° or 90°C. In the following, we will then look for an alternative mechanism which could have a smaller barrier than the classical transmetalation.

3.1.3.3 Carbometalation mechanism

We first envisioned a carbometalation-like mechanism. A carbometalation is a nucleophilic addition of an organometallic reagent to an alkene or an alkyne. Its schematic representation is depicted in Figure 3.1.13. The biaryl formation from the (Ph)(R_3P)PdOSi(Me_2)Ph complex could be conceived as the attack of the palladium to the double bond of the aromatic ring vicinal to the C(aromatic)-Si bond, in a kind of intramolecular carbometalation.

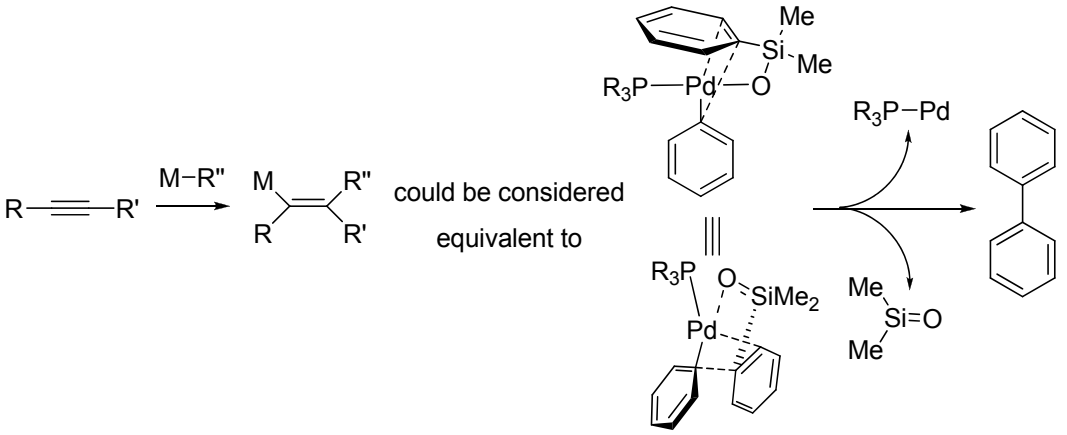

Figure 3.1.13 Schematic representation of a carbometalation mechanism on the (Ph)(R_3P)PdOSi(Me_2)Ph complex.

We located some transition states corresponding to such a process. All are very high in energy. Three of them are reproduced in Figure 3.1.14. **Carbom_TS1** lies 63.9 kcal/mol higher in free energy than **Conf_1**. **Carbom_TS2** and **Carbom_TS3** are even higher, at 72.6 and 69.2 kcal/mol respectively.

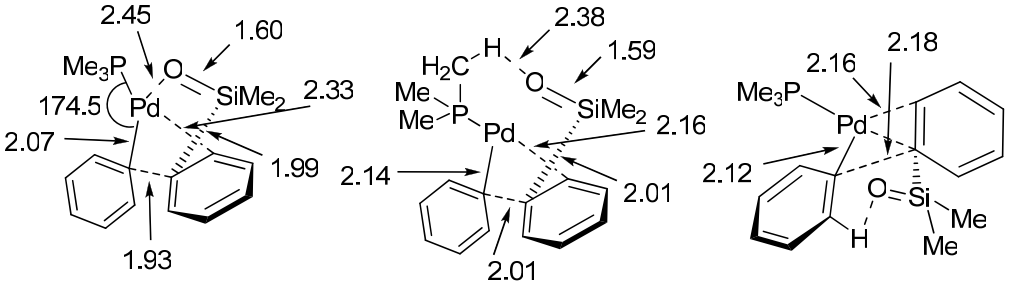

Figure 3.1.14 Computed transition states for a carbometalation process for the (Ph)(Me_3P)PdOSi(Me_2)Ph complex.

The arrangement of the ligands is different in these three transition states. However, these structures share similar geometrical features around the palladium center. They can all be viewed as a four-membered ring metallacycle between the

palladium, the alpha carbon of the phenyl ring bound to the palladium, and the alpha and beta carbons of the phenyl ring of the silanolate backbone. All these four bond distances are broadly similar. For instance, in **carbom_TS2**, Pd-C(α) = 2.14 Å, Pd-C(Ph_sil-β) = 2.16 Å, and C(α)-C(Ph_sil-α) = 2.01 Å.

The carbometalation-like process does not seem to be a feasible mechanistic pathway for the biaryl formation for this system. The very high barriers of the process (almost the double compared to the one obtained for a classical transmetalation) allow us to confidently discard this possibility.

3.1.3.4 Rearrangement of the (Ph)(R_3P)PdOSi(Me_2)Ph complex

In the next attempt, we imagined the rearrangement of the Pd-O-Si type complex. We tried to assess the possibility for the Pd-O-Si linkage containing complex to rearrange towards a "Pd-Si-O" type complex. As depicted in Figure 3.1.15, we go from complex (Ph^1)(L)PdOSi(Me_2)Ph^2 (labelled as **switch_1** in Figure 3.1.15) to (Ph^2)(L)PdSi(Me_2)OPh^1 (labelled as **switch_4**). Note that this process has been computed with Me_3P- and *t*Bu_3P- (this last case is reproduced in Figure 3.1.15). No significant differences were observed between these two systems.
The first step is the Pd-O bond formation through the transition state **switch_TS12** which lies 20.2 kcal/mol higher than **switch_1**. A PhSi(Me_2)OPh complex with a weak interaction between the palladium and the oxygen atom is generated (**switch_2)**. The phosphine is still bound to the metal. Such interaction is expected to be in equilibrium with complexes such as **switch_3** which shows an interaction between the metal and the phenyl ring. The transition state between **switch_2** and **switch_3** has not been computed, but the barrier should be low. Then, a C-Si bond cleavage takes place concomitantly with C-Pd and Pd-Si bond formations. A three membered-ring transition state was located with a reasonable barrier (around 16.6 kcal/mol). We end up with a Pd-Si-O linkage containing complex which is slightly stabilized compared to the Pd-O-Si type complex (by 6.1 kcal/mol in free energy). In summary, the phenyl group bound to the silicon in **switch_1** (in red in Figure 3.1.15) migrates to the metal center, and the phenyl previously bound to the palladium is then bound to the oxygen in **switch_4**. Note that **switch_1** is very similar structurally and energetically (for the process computed with the model system) to **Conf_2** (phenyl group *trans* to the vacant site and no η^2 interaction between the phenyl ring bound to the silicon atom and the metal center). The whole exchange process appears to be feasible (highest energy barrier around 20 kcal/mol) under the experimental conditions.

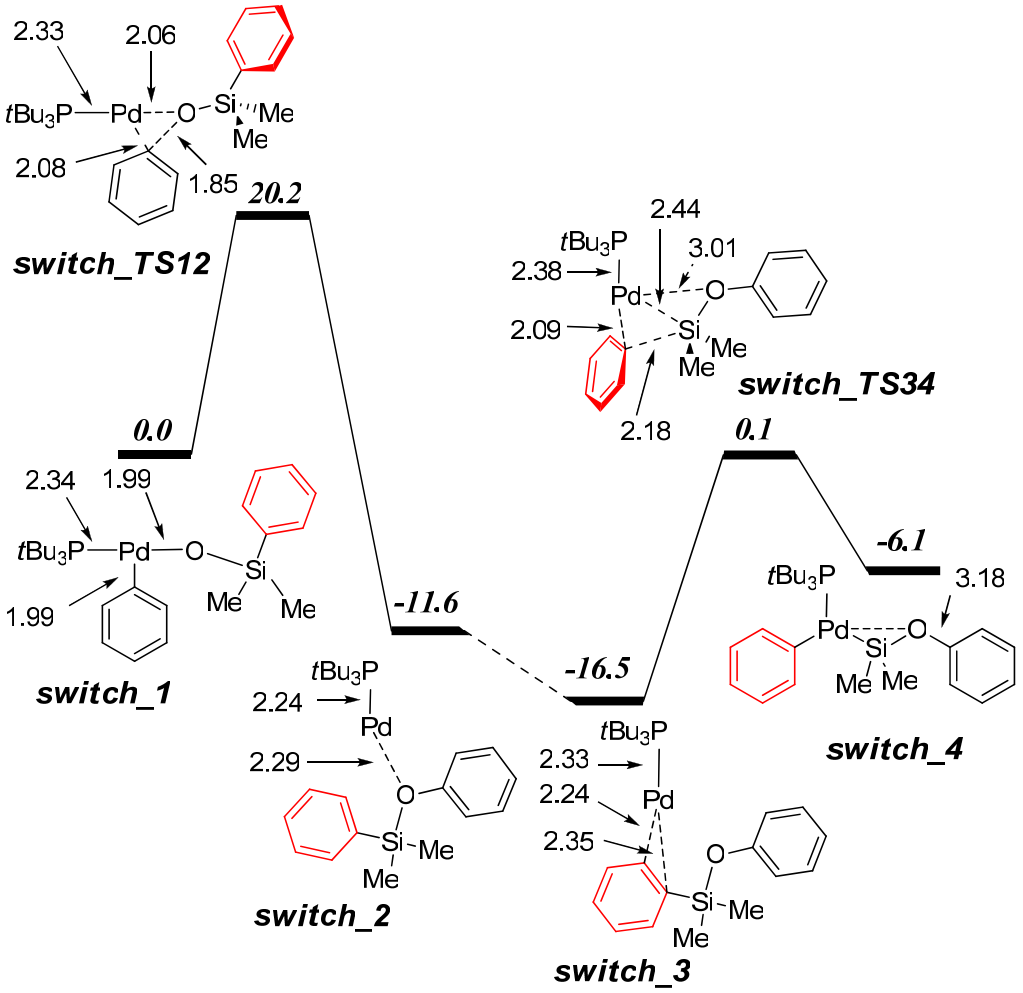

Figure 3.1.15 Rearrangement of the Pd-O-Si linkage containing complex towards a "Pd-Si-O" type complex. Free energy values in kcal/mol.

The following step would be the migration of the phenyl group Ph[1] towards the palladium or, in other words, a transmetalation process starting with a Pd-Si-O type complex (**switch_4)**. Intuitively, we thought that the transmetalation would be easier in this case because breaking of the O-C bond to afford the transmetalation product should be easier than the breaking of the Si-C bond previously envisioned. Unfortunately, despite much effort, we did not succeed in finding a reasonable barrier for the subsequent step. As an example, we show the transition state for the phenyl transfer from the oxygen atom to the palladium in Figure 3.1.16. This transition state lies 83.3 kcal/mol higher than **switch_1** (in free energy).

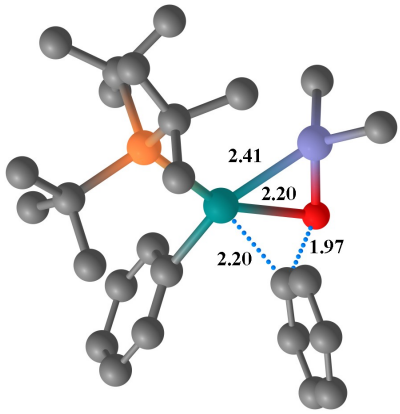

Trans_Pd_Si_O

Figure 3.1.16 Transition state for the phenyl transfer from the oxygen of the Pd-Si-O linkage to the palladium. All hydrogen atoms were removed for clarity.

3.1.3.5 Reductive elimination

Subsequent isomerization of **Prod_trans_trans_bulk** (minimum connected to **TS_trans_trans_bulk**) is expected in order to bring the two phenyl rings in *cis* to allow the reductive elimination. Such a process was found difficult to compute because further recombination of the $Me_2Si{=}O$ unit is very likely once the **Prod_trans_trans_bulk** complex is formed. More importantly, we were unable to locate any minimum with the two phenyl rings in *cis*, together with the phosphine and the $Me_2Si{=}O$ unit. All our attempts converged to **Conf_1** or similar structures. This strongly suggests that one of the two groups (phosphine or $Me_2Si{=}O$ unit) must leave the metal coordination sphere to allow the reductive elimination.

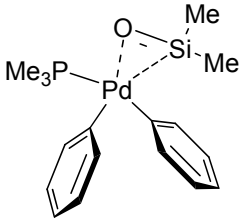

not obtained

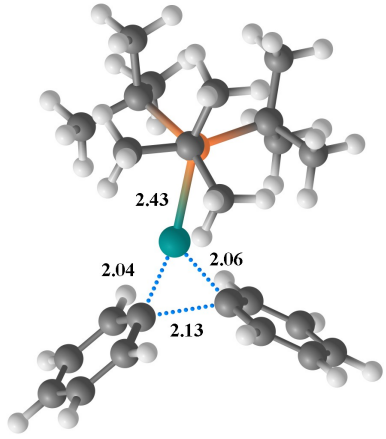

Ph_cis ***Bulk_Red_Elim***

Figure 3.1.17 Putative intermediate with the two phenyl groups in *cis* (left) and transition state (right) of the reductive elimination process with the bulky phosphine.

The barrier for the reductive elimination process itself is, as expected, very low.[102] The transition state **Bulk_Red_Elim** depicted in Figure 3.1.17 is 4.6 kcal/mol higher in energy than the connected reactant.

3.1.4 Feasibility of biaryl formation from a bisphosphine ligated Pd-O-Si type complex

In the previous subsection, we computed tBu$_3$P as a phosphine ligand, which is the most efficient phosphine for the catalytic cross-coupling of aromatic and heteroaromatic silanolates with aromatic (and heteroaromatic) halides.[219] This is also the phosphine used to run the kinetic experiments.[215] This phosphine appears to be very efficient, and a Pd-O-Si type complex bearing this ligand was detected in the reaction media.[215] Nonetheless, it came to our attention that in this case, the biaryl formation occurred in the presence of other reagents, such as the silanolate salt and the aryl bromide. As stated in the 2010 JACS paper,[215] "Simply heating complex **5** (formed in situ) in toluene at 50 °C resulted in the formation of the biaryl product in 80−90% yields with concomitant formation of PdL$_2$." Complex **5** ((Ph)(tBu$_3$P)PdOSi(Me$_2$)Ph) was then formed in situ (and X-Ray analysis could be performed) and heated in presence of other reagents still in the reaction media. It is not explicitly reported that the Pd-O-Si type complex **5** was independently synthetized and that it afforded the biaryl product. In consequence, it is not totally clear if the biaryl formation occurs from the Pd-O-Si type complex bearing the tBu$_3$P phosphine ligand, or if other species could be involved in the process (but keeping at the same time the mechanism non-activated, meaning without involvement of a pentacoordinate silicon atom). In contrast, the ability of another Pd-O-Si type complex, this time bearing the PPh$_2$CH$_2$CH$_2$CH$_2$Ph$_2$P ligand instead of tBu$_3$P, was unambiguously demonstrated. A simple heating to 100 °C afforded the biaryl product in that case.[88, 230] Therefore, we decided to compute the transmetalation process using the PPh$_2$CH$_2$CH$_2$CH$_2$Ph$_2$P ligand in order to assess the role of the phosphine on the reaction barrier. The transition state (**TS_trans_trans_biphos**) is depicted in Figure 3.1.18, and the energy is reported in Table 3.1.3, together with that obtained with the monophosphine ligand. The transition state lies 30.1 kcal/mol higher in energy that the corresponding reactant (Pd-O-Si type complex with the two phenyl ligands *trans* to each other), which is 15 kcal/mol lower than the value obtained with tBu$_3$P.

Remarkably, the C-Pd-C angle (formed between the carbon in *para* position of the phenyl group bound to the metal (carbon at the far left in Figure 3.1.18), the palladium, and the carbon in *para* position of the migrating phenyl group (carbon at the far right in Figure 3.1.18)) is around 165°, which is close to the value found for **TS_trans_trans**, (transition state for transmetalation computed with the model system). It is less acute than the angle found for the real system bearing a monophosphine (C-Pd-C angle of 145°, see sub-subsection 3.1.3.2). The distortion induced by the tBu$_3$P ligand is thus not observed with this bisphosphine ligand. It is interesting to note that the energy barrier for the bisphosphine is very similar to that of the model system (with PMe$_3$ as the computed ligand). There is therefore a

correlation between the geometrical distortion of the system and the energy barrier of the transmetalation. The energy barrier obtained for the real system bearing the *t*Bu$_3$P ligand is 15 kcal/mol higher than with the model phosphine or the bisphosphine.

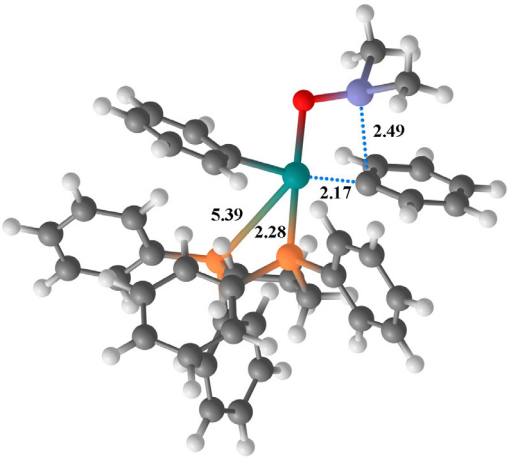

TS_trans_trans_biphos

Figure 3.1.18 Transition state for the transmetalation starting with a Pd-O-Si type complex bearing a bidentate phosphine.

Table 3.1.3. Free energy barrier (gas phase) in kcal/mol of the transmetalation process bearing two different phosphine ligands. Values are relative to their respective Pd-O-Si type complexes.

Phosphine ligand	Transition state
$PPh_2CH_2CH_2CH_2Ph_2P$	30.1
*t*Bu$_3$P	46.0

We note that a conformational analysis should be undertaken due to the high flexibility of the phenyl rings of the ligand. One of the two phosphine arms is clearly dissociated, being 5.39 Å away from the metal center. The barrier could be slightly lowered if a more favourable conformation can be found. However, the barrier found is already in agreement with the experimental data which report a transmetalation from a Pd-O-Si type complex bearing a bidentate phosphine under heating of 100°C.[88, 230]

These results also suggest that the mechanism of the transmetalation might be different between the two systems differing only with the phosphine ligand attached to the palladium.

3.1.5 Concluding remarks

We rationalized the non activated intramolecular cross-coupling of aryl silanolates with aryl halides. A transmetalation mechanism is possible starting with a "Pd-O-Si" type complex, if the two phenyl groups are *trans* to each other. The high barrier found for this mechanism makes the phosphine dissociation probable. When the normal reaction conditions apply (starting from a Pd(0) or a Pd(II) catalyst), our results suggest than the transmetalation is easier after phosphine dissociation, and in presence of the bromide ligand on the palladium. These results are in line with the recent results of Hartwig, where they isolated some "ligandless" palladium catalysts, where the halide is crucial for the reactivity.[231, 232] Changing the phosphine ligand is critical regarding the transmetalation mechanism. The bisphosphine ligand computed induced less geometrical distortion of the transition state structure than when the tBu$_3$P ligand is used, and the barrier of transmetalation is consequently much lower.

We also showed the importance of the ligand arrangement around the metal center. Two forms of the T-shaped catalyst were found competent (the ground state structure **P_Br_1_Bulk**, but also **P_Br_2_Bulk**) for the transmetalation. The model phosphine and the real phosphine give very different results. Introducing the bulky groups on the tBu$_3$P phosphine appeared crucial. The substituents groups on the phosphine have an influence on both the Pd-O bond formation and transmetalation. The first process is hindered by the bulkiness of the methyl groups, and the latter is facilitated by dissociation of the phosphine.

In the following section, we will study the role of activating molecules on these mechanisms.

3.2 Activated mechanism

The main aim of this section is the investigation of the activated mechanism in the cross-coupling of silanolates. Two other topics will be tackled in this section: the role of dibenzylideneacetone (dba), and the selectivity issues in the coupling of crotyl silanolates.

As stressed in the introductory paragraph of this chapter, the cross-coupling of silanolate salts with halide compounds can be achieved through a thermal, intramolecular, and non-activated mechanism. In the previous section, we developed computationally the feasibility of this hypothesis. Nevertheless, it has been recently proved that an activated mechanism could be also operative for this coupling depending on the experimental conditions used.[215] Significantly higher kinetic rates were obtained in some of the cases where an activated mechanism is suspected (for instance in presence of an excess of silanolate salt in the reaction media). By activated, we mean that a pentavalent silanolate is involved at some stage during the mechanism (see Figure 3.2.1 below). This is reminiscent of the mechanism proposed by Hiyama, which required a hypervalent silicon atom (see

Figure 3.1.2). This can be in principle achieved through the intervention of another molecule (ligand, solvent, siloxane released in the reaction media), or by an excess of the silanolate salt. In any case, this mechanism will convert this process to an intermolecular reaction. In this section, we will study this so-called activated mechanism.

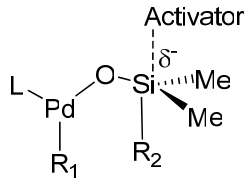

Figure 3.2.1. Schematic representation of an activated Pd-O-Si type complex.

Along these lines, the intriguing role of dibenzylideneacetone (dba) on the coupling will also be taken into account. Dba is a π-olefinic ligand (see subsection 1.2.3 in chapter 1), and as such, its effect is viewed as that of an a olefinic ligand. We will take advantage of this study on the activated mechanism to investigate in more detail the role of dba on the transmetalation step. Dba is an efficient pre-catalyst and/or ligand in the case of the cross-coupling of aryl halides with allylic[218] and heterocyclic[233] silanolate salts. It shows some positive effects in some cases when using alkenyl silanolates.[216]

Among the available allylation methods available for the chemist, the cross-coupling of aryl halides with allylic compounds catalyzed by a late transition metal has been found very efficient. The reaction of aryl halides with allyl silanolates has been recently developed,[218, 234] and we present here a computational study of these developments. The coupling can be achieved through the competitive α- and γ-positions. Indeed, depending on the reaction conditions, the catalyst, and the starting reagents used, selective α- or γ- couplings can be obtained. In our case, the γ-selectivity is typically obtained in fairly good yields. The introduction of the methyl group at the γ carbon of the silanolate will allow treatment of the Z/E configurational issue.

The activated mechanism being the guiding line of the whole section, we will first treat the cross-coupling of allylic and heterocyclic silanolates with aryl halides in an activated mechanistic perspective (sub-sections 3.2.2, 3.2.3, 3.2.4). Following this approach, the particular role of dba will be investigated. Selectivity issues (regio- and stereo-selectivity) of the coupling of crotyl silanolates will be explored (sub-section 3.2.3). Finally, the role of an excess of silanolate salt in the reaction media will be studied, and the effect of the released dimeric siloxane discussed (sub-sections 3.2.5 and 3.2.6).

3.2.1 Computational methods

This section was computed by means of DFT methods (Gaussian 03[163] and Gaussian09[178] suite of programs), using the B3LYP formalism[127, 132] and the SDD pseudo-potential and its associated basis set[179] for palladium and the 6-31G(d) basis for the other atoms (BS1).[167, 168] In the cases where the molecule is anionic, a diffuse function was added (e.g. atoms were described with 6-31+G(d)) (BS2).[224] Direct comparison of energy values obtained with BS1 and BS2 is not strictly correct, but is indicative of the pathways followed. The nature of each optimized minimum was characterized by means of a vibrational analysis. All transition states computed have only one imaginary frequency, and were connected to the corresponding minima. All reported values are free energy values, except otherwise stated in the text. Solvation was not taken into account. Energy values are all expressed in kcal/mol, and distances in angstrom. Charged complexes are represented between brackets.

3.2.2 Transmetalation step for the coupling of crotyl silanolates

Figure 3.2.2 shows three isomers of the Pd-O-Si type complex obtained after Pd-O bond formation between the 2-butenyldimetylsilanolate and an aryl halide palladium catalyst. On the left side, the ligand-free structures are shown, and on the right side are depicted the complexes which have a molecule of dba ligated to the metal center through the double bond. The relative free energies are reported below each complex. We collect only the structures with the double bond of the alkyl chain of the silanolate in the Z configuration. **free_crot_1** shows the phenyl group *trans* to the oxygen of the silanolate, and the double bond of the silanolate alkyl chain *trans* to the vacant site. The arrangement of ligands is similar to the one adopted in **Conf_1** (see Figure 3.1.10) but without the phosphine. The other conformer showed is **free_crot_2** which has no η^2-interaction between the double bond and the metal center. This complex is highly unstable and lies 15.0 kcal/mol higher than **free_crot_1**. This is not surprising due to the fact that the former is a well-defined T-shaped complex, when the latter has the palladium poorly coordinated. The energy gap between the two corresponding dba-coordinated structure (**dba_crot_1** and **dba_crot_2**) is much lower, with very similar free energies. Both structures have a square planar geometry, and the various *trans* influence of the ligands make the relative energy of these two complexes close. To be exhaustive, we also computed **free_crot_3**, with the phenyl group *trans* to the double bond. The free energy is 4.2 kcal/mol higher than the most stable complex, and the ligated species is also marginally destabilized compared to **dba_crot_1** and **dba_crot_2**.

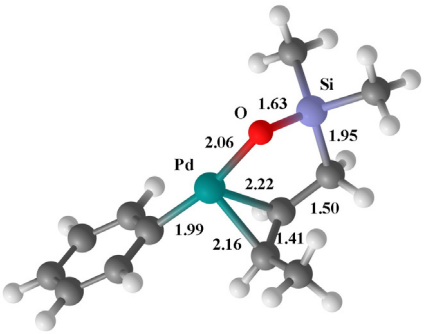

free_crot_1
0.0

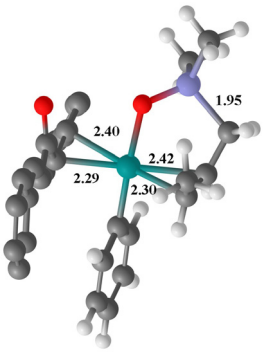

dba_crot_1
0.0

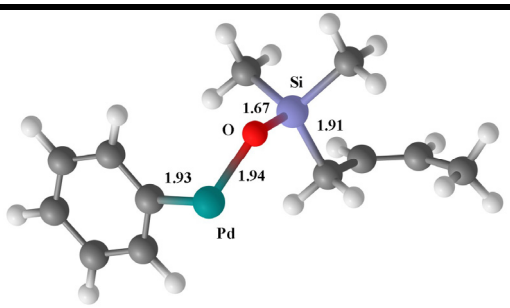

free_crot_2
15.0

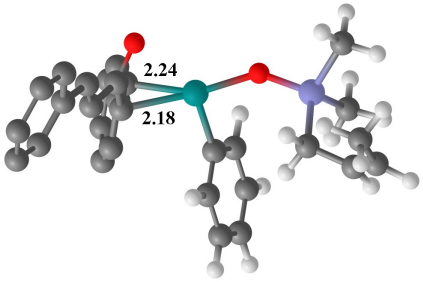

dba_crot_2
-0.7

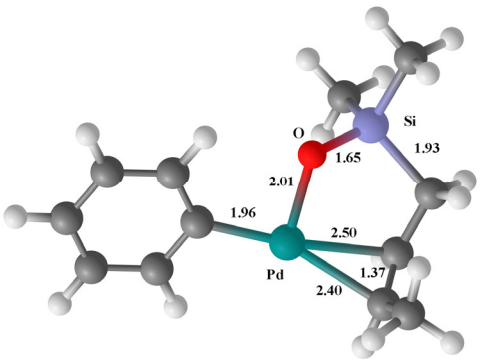

free_crot_3
4.2

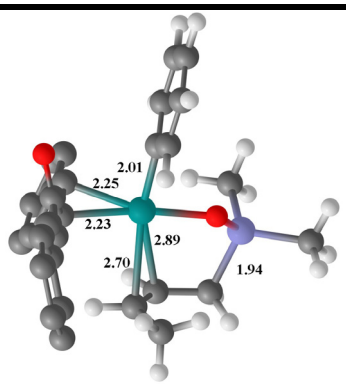

dba_crot_3
1.2

Figure 3.2.2. Computed isomers of the complex PhPd(OSi(Me_2)CH_2CHCHCH$_3$). Free energies relative to **free_crot_1** for the ligand free complexes (left side), and relative to **dba_crot_1** for the ligated ones (right side). Hydrogen atoms on dba were removed for clarity.

In the following, we will use **free_crot_1** as the starting complex for the profiles involving a crotyl group. The separated reactants will then be this complex plus a molecule of dba.

*3.2.2.1 Dibenzylideneacetone-assisted transmetalation of **dba_crot_1***

In this sub-subsection, we study the role of the olefin-ligated palladium pre-catalyst $Pd(dba_2)$ (sometimes used through the form $Pd_2(dba_3)$). We will focus on the effect of the dibenzylideneacetone (dba) ligand on the transmetalation step. Figure 3.2.3 depicts the whole profile.

We start the profile with the η^2-ligated complex **dba_crot_1**. The ligands around the palladium coordination sphere are the aryl, the oxygen atom coming from the silanolate salt, the double bond of the alkyl chain of the silanolate, and one of the double bond of dba. We then found a transition state (**all_dba_TS12**) where the carbonyl of dba attacks the Si=O unit of the silanolate, which gives the four-membered ring complex **all_dba_2**. In that particular structure, the silicon atom is pentavalent and is part of the four-membered ring formed between the carbonyl of dba and the Si=O unit of the silanolate. This intermediate is rather unstable, lying 17.8 kcal/mol higher than the separated reactants. The following transition state (**all_dba_TS23**), which is only 1 kcal/mol higher in energy, shows the cleavage of the Si-C bond. Finally, the last transition state (**all_dba_TS34**) corresponds to the cleavage of one of the C-O bond and thus allows the ring to open and generate a silicon analogue of a carboxylic acid. In this structure (**all_dba_4**), the oxygen atom is 2.11 Å away from the palladium. The whole profile is slightly exothermic (**all_dba_4** is 0.6 kcal/mol lower than the separated reactants) and the highest barrier is about 25.3 kcal/mol. This is largely feasible considering the experimental conditions encountered in the coupling with dibenzylideneacetone (temperature around 50-70°C). Table 3.2.1 shows in more detail the energetics of this profile, in order to compare the potential energies, the ZPE energies, and the free energies. No significant differences are found between the three. Though, **all_dba_TS12** lies 25.3 kcal/mol higher than the separated reactants in free energy, which is around 4 kcal/mol higher than the other two parameters.

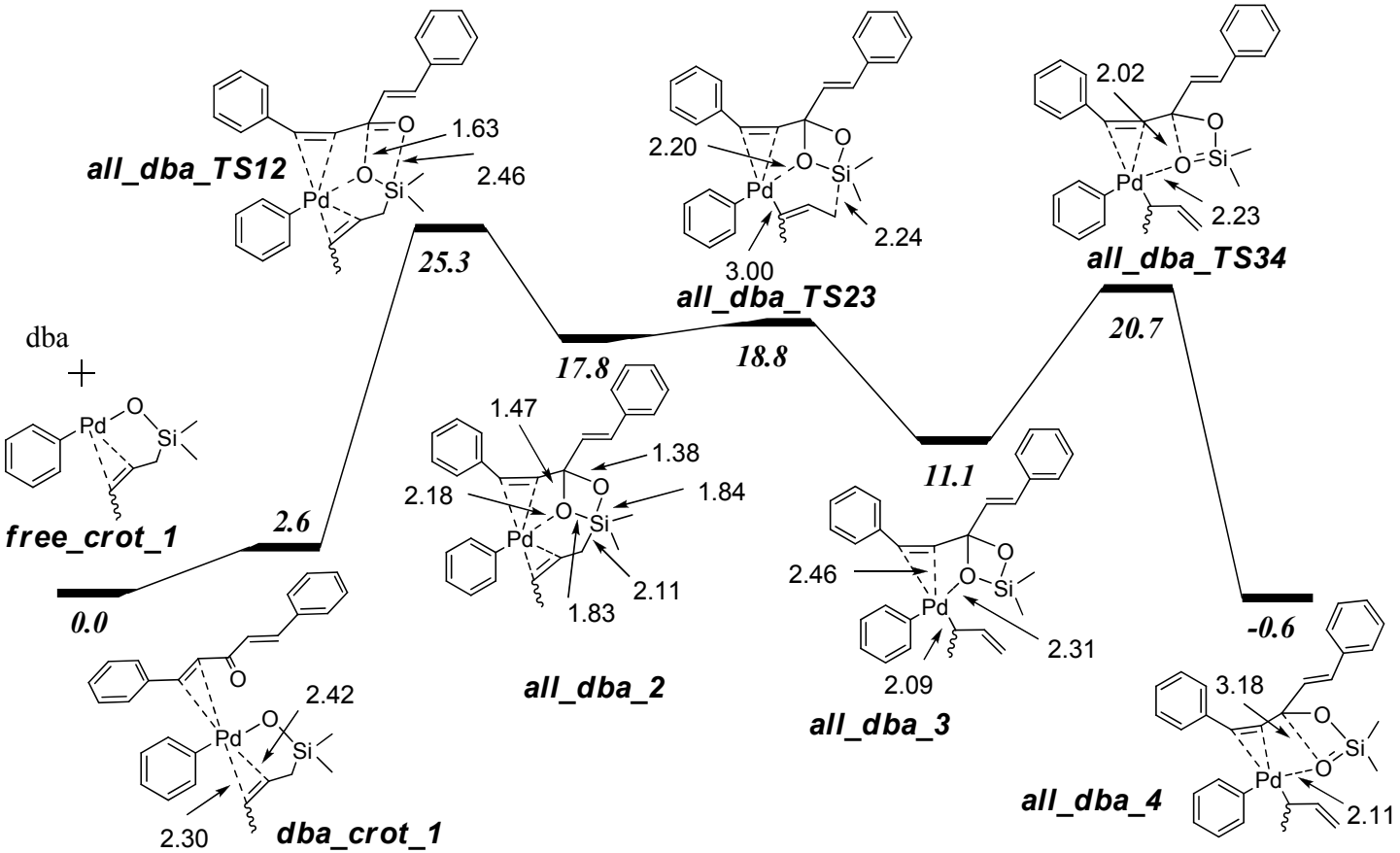

Figure 3.2.3 Dba-assisted transmetalation step of **free_crot_1**. Free energy values in kcal/mol. Double bond in Z configuration.

Table 3.2.1 Computed energy values (potential energy, ZPE corrected energy, and free energy) for the dba-assisted transmetalation step of a Pd-O-Si type complex generated from a crotyl silanolate and an aryl halide. Comparison between Z- and E-silanolates.

	Potential energy		ZPE energy		Free energy	
	Z[a]	E[b]	Z[a]	E[b]	Z[a]	E[b]
all_dba_1	-13.0	-12.1	-11.8	-11.1	2.6	2.1
all_dba_TS12	8.5	9.6	9.2	10.2	25.3	25.7
all_dba_2	1.1	1.9	2.4	3.3	17.8	18.8
all_dba_TS23	1.2	2.0	2.4	3.1	18.8	18.9
all_dba_3	-3.5	-3.1	-2.7	-2.5	11.1	10.4
all_dba_TS34	5.7	5.7	5.8	5.4	20.7	18.6
all_dba_4	-16.5	-18.6	-15.4	17.7	-0.6	-4.6

[a] Double bond in the Z configuration. [b] Double bond in the E configuration.

We also computed the dba-assisted transmetalation using a starting complex generated from an aryl halide and a (E)-2-butenyldimethylsilanolate (similar to **all_dba_1** but with the double bond in the E configuration). The γ-selectivity experimentally observed when using this silanolate geometry is usually slightly higher. As it can be seen in Table 3.2.1, the energy values for the transition states and the intermediates are very similar for both silanolate geometries, with differences around 1 kcal/mol or less. However, the last transition state corresponding to the opening of the four-membered ring is 2.1 kcal/mol lower in the case of the (E)-silanolate (in free energy), and the final product is significantly more stable by 4 kcal/mol. This difference follows the experimental trend. However, since the barriers for the rate determining transition state (**all_dba_TS12**) are very similar in both cases (E and Z configuration), the explanation of experiment is not satisfactory at this point.

The main point here is the key role of the carbonyl of dba in the transmetalation step. As we emphasized in Chapter 1, dibenzylideneacetone is widely considered as a π-olefinic ligand.[235] In our case, we have an active role of the carbonyl of dba in the reaction. The carbonyl assists the transmetalation, facilitating the cleavage of the Si-C bond of the silanolate part. Nevertheless, the double bond of dba stays bound to the metal center along the profile. Indeed, in all the structures depicted in Figure 3.2.3, there is free space for the double bond to bound the palladium, without distorting too much the dba molecule during the transmetalation process. To assess the olefinic character of the ligand, we computed a range of dba-type ligands (depicted in Figure 3.2.4.) which were previously studied in various coupling reactions. We decided to compute 4,4'-(trifluoromethyl)benzylideneacetone (**dba_F**), 4,4'-(methoxy)benzylideneacetone (**dba_MeO**), and 2,2'-(dinitro)benzylideneacetone (**dba_NO_2**).[235] The transmetalation step was then recomputed for these three ligands and we collected the results in Table 3.2.2. The strength of the interaction between dba and the metal

is different when the substituents in the aryl ring change. It has been found that in the Suzuki-Miyaura coupling, electron donating substituents on the ligand improve the reaction yield.[236] On the opposite, electron withdrawing groups were generally associated with poor outcomes. The reason for this is not clear, because alkene ligands can affect the reaction during all the steps of the coupling (oxidative addition, transmetalation, reductive elimination) and this is hard to follow along the whole process. However, it has been established that such π-olefinic ligands disfavour the rate of the oxidative addition step, and enhanced the reactivity of the complexes during the reduction elimination. Regarding the transmetalation step, the exact role of the olefinic ligand is broadly unknown (see Chapter 1). Concerning the coupling of allyl silanolates, it has been found experimentally that increasing the π-acidity of dba affords improved the γ-selectivity. Similarly, the use of 4,4'-(trifluoromethyl)benzylideneacetone revealed compulsory for the coupling of α-substituted allylic silanolates.[218]

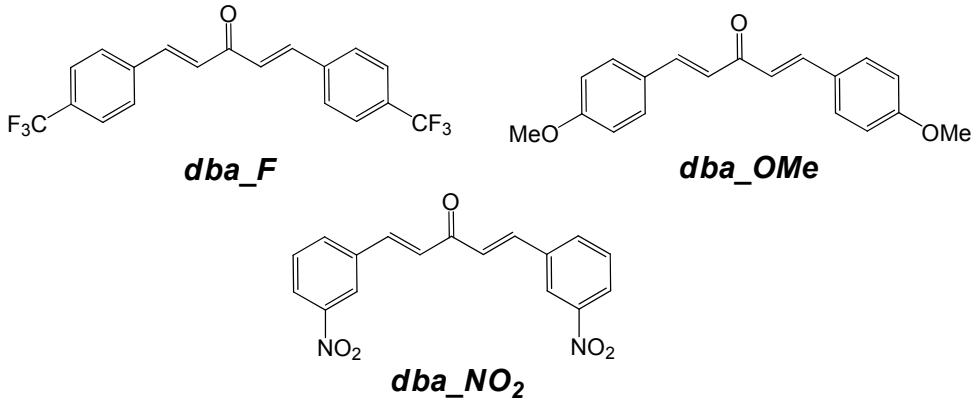

Figure 3.2.4. Structures of the dba-based ligands studied.

Table 3.2.2. Influence of the substituent using various dba-based ligands on the energy barriers of the transmetalation step of the cross-coupling of silanolates. Free energy values compared to each respective reactants (**free_crot_1** complex and corresponding dba-like ligand). Double bond in Z configuration.

	dba_NO_2	dba_F	dba_MeO
all_dba_1	2.0	4.8	1.3
all_dba_TS12	22.9	24.3	25.0
all_dba_2	16.9	18.5	18.8
all_dba_TS23	17.5	18.9	18.9
all_dba_3	10.4	11.2	11.8
all_dba_TS34	21.2	22.3	19.1
all_dba_4	-0.3	-0.0	-1.4

The values for the three ligands are broadly similar and no differences in the mechanism are found when varying the substituents on dba. However, we note that the energy barrier of the first step (formation of the four-membered ring, see Figure

3.2.3) is the lowest with **dba_NO$_2$**, and the highest using the electron donating **dba_MeO**. Experimentally, **dba_F** afforded better γ-selectivity, and this is not translated in the barriers of the transmetalation step. This is not surprising since, as we stressed before, the dba ligand (and then its substituents) could influence the reaction along the whole profile, and looking only at this step is not enough to rationalize the experimental observations on the selectivity. Nevertheless, what we wanted to show here is that the substituent on the aryl *does* have an effect on the transmetalation step. Then, even if the mechanism found for this step features mainly the carbonyl group, the dba-based ligand keeps its olefinic character.

3.2.2.2 Dba-assisted transmetalation through weak carbonyl interactions

We also considered the possible coordination of dba to the palladium through the carbonyl. Figure 3.2.5 depicts the transmetalation step when the silicon-carbon bond cleavage is not actively assisted by dba. The ligand is only spectator in this case, and weak hydrogen interactions take place between the oxygen atoms and the metal center (2.17 Å in **dba_O_1**) and one hydrogen of dba (1.98 Å in **dba_O_1**). The reaction barrier is here 7.2 kcal/mol higher in energy than when dba is actively involved in the transmetalation through its carbonyl, as reported in Figure 3.2.3.

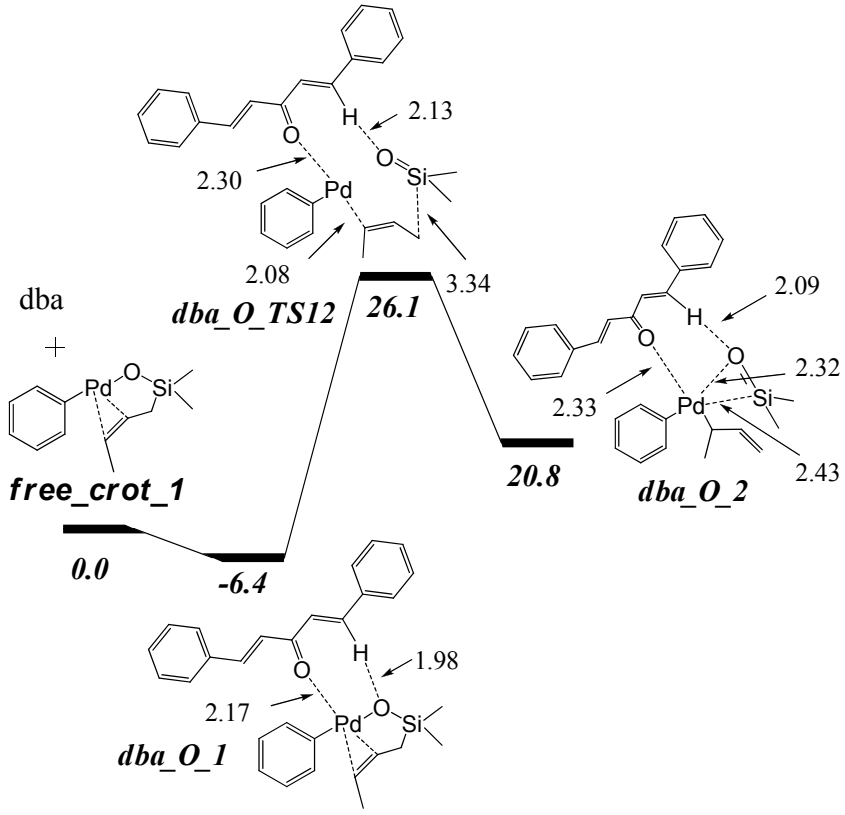

Figure 3.2.5 Transmetalation step of **free_crot_1** supported by weak interactions with dba. Free energy values in kcal/mol.

3.2.2.3 Benzoquinone-assisted transmetalation

We then computed the same profile using 1,4-benzoquinone instead of dba. This ligand gave very good selectivity (with a γ:α ratio as good as 61:1), but the yields were poorer than when using dba. The profile depicted in Figure 3.2.6 shows lower barriers than with dba (highest barrier around 20 kcal/mol), and the process is slightly endothermic. We note that the Si-C bond cleavage is concomitant with the four-membered ring formation. The disappearance of the barrier is not surprising since in the profile depicted in Figure 3.2.3, the silicon-carbon bond cleavage was a very easy process. The double bond of benzoquinone stays equally bound along the process.

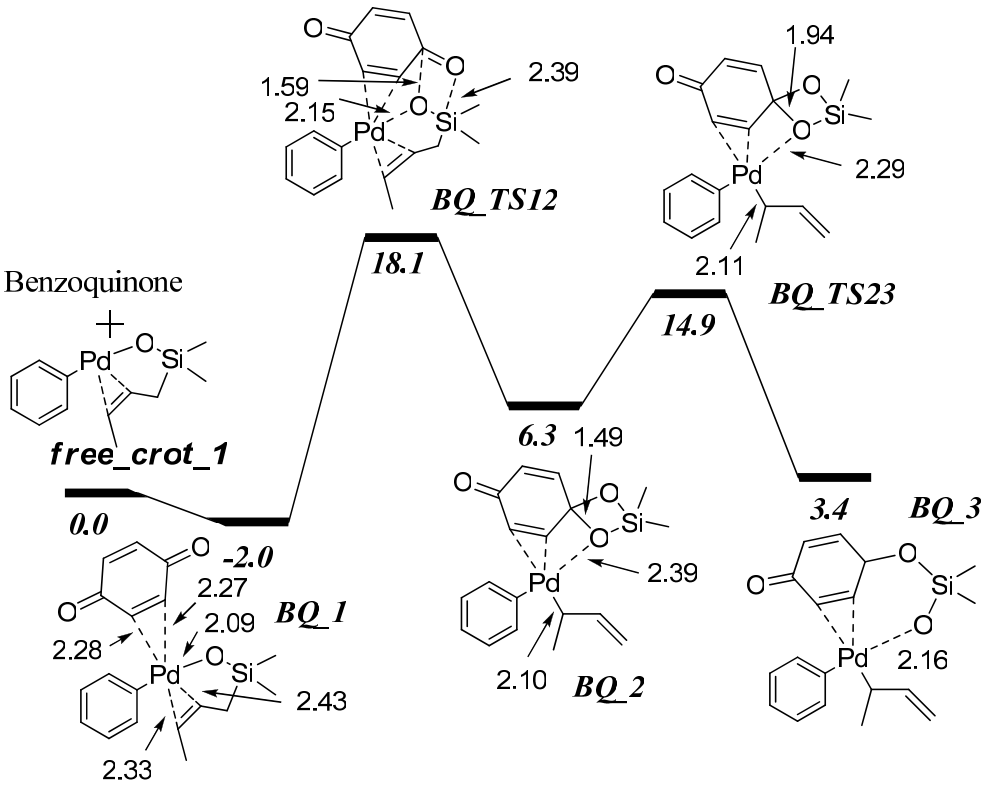

Figure 3.2.6 Benzoquinone-assisted transmetalation step of (Z)-crotyl silanolates. Free energy values in kcal/mol.

Such a process is consistent with the fact that 1,4-benzoquinone is a good ligand for the coupling, but the poor yields cannot be rationalized looking at the transmetalation.

3.2.2.4 CO_2-assisted transmetalation

Finally, we undertook similar calculations using carbon dioxide. There are no experimental data on the effect of carbon dioxide on the coupling. However, we

decided to test the effect of a very simple molecule bearing a carbonyl to assess the importance of the double bond of dba and its coordination to the metal center during the transmetalation. Figure 3.2.7 depicts the corresponding energy profile. In this case, after bonding of CO_2 to the metal center (**co2_1**), a four-membered ring is formed very easily (barrier of 1.7 kcal/mol), this time between the palladium and the oxygen of the Si=O unit of the silanolate and the C=O unit of carbon dioxide (**co2_2**) Then **co2_TS23** shows the cleavage of the Pd-O bond and a Si-O bond formation. We obtained an intermediate similar to the ones obtained with 1,4-benzoquinone and dba (**co2_3**), which is 12.7 kcal/mol higher in energy than the separated reactants. Following this, the Si-C bond cleavage generates the product of transmetalation **co2_4**. The transmetalation appears even more easier than when using dba or 1,4-benzoquinone (difference between the lowest and the highest points of only 16.8 kcal/mol). However, the overall step is largely endothermic, **co2_4** being 10.7 kcal/mol higher than the separated reactants. This is possibly due to the lack of coordinating agent at the metal center in this complex. There is indeed a large free space around the coordination sphere of palladium, which presumably destabilizes the complex.

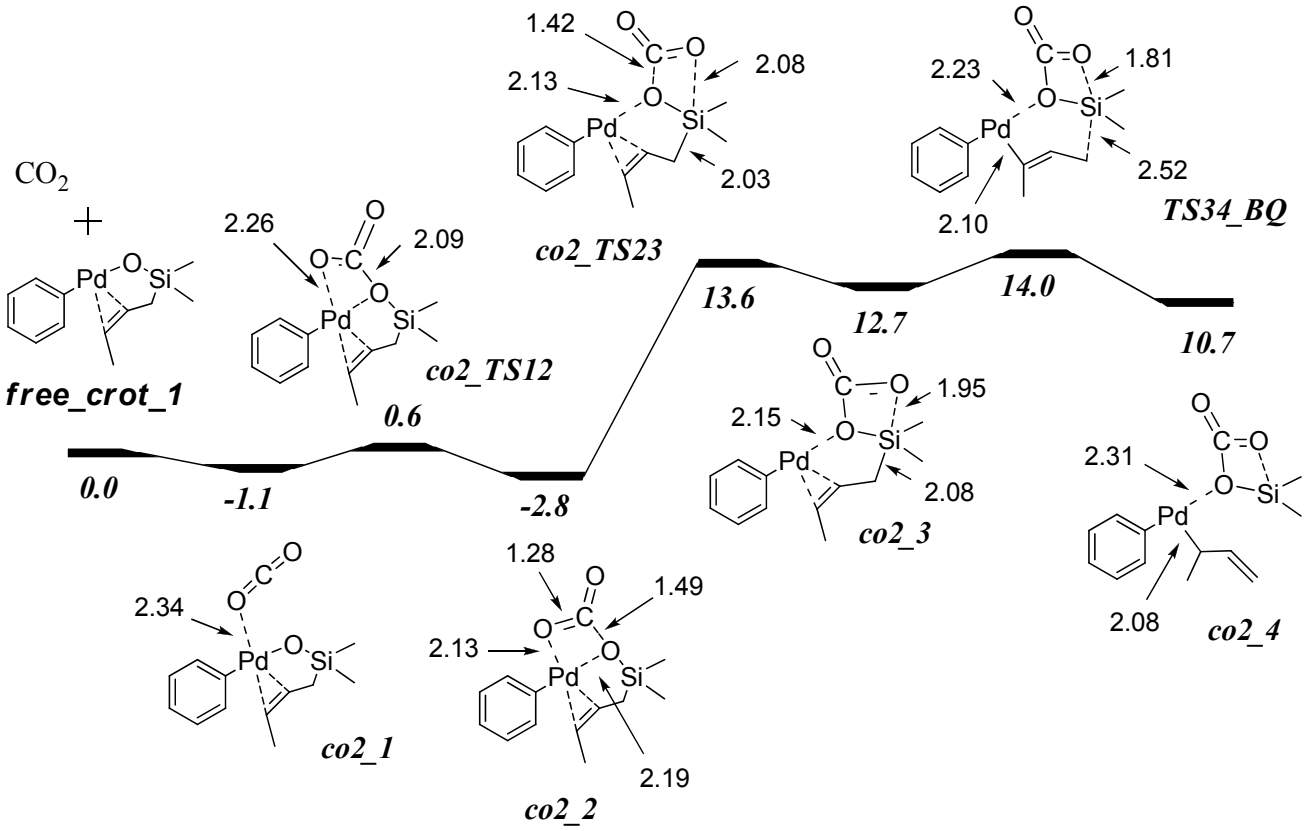

Figure 3.2.7 Carbon dioxide-assisted transmetalation step of a (Z) crotyl silanolate. Free energy values in kcal/mol.

3.2.2.5 Transmetalation with a phosphine ligand (PMe_3)

To verify the role of dba in lowering the reaction barrier, we computed the transmetalation of a Pd-O-Si type complex generated from a crotyl silanolate, with no activator. We tested the model phosphine PMe_3 and the schematic representation of the process is depicted in Figure 3.2.8. We note that the starting structure is very similar than that used for all the previous profiles using a Pd-O-Si type complex generated from a crotyl silanolate (**free_crot_1**). The transmetalation occurs by transfer of the γ carbon to the metal center, and release of the $(Me)_2Si{=}O$ unit. The phosphine ligand stays bound to the complex, including in the transition state. The reaction has a barrier of 43.1 kcal/mol in free energy relative to the starting complex (**1_Phos**). This is significantly higher than when the transmetalation process is assisted by dba (25.3 kcal/mol), benzoquinone (20.1 kcal/mol), or CO_2 (16.8 kcal/mol). The activator is then critical to lower the barrier and allow the transmetalation of these complexes. The process is also thermodynamically disfavoured, with a product of transmetalation (**2_Phos**) highly endothermic.

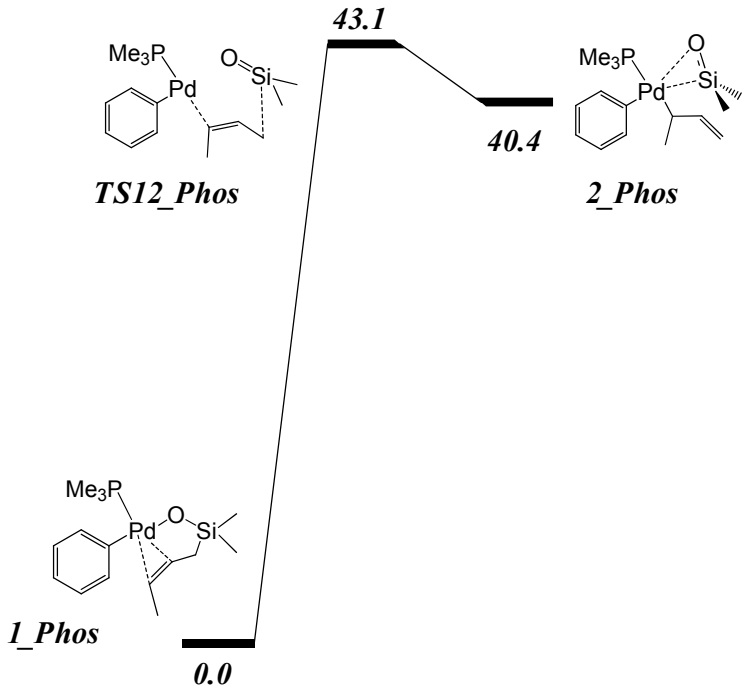

Figure 3.2.8 Transmetalation step using a Pd-O-Si type complex generated from a crotyl silanolate with a phosphine ligated to the metal center. Free energy values in kcal/mol.

We also used a bisphosphine ($PH_2CH_2CH_2CH_2PH_2$) as a ligand to take into account the possibility of a double coordination of the phosphine to the metal center. All our attempts to compute a dicoordinated phosphine failed. One of the phosphine

arms systematically dissociates from the metal center. The presence of an η^2 interaction between the alkyl chain of the silanolate and the palladium, together with the bound oxygen atom, the phenyl group and one arm of the phosphine saturate electronically the metal center, and this most probably prevents a double coordination of the bisphosphine ligand.

3.2.3 Qualitative study of the γ:α selectivity in the coupling of allylic silanolates

The cross-coupling of allylic reagents is highly versatile, and many systems were reported with numerous catalysts.[237-242] Among the available methods for the allylation of organic compounds, the regioselective cross-coupling of allylic silanolates with aryl halides was recently developed by the group of Denmark.[218, 234, 243-245]

The presence of a methyl group at the γ carbon of the allyl chain introduces selectivity issues and the possible outcomes are collected in Figure 3.2.9.

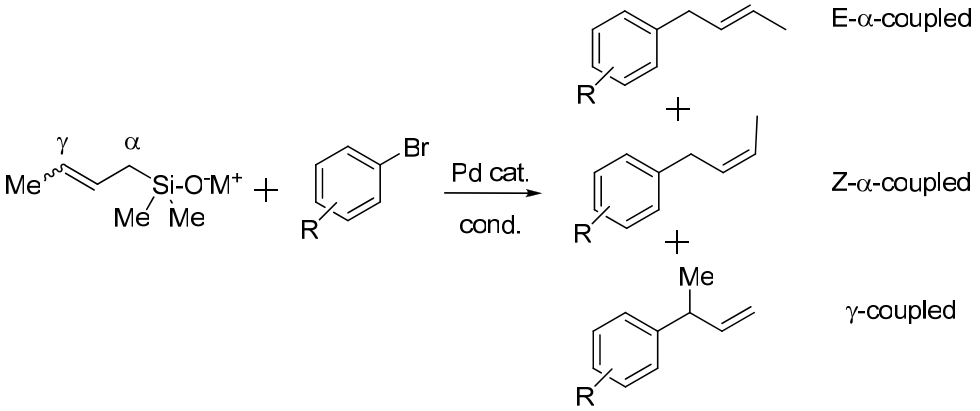

Figure 3.2.9 Products obtained in the palladium-catalyzed crotylation of aryl halides with crotyl silanolates.

The approach developed for the allyl (and crotyl) silanolates affords moderate to good selectivities towards the γ coupled product. Whatever the substituents on the aryl bromide, the γ compound is the major isomer, and the selectivity is best when using the *tert*-butyl 4-bromobenzoate ester as the starting halide. In that case, the γ : α ratio obtained is as high as 25 : 1 (see Table 3.2.3). Interestingly, when the *tert*-butyl 2-bromobenzoate ester is used, the regioselectivity is reversed and the α-coupled product is obtained with a γ : α ratio of 1 : 2.5. It was suggested that the origin of this phenomenon lies in the interconversion process commonly described in allylic reactions. As we stressed in the introductory paragraph of this section, dba is the best pre-catalyst for the coupling of allylic and crotyl silanolates, and the addition of dba as a ligand improved even more the selectivity, the rate, and the yield of the reactions.[218] The best experimental conditions are depicted in the upper portion of Table 3.2.3. We note that (E)-silanolates are typically synonyms of

better regio-selectivity than (Z)-silanolates,[218] but only calculations performed with the (Z)-silanolate will be considered in this subsection.

Table 3.2.3 Optimized conditions for the coupling of aryl halides with crotyl silanolates, and major isomers obtained depending on the substituent on the aryl halide.

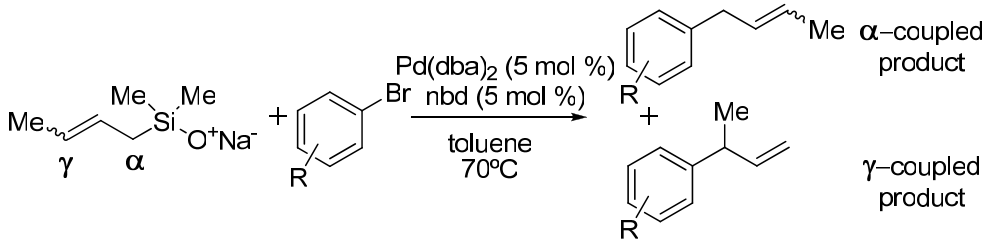

Starting halide	Major product	Ratio γ:α
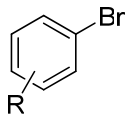	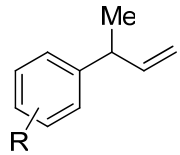	3.4-25 : 1
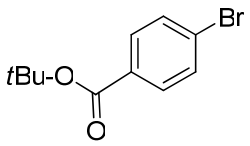	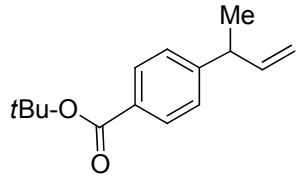	25 : 1
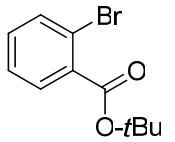	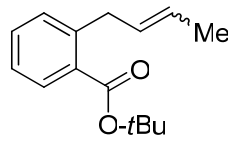	1 : 2.5

We show the full proposed catalytic cycle with crotyl silanolates in Figure 3.2.10. After oxidative addition and generation of the Pd-O-Si type complex, the Pd(II) complex **Pd_all_int** is formed through transmetalation at the γ-carbon. The reductive elimination can take place to give the final γ-coupled product. Alternatively, a σ-π isomerization process can occur through a π-allylpalladium intermediate which allows formation of the α-coupled product. A transmetalation at the α-carbon from the Pd-O-Si type complex (also followed by a reductive elimination) is unlikely, but this possibility will also be tested.

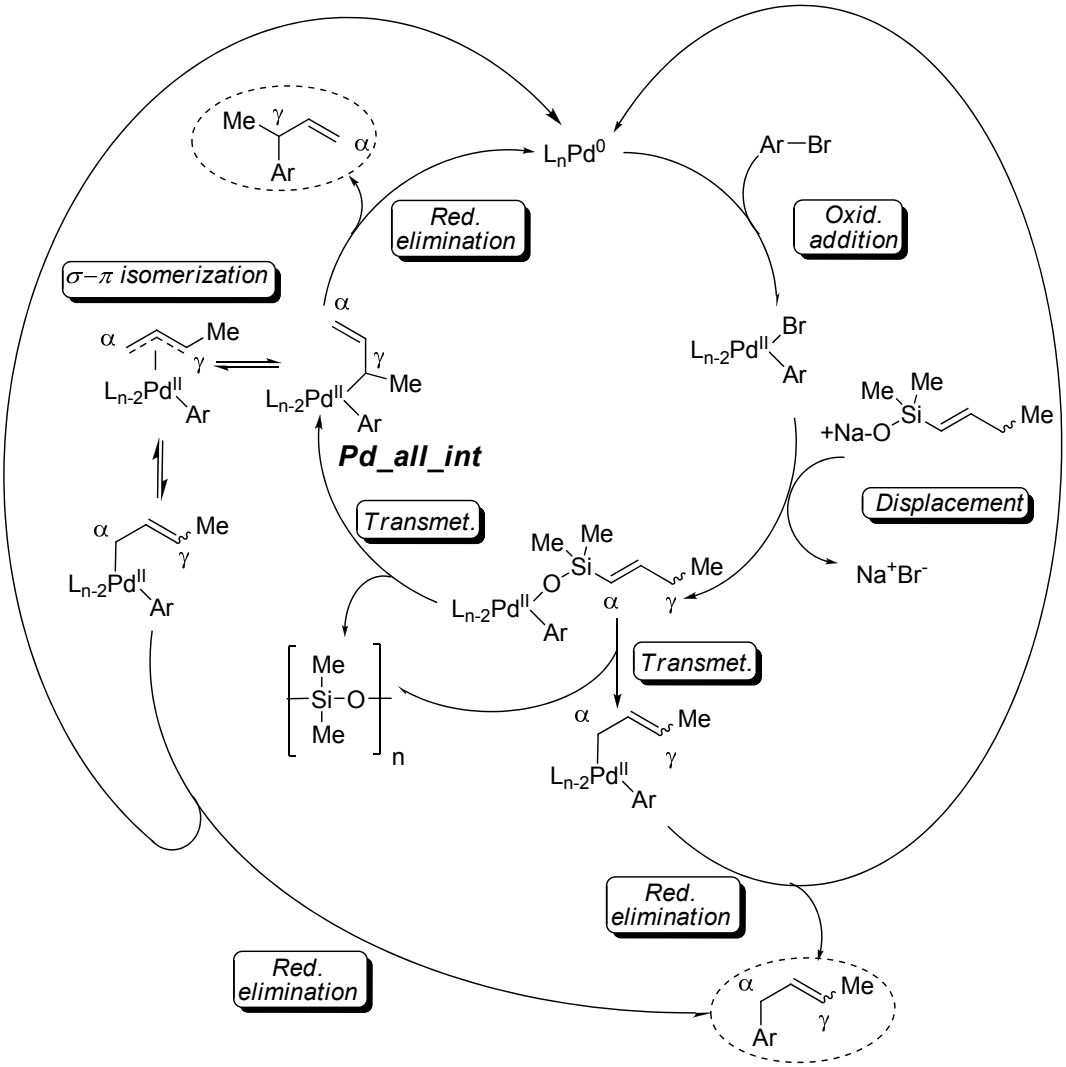

Figure 3.2.10 Proposed catalytic cycle of the cross-coupling of allylic silanolates.

We decided to study the viability of this cycle, and the key steps will be analyzed. To address the selectivity differences induced by the substituents, three complexes generated by three different starting organic halides will be considered. These halides are the simple phenyl bromide, the *tert*-butyl 4-bromobenzoate ester, and the *tert*-butyl 2-bromobenzoate ester (see structures in Table 3.2.3). In all cases, we will start the mechanism with the corresponding Pd-O-Si type complex. The transmetalation at α and γ carbons will be first tested to check the variations induced by the substituents on the reaction barriers of this process. Then, the energy barriers for the reductive elimination for both regio-isomers will be compared. Finally, we will look at the σ-π isomerization process for these three complexes.

3.2.3.1 Transmetalation at the α carbon

We first tested the possibility of a transmetalation at the α carbon (bound to the silicon) to the palladium. The structure of the corresponding transition state (labelled as **alpha_transmet_ester_TS**)for the system bearing an ortho ester substituent is showed in Figure 3.2.11. A very long C(alpha)-H bond is observed (at 1.17 Å) suggesting an agostic interaction, the C(alpha)-Si distance is 2.09 Å and the C(alpha)-Pd is 2.54 Å. This transition state lies 54.5 kcal/mol higher in free energy relative to the separated reactants (Pd-O-Si type complex and dba). We note that only one molecule of dba is needed to allow the transmetalation because the ester substituent stabilizes the metal center through the carbonyl. We located a similar transition state when no ester substituent is located on the aryl group, and the transition state lies similarly very high in energy, around 47.4 kcal/mol higher in free energy that the corresponding reactants (**free_crot_1** and two dba molecules), which is much higher than the transmetalation at the γ carbon depicted in Figure 3.2.3 (free energy barrier of 25.3 kcal/mol). The energy difference of 22 kcal/mol confirms that a transmetalation at the α-carbon from the silicon to the palladium is unlikely, and that an isomerization process should take place after the transmetalation at the γ carbon. When there is no substituent on the aryl group, two molecules of dba are needed to account for the saturation at the metal center to locate the transition state (this issue will be tackled in the next subsection). A barrier of 54.5 kcal/mol (for the system bearing an ortho ester substituent) is too high to account for the α-coupled product obtained with the experimental conditions reported for the *o*-ester substituted system. We can then confidently discard the possibility of a direct transmetalation at the α-carbon.

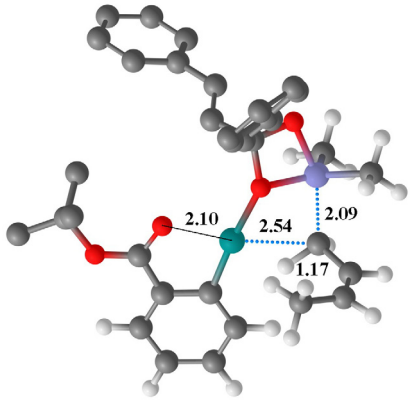

alpha_transmet_ester_TS

Figure 3.2.11 Transition state for the transmetalation at the α carbon of the crotyl group. Hydrogen atoms on dba and the ester were removed for clarity.

3.2.3.2 Transmetalation at the γ carbon

Regarding the transmetalation at the γ-carbon, we computed the same pathway as the one depicted in Figure 3.2.3 consisting of a transmetalation process starting with a Pd-O-Si type complex and assisted by dba. We report the energy barriers for three systems, the para and ortho ester substituted Pd-O-Si type complexes and the complex with no substituents on the aryl ring. Free energy values are collected in Table 3.2.4. For the non-substituted system, we reproduce the values collected in Figure 3.2.3. In all cases, the first transition state corresponds to the four-membered ring formation concomitant with Pd-C(γ) bond formation and Si-C(α) bond cleavage. In other words, the transmetalation takes place in the first step, so the subsequent steps applicable in Figure 3.2.3 will not be discussed here.

Table 3.2.4. First step of the dba-assisted transmetalation process depending on the substituent present on the aryl group. Free energies in kcal/mol are relative to the separated complexes, meaning the ligand-free Pd-O-Si type complexes and dba. Double bond in Z configuration.

	Substituent		
	none	para ester	ortho ester
dba-ligated complex	2.6	0.4	19.4
Transition state	25.3	24.7	41.1
Product	17.8	10.5	26.5

The "dba-ligated complexes" of Table 3.2.4 are Pd-O-Si type complexes with a molecule of dba ligated to the palladium center (complex labelled as **dba_crot_1** in Figure 3.2.3 in the case of the non-substituted system).
For the ortho substituted complex, the energy barrier is much higher than its *para* substituted and non-substituted counterparts. The reason can be found in the higher stability of the *o*-ester substituted Pd-O-Si type separated complex (without dba on the metal center). The **free_crot_o_ester** complex is indeed 15.7 kcal/mol more stable than **free_crot_p_ester**. Both complexes are shown in Figure 3.2.12, and we can observe the additional stabilization at the metal center induced by the ester substituent in the case of **free_crot_o_ester**. The *p*-substituted complex has a structure very similar to **free_crot_1** (the non-substituted Pd-O-Si type complex), which is translated into similar energy barriers for the transmetalation step.

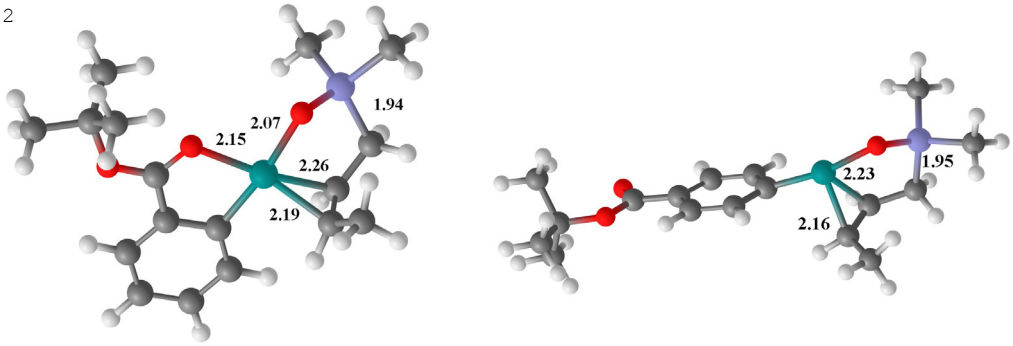

free_crot_o_ester ***free_crot_p_ester***

Figure 3.2.12 *Ortho*- and *para*-ester substituted Pd-O-Si type complexes.

The very high energy barrier for the transmetalation of **free_crot_o_ester** is thus a consequence of the high stability of this ligand-free Pd-O-Si type complex compared to its *para* substituted counterpart. This would suggest that the transmetalation step in the case of the ortho substituted Pd-O-Si type complex takes place without involvement of dba, due to the electronic saturation of the metal center. The process would thus become non activated.

3.2.3.3 Reductive elimination depending on the ester position and the carbons coupled

Following this, we looked at the reductive elimination step. We computed this process at the α and γ carbons.
To highlight the importance of the substituent position in this process, we reproduce in Figure 3.2.13 two different views of two transition states, namely **ER_TS_γ_est_pos1** and **ER_TS_γ_est_pos2** which both correspond to a reductive elimination process affording the γ-coupled product. They correspond to the same carbon-carbon bond formation between the γ carbon of the silanolate unit and the carbon of the aryl halide. However, they differ by the position of the ortho ester substituent. In **ER_TS_γ_est_pos1**, the ester substituent faces the approaching carbon chain on the right side (we called it "position 1", see Figure 3.2.13). In contrast, the ester group is on the other side in the case of the transition state **ER_TS_γ_est_pos2** ("position 2").

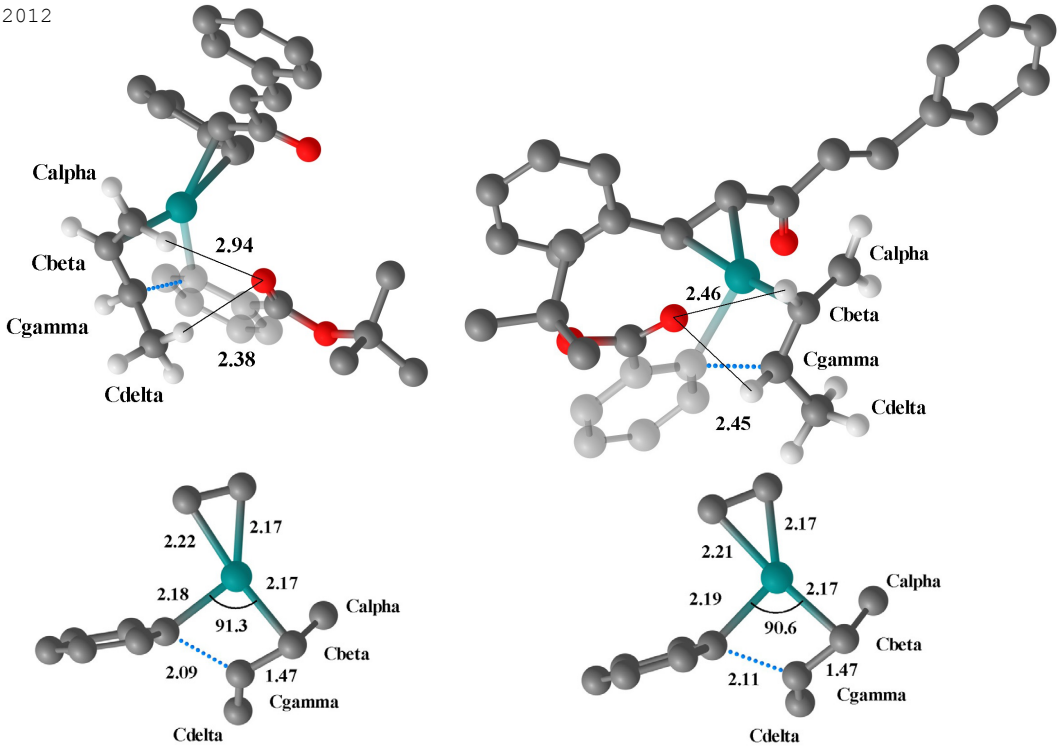

ER_TS_γ_est_ pos1 ***ER_TS_γ_est_ pos2***

Figure 3.2.13 Two representations of **ER_TS_γ_est_pos1** (left) and **ER_TS_γ_est_pos2** (right). Transition states for the reductive elimination step, affording the γ-coupled product in the case of crotyl silanolates with the aryl halide bearing an ortho ester group. Several atoms were removed for clarity.

The geometrical features appear very similar for both transition states. The distances around the metal center are virtually the same (see pictures in the lower portion of Figure 3.2.13). Regarding the interactions between the oxygen of the ester group and the carbon chain, things are different. In the case of **ER_TS_γ_est_pos1**, weak interactions (C-H···O distances of 2.94 Å and 2.38 Å) can be observed between the oxygen of the carbonyl and the α and δ carbons of the carbon backbone (labelled Calpha and Cdelta in Figure 3.2.13). In contrast, distances of 2.46 Å and 2.45 Å between the oxygen and the β and γ carbons (Cbeta and Cgamma in Figure 3.2.13) are observed for **ER_TS_γ_est_pos2**, but no interactions with the α and δ carbons are apparent.
Energy values corresponding to these transition states are collected in Table 3.2.5. The values for the α- coupled products (with an *o*-ester substituent) are also shown. We can then compare the energy values depending on the carbon bond formation (α or γ coupling), and the position of the *o*-ester group in the transition states. Other systems bearing various groups were also computed (among them, an ester substituent at the para carbon), but we will only discuss the results obtained with the representative ortho ester substituent.

Table 3.2.5 Reductive elimination barriers depending on the regioselectivity and the position of the ortho-ester substituent. Free energy in kcal/mol relative to the corresponding intermediates. (Z)-silanolates were computed and dba is ligated to the palladium through one of its double bond in all cases.

Transition state	Regioselectivity	Ester position	Free energy[a]	*Product*
ER_TS_α_est_pos1	α-coupled	position 1	14.2	*-23.7*
ER_TS_α_est_pos2		position 2	11.6	*-25.7*
ER_TS_γ_est_pos1	γ-coupled	position 1	17.9	*-16.9*
ER_TS_γ_est_pos2		position 2	15.0	*-21.8*

[a] Relative to the dba-ligated Pd-O-Si type complex, after loss of the $(Me)_2Si=O$ unit.

For both ester positions, the reductive elimination at the α-carbon is favoured by around 3.5 kcal/mol compared to the γ-coupled product, as reported in Table 3.2.5 (see **ER_TS_α_est_pos1** is lower than **ER_TS_γ_est_pos1**, and **ER_TS_α_est_pos2** is lower than **ER_TS_γ_est_pos2).** The magnitude of the energy difference is similar for both positions of the ortho ester group. The fact that the α-coupled is kinetically favoured by 3 kcal/mol over the γ-coupled product is in agreement with the fact that the α-coupled product is the main isomer obtained for the system bearing an *o*-ester group. However, we found the same trend with the para-substituted systems. Even for the non-substituted complex, the reductive elimination at the α-carbon is favoured over the one at the γ-carbon (results not reproduced here). This leads us to believe that the regioselectivity is not determined in the reductive elimination process.
The other important point is that the reductive elimination with the ester group in position 2 (interactions between the carbonyl and the β and γ carbons) is around 3 kcal/mol easier than when the ester is in position 1. Position of the ester substituent is then critical for the accurate description of the reductive elimination process.
We then turned our attention to the interconversion process.

3.2.3.4 Interconversion process

Figure 3.2.14 depicts the interconversion process which brings the crotyl group from a η^2-coordination between the β- and γ-carbons and palladium (**inter_1_nosubs**) to a η^1-coordination between the α-carbon and the metal center (**inter_2_nosubs)**. The transition state (**inter_TS_nosubs**) is significantly high in energy, lying 25.5 kcal/mol higher that the starting η^2 complex. If we compare this value with the reductive elimination barriers (around 12-15 kcal/mol), it can be deduced that the latter is greatly favoured, and no α-coupled product should be formed. This is in contradiction with the experimental results, in which an appreciable amount of α-coupled product is always observed.

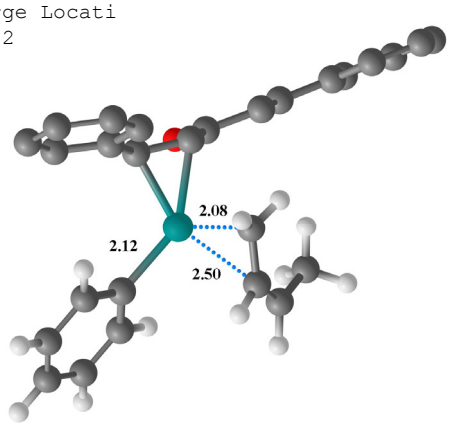

inter_TS_nosubs

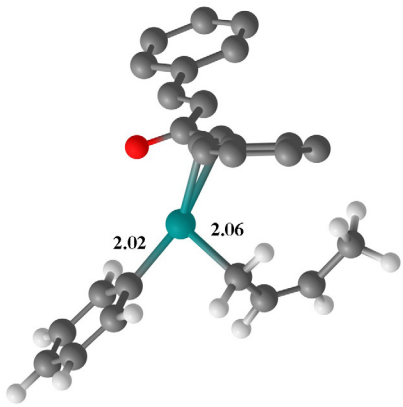

inter_2_nosubs

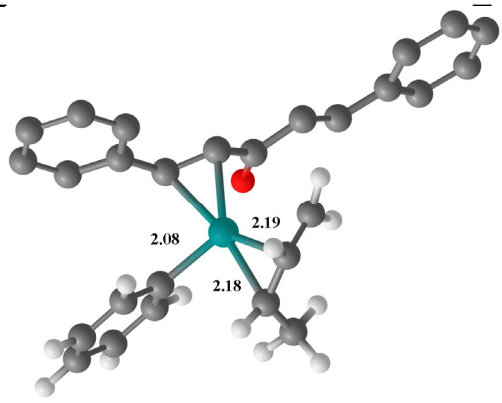

inter_1_nosubs

Figure 3.2.14 Interconversion process for the non-substituted system. Hydrogen atoms on dba were removed for clarity.

In contrast, the corresponding barrier for the *o*-ester substituted system is considerably reduced, with a barrier of only 15.6 kcal/mol relative to the corresponding η^2-coordinated complex. This would allow the interconversion process to compete with the reductive elimination at the γ-carbon (barrier around 15 kcal/mol, see Table 3.2.5), and would broadly rationalize the mixture obtained with the *o*-ester substituted aryl bromide. Since the γ : α ratio is 1 : 2.5 in this case, the barrier of the isomerization process should be slightly lower than that of the reductive elimination at the γ-carbon. We note that the weak interactions that take place in the reductive elimination and the interconversion processes should be described more accurately by functionals which were designed to account for these (like M06 or B97D). We are confident in the relative energy barriers of the catalytic cycle, and our values allow us to have determined the importance of the competition between reduction elimination at the γ position, reductive elimination at the α carbon and the σ-π isomerization process. Nevertheless, the small energy differences between these processes require a better description of the weak interactions found in the transition states in order to rationalize the regioselectivities obtained experimentally.

The reason why a significant amount of α-coupled product is experimentally obtained with the systems bearing para substituents still has to be determined. The high barrier of the interconversion process compared to that of the reductive elimination at the γ carbon is indeed in apparent contradiction with the experimental observations.

We mention that the transition states for the σ-π interconversion process are not easy to locate due to the very low imaginary frequencies which are typical for rotation processes of carbon chains.

The calculations confirm that the interconversion process is key for the regioselectivity in allylic (and crotyl) systems. Competition between the reductive elimination and the interconversion is critical regarding the selectivity of these systems. The lowering of the interconversion barrier for the system bearing an *o*-ester substituent is likely to be responsible of the domination of the α-coupled product for the *o*-ester substituted system. This is likely due to subtle effects between the carbonyl of the ester group and the hydrogen atoms of the carbon chain, but steric effects should be also important. More work is needed to better rationalize the experimental outcomes.

3.2.4 Dba and carbene effects on the transmetalation step in the coupling of heterocyclic silanolates

We also got interested in the coupling of pyrrolic systems. Various five-membered heterocyclic silanolates have been shown to couple with aryl halides under palladium-based catalysts.[233] Coupling reactions with 2-indolyl-, 2-pyrrolyl-, 2-furyl-, and 2-thienylsilanolates were developed. $Pd_2(dba_3)$ has been shown to be an efficient catalyst for these. We decided to test the viability of the mechanism presented in Figure 3.2.3 in the particular case of the N-methyl-2-dimethyl(2-pyrrolyl)silanol. The development of the cross-coupling of heterocyclic silanolates revealed that the best conditions (depicted in Figure 3.2.15) for this coupling consist (together with the presence of a base such as NaH to generate the silanolate from the silanol) in the use of $Pd_2(dba_3).CHCl_3$ as the palladium source in a toluene solvent. Some other catalyst precursors were found to be competent, such as the palladacycle depicted in the same figure, which is needed when using aryl chlorides and bromides, presumably to facilitate the oxidative addition. However, our aim here is to focus on dba, consequently, we will not expand our study to this particular catalyst. It has also been found that $Pd_2(dba_3).CHCl_3$ affords much better results than $Pd_2(dba_3).CH_2Cl_2$ or $Pd_2(dba_3)$ alone. The addition of chloroform into a reaction mixture containing $Pd_2(dba_3)$ provides similar results that when using $Pd_2(dba_3).CHCl_3$. The role of $CHCl_3$ is rather unknown. However it has been recognized for a long time that dichlorocarbenes are formed upon basic treatment of chloroform.[246] The schematic mechanism of dichlorocarbene formation is represented in Figure 3.2.16. Such species readily react with alkenes to form cyclopropane derivatives.[247, 248] More recently, Ong *et al* explored the reactivity of such intermediates.[249] The basic conditions reported in that paper were very similar

to that of the cross-coupling of heterocyclic silanolates with aryl halides that we are interested in.

It is then likely that in this present case, chloroform will generate a dichlorocarbene under the basic conditions experimentally described. Since this carbene could affect the catalyst and the reaction barriers, we therefore decided to study its possible role on the transmetalation step.

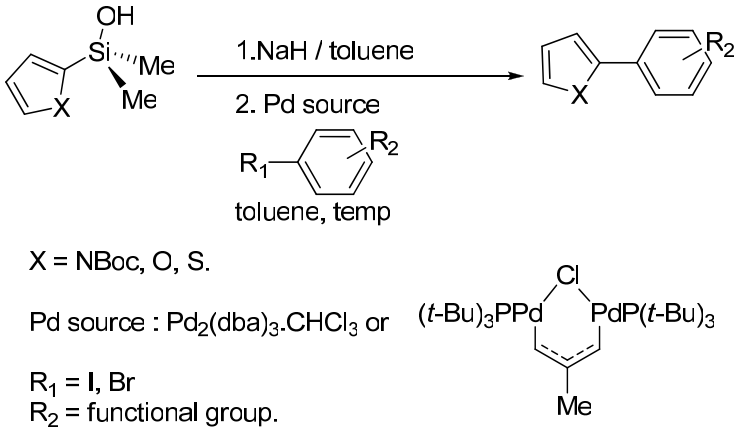

Figure 3.2.15 Experimental conditions for the coupling of heterocyclic silanolates with aryl halides.

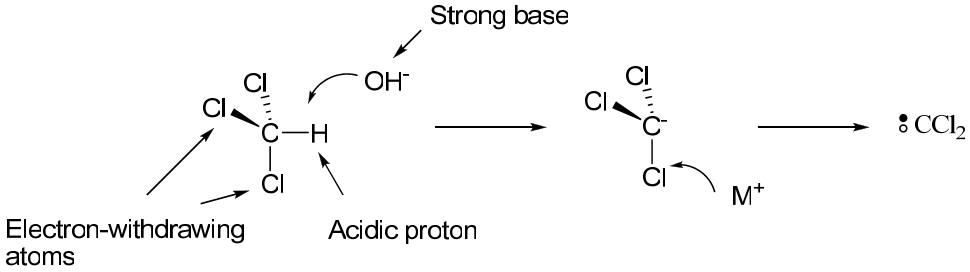

Figure 3.2.16 Dichlorocarbene formation under strong basic conditions.

Our goal in this subsection is then two-fold. We first want to test the effect of dba on the transmetalation step in the case of heterocyclic silanolates, and generalize the process depicted in Figure 3.2.3. We will also attempt to give some insights on the effect of the putative dichlorocarbene species.

To explore the conformational issue, we started this study by computing several complexes containing a CCl_2 ligand. Figure 3.2.17 shows two isomers of the Pd-O-Si type complex. In **pyr_carb_cis**, the phenyl group is *trans* to the heterocyclic group, and in **pyr_carb_trans**, the carbene is located *trans* to the pyrrolyl group. The former complex is more stable by 3.2 kcal/mol in free energy.

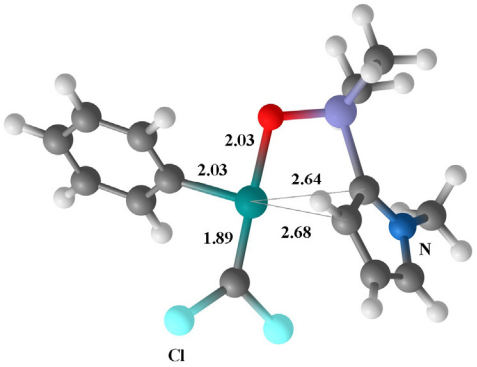

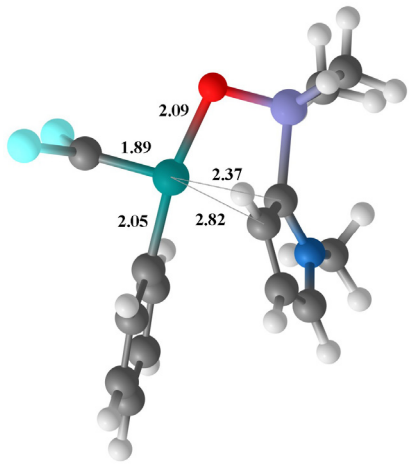

pyr_carb_cis ***pyr_carb_trans***
0.0 ***3.2***

Figure 3.2.17 Two isomers of the Pd-O-Si type complex stabilized by a dichlorocarbene ligand. Relative free energy values in kcal/mol depicted below each complex.

We reproduce in Figure 3.2.18 the full profile for the transmetalation with (Ph)(dba)PdOSi(Me_2)(Het) and (Ph)(CCl_2)PdOSi(Me_2)(Het) (Het=$C_4H_3NCH_3$). In the first case, the energy barrier of the highest transition state is 27.2 kcal/mol above the separated reactants. This is slightly higher than in the case reported in Figure 3.2.3, but still reasonable for the experimental conditions. The process is also significantly endothermic (by 9.6 kcal/mol), but the thermodynamical driving force of the subsequent reductive elimination should compensate this. We then considered the effect of CCl_2 on the species active in the transmetalation step, to assess the capacity of the carbene to stabilize the Pd-O-Si type complex. If we replace one of the molecules of dba (the one bound to the metal through its double bond, which is not involved in the four-membered ring formation), by a dichlorocarbene, the energetics are dramatically different. Indeed, changing the ligand provokes a stabilization of around 30 kcal/mol of the complex (**pyrr_carb_1**). Starting from this, the transmetalation occurs similarly, with a barrier of 23.4 kcal/mol through a transition state whose structure is similar to that of **pyrr_TS12**. The barrier is around 4 kcal/mol lower in presence of dichlorocarbene. We note that the reductive elimination can take place after **pyrr_2**, **pyrr_3**, or **pyrr_carb_2** since in all these cases, the aryl groups are in a favourable position (in *cis*) for this process. Subsequent dissociations of the $(Me)_2Si{=}O$ unit and dba are trivial at this stage.

The better results obtained when adding $CHCl_3$ in the reaction media are then a consequence of the much higher stabilities of the CCl_2 ligated complexes. The fact that CCl_2 is very reactive is directly related to the higher stability of **pyrr_carb_1** compared to **pyrr_1**. The transition state energy barrier of the transmetalation are somewhat similar for both species (but 4 kcal/mol lower with the carbene complexes) but the ligand exchange between (Ph)(dba)PdOSi(Me_2)(Het) and (Ph)(CCl_2)PdOSi(Me_2)(Het) is extremely favoured towards the carbene complexes.

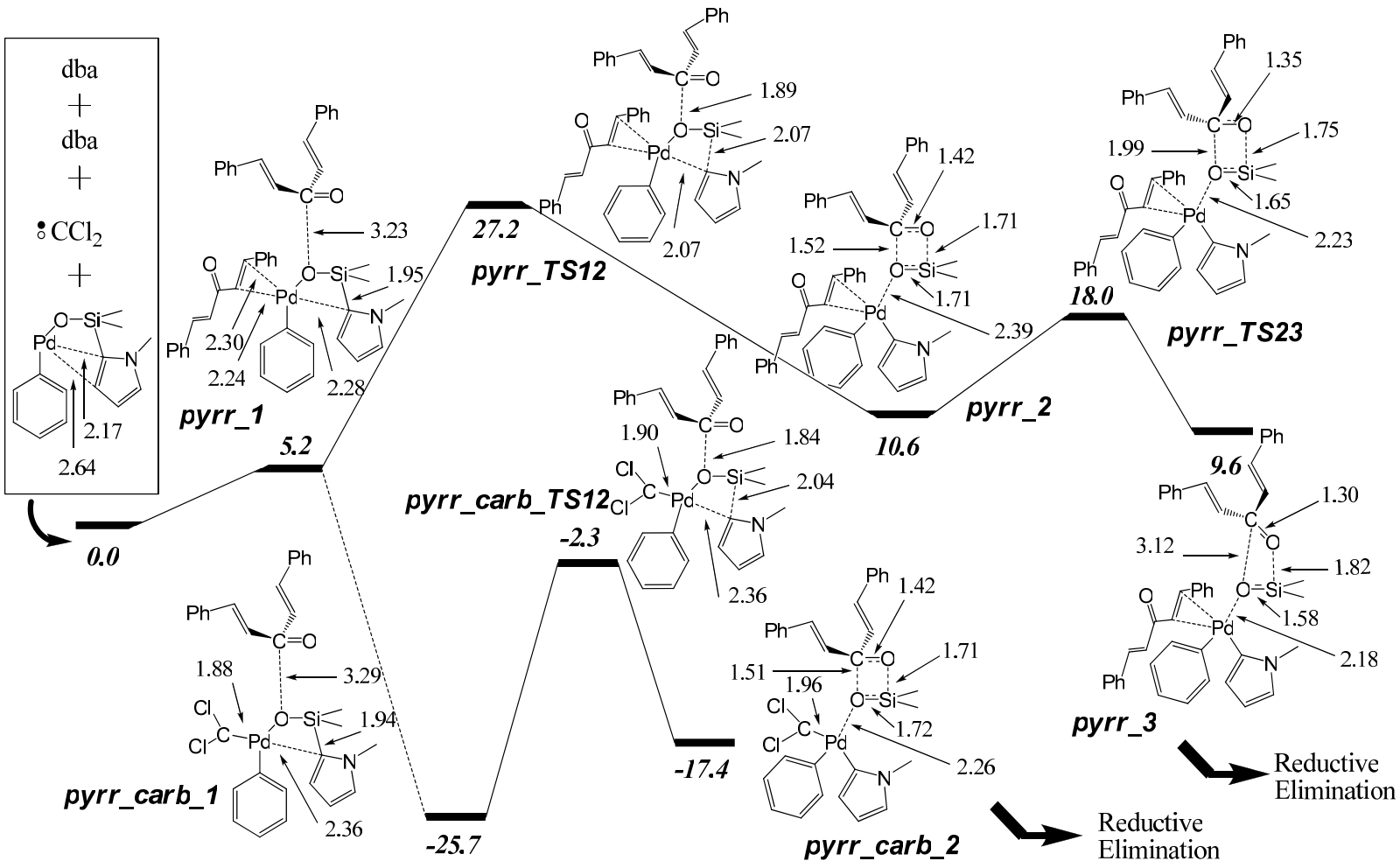

Figure 3.2.18 Free energy profile of the transmetalation with pyrrolyl silanolates. Complexes with dba and CCl_2 are considered.

The next question would be why two molecules of dba (or one dba, and one CCl_2) are needed in the case of pyrrolyl compounds, when one is sufficient when crotyl (or allyl) species are used. Indeed, all our attempts to compute a transition state for the transmetalation step with only one molecule of dba in the case of heterocyclic silanolates failed. They all produce some rearranged species of high energy, irrelevant to the mechanism considered. To address this issue, we compare **all_dba_TS12** (which is the first transition state of the transmetalation step using crotyl silanolates, see Figure 3.2.3) and **pyrr_TS12** (transition state of the transmetalation step using pyrrolyl silanolates, see Figure 3.2.18). Figure 3.2.19 shows these two transition states structures. The arrangement of the ligands around the metal center is similar in both cases. A η^2 interaction is adopted between the silanolate part (crotyl or pyrrolyl compounds) and the metal, thus no electronic deficiency on the palladium is expected. Importantly, in **all_dba_TS12**, dba can stretch enough to interact in a η^2 manner with the palladium through one of its double bonds, and, at the same time, initiate the transmetalation through its carbonyl by attacking the $(Me)_2Si=O$ unit and subsequently form the four-membered ring. The η^2 interaction established between the carbon chain and the metal is done through the β (labelled as Cbeta in Figure 3.2.19, left) and γ (Cgamma) carbons. In contrast, in **pyrr_TS12**, the interaction is made through the α (Calpha) and β (Cbeta) carbons. The structure of the Pd-O-Si-Calpha-Cbeta-Cgamma backbone is therefore significantly different between the two.

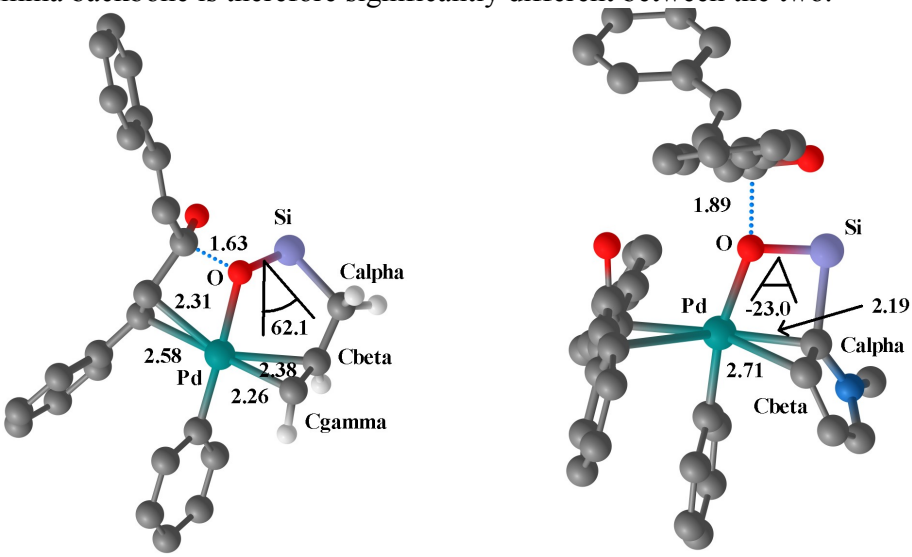

all_dba_TS12 ***pyrr_TS12***

Figure 3.2.19 Structures of the transition states found for the transmetalation step of crotyl and pyrrolyl silanolates. Most of the hydrogen atoms, the methyl groups on silicon, and the δ carbon of the crotyl chain of **all_dba_TS12** were removed for clarity.

This can be clearly illustrated by the dihedral angles formed by the Pd-O-Si-Calpha atoms of these two complexes. In **all_dba_TS12** the dihedral angle is about 62°,

when that of **pyrr_TS12** is -23°. The lower dihedral angle in the latter case prevents dba from concomitantly interacting with the metal through its double bond and attacking the $(Me)_2Si=O$ unit in order to form the four-membered ring which will facilitate the transmetalation. Then another molecule of dba or a dichlorocarbene is necessary to stabilize the metal. This is directly related to the higher performance of the chloroform solvated catalyst with heterocyclic silanolates. This also suggests that chloroform (and by extension CCl_2) is not required in the coupling of allyl (and crotyl) silanolates because dba is able to undertake the activated transmetalation alone in that case.
Several computational papers appeared recently in the literature regarding the reactivity or the role of CCl_2 in various reactions.[250] However, to our knowledge, it is the first time that a study on the effect of such a carbene in a cross-coupling reaction is reported.

Finally, we note that the arrangement of the ligands around the metal center in **pyrr_carb_1** is similar to **pyrr_carb_trans**, which is slightly unstable compared to **pyrr_carb_cis** (by 3.2 kcal/mol). We did not locate a transition state for the transmetalation corresponding to the latter but it is likely to be of similar energy. In any case, the reasonable barrier (23.4 kcal/mol) of the transmetalation step with a carbene ligand leads us to believe that the small difference between the starting species should not be significant.

3.2.5 Effect of an additional silanolate on the reaction barriers (excess of silanolate in the reaction media)

In the catalytic conditions, the silanolate is typically in excess compared to the palladium catalyst. After having considered the feasibility of the intramolecular non-activated mechanism (section 3.1), and the role of dba on the transmetalation step (subsections 3.2.2, 3.2.3, and 3,2,4), we then studied the role of the silanolate salt on this process. Experimentally, it has been found that the presence in excess of the silanolate salt increases the reaction rate significantly. The presence in excess of this species makes by-itself the silanolate salt of tremendous importance regarding the general picture of the mechanism, and we then decided to address this issue computationally. We note that changing the counter ion has also important effects on the reaction rates. Indeed, when the cesium salt was employed instead of potassium, the reaction rate was 4.5 times faster. In this subsection, we will treat the transmetalation step using the silanolate as an activator, but the role of the counter ion will not be analyzed.

3.2.5.1 Isomers of (Ph)(PhSiMe$_2$O)Pd(OSi(Me$_2$)Ph)

Figure 3.2.20 depicts two stable isomers of the (Ph)(PhSiMe$_2$O)Pd(OSi(Me$_2$)Ph) complex. These complexes are negatively charged, and were thus computed using BS2 (see computational methods). The most stable (**Sil_1**) will be taken as a reference for the energy profiles with added silanolates, in absence of phosphine ligand.

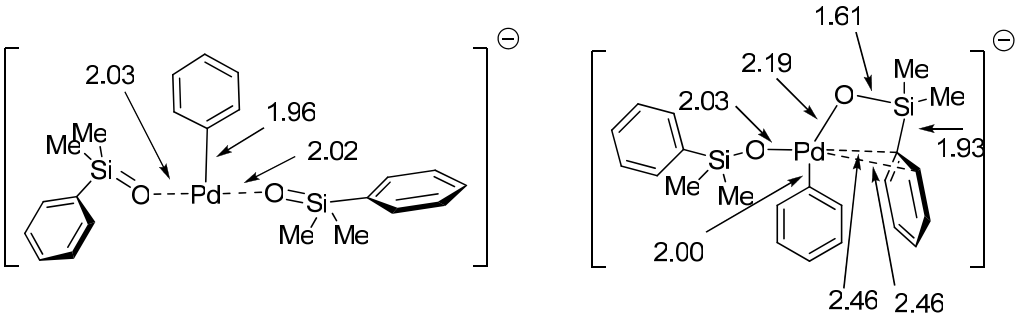

0.0 ***17.3***

Sil_1 **Sil_2**

Figure 3.2.20 Computed isomers of the (Ph)(PhSiMe$_2$O)Pd(OSi(Me$_2$)Ph) complex. Relative stabilities in free energy (kcal/mol) are indicated below each structure.

The most stable isomer (**Sil_1**) has the phenyl group *trans* to the vacant site, and the two silanolate groups in *trans* from each other. It is interesting to note that replacing the phosphine ligand of **Conf_1** (which was the most stable isomer found, see Figure 3.1.10) by a silanolate gives a similar structure, labelled as **Sil_2**, which is much less stable in that case, being 17.3 kcal/mol higher that **Sil_1**.

3.2.5.2 Transmetalation step starting with the (Ph)(L)Pd(OSi(Me$_2$)Ph) complex, with L= PhSiMe$_2$O$^-$. Added silanolate in a non activated process

We first tried the possibility for the additional silanolate to coordinate the palladium center, without been actively involved in the release of the (Me)$_2$Si=O unit. The upper portion of Figure 3.2.21 shows the transition state of the transmetalation step using a PhSiMe$_2$O$^-$ group as a ligand, and below are shown the corresponding reactant (left side) and product (right side).

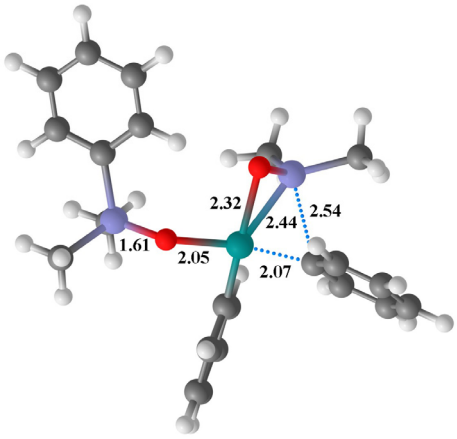

add_sil_TS

29.8

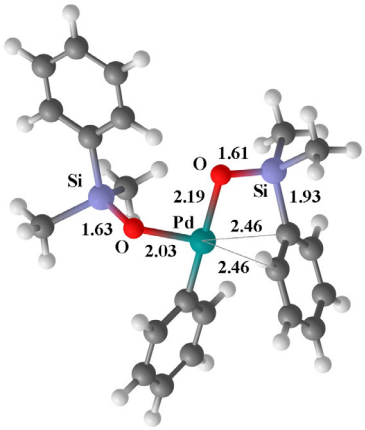

Sil_2

17.3

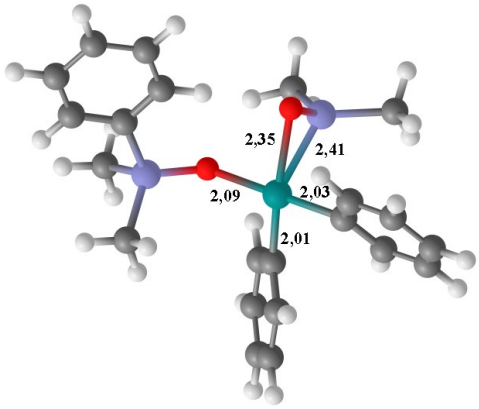

add_sil_2

25.9

Figure 3.2.21 Transmetalation step of a Pd-O-Si type complex using a silanolate ligand. Reactant, transition state and product with their corresponding free energies relative to **Sil_1**.

The transmetalation appears feasible with a barrier of 29.8 kcal/mol in free energy compared to **Sil_1**. However, the process depicted in Figure 3.2.21 cannot be considered as activated as defined in the introductory paragraph of this section. In this case, the phosphine ligand has simply been swapped by a silanolate. Indeed, the silanolate is *trans* to the phenyl group transferred, and does not activate the silicon atom of the "Pd-O-Si" type complex. The fact that we have a large barrier for this process would mean that the silanolate does not accelerate the rate of the reaction by replacing the phosphine group, but instead by activating the silicon atom of the "Pd-O-Si" type complex. This would confirm the activating role (meaning by creating a pentavalent silicon atom on the Pd-O-Si type complex) of

the silanolate in the improvement of the reaction rate. We note that we could not locate a transition state with both phenyl groups *trans* to each other.

We also collect in Figure 3.1.22 a transition state found for a carbometalation process, but this time with a silanolate ligand instead of the phosphine. Analogously, it lies very high in energy, being 59.0 kcal/mol higher than **Sil_1**.

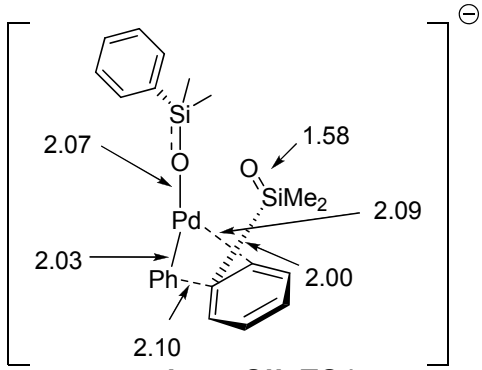

carbom_Sil_TS1

Figure 3.1.22 Representation of the computed transition state for a carbometalation process for the (Ph)(PhSiMe$_2$O)PdOSi(Me$_2$)Ph complex.

3.2.5.3 Transmetalation step starting with the (Ph)(L)Pd(OSi(Me$_2$)Ph) complex, with L= Ø. Added silanolate in an activated process

We then computed two transition states where the silanolate is truly involved in the transmetalation step as an activator, meaning that a pentavalent silicon is generated.

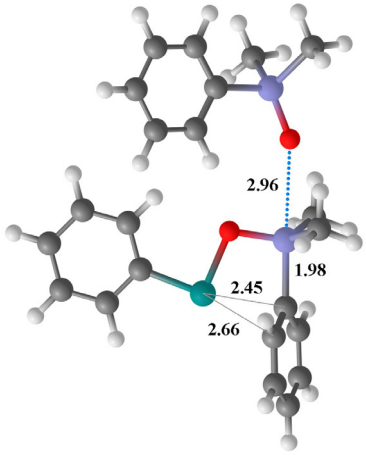

act_sil_TS1

53.9

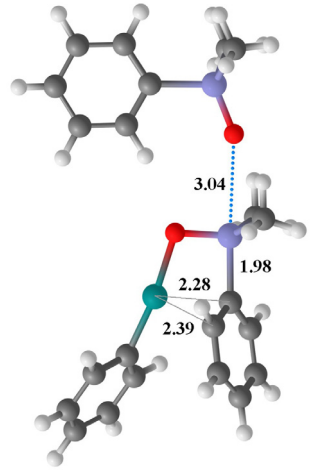

act_sil_TS2

58.1

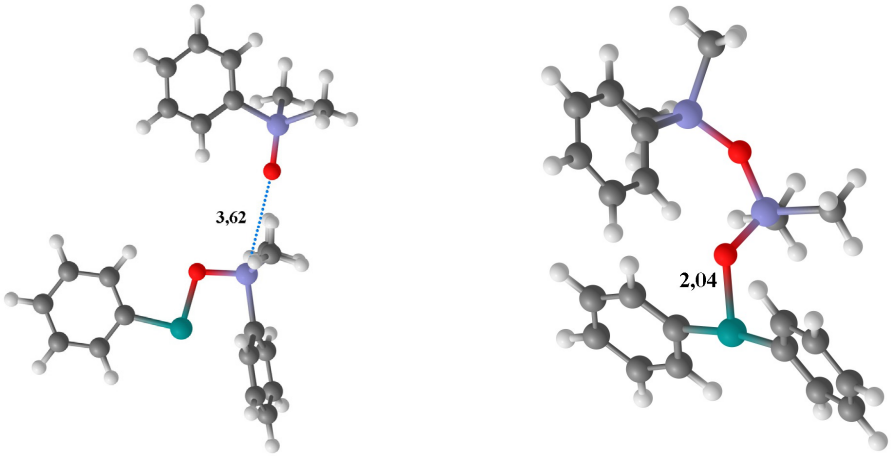

act_sil_1 ***act_sil_2***

50.7 ***7.0***

Figure 3.2.23 Transmetalation step of a Pd-O-Si type complex using a silanolate activator. Computed transition states are in the upper part. Corresponding reactant and product of transition state **act_sil_TS1** in the lower part. Free energy values in kcal/mol relative to **Sil_1**.

The two transition state structures depicted in the upper part of Figure 3.2.23 correspond to a true activated process, where the oxygen atom of the additional silanolate is attacking the silicon atom of the Pd-O-Si type complex. The structure reproduced on the left (**act_sil_TS1**) has the phenyl group *trans* to the migrating phenyl group. In contrast, **act_sil_TS2** shows the phenyl group transferred *trans* to the vacant site of the palladium. Surprisingly, **act_sil_TS2** lies 4.2 kcal/mol higher than **act_sil_TS1**. The strong *trans* influence of the phenyl group, and the fact that the structure resembles the most stable Pd-O-Si type complex (**Conf_1** depicted in Figure 3.1.10) would intuitively imply that the former should be more stabilized. However, the absence of phosphine in that case modifies the electronic configuration at the metal center, and guesses regarding the stabilities of these complexes are a hard task. We also collected in the lower part of the figure the structures of the reactant and product corresponding to **act_sil_TS1**. The additional silanolate is 3.62 Å away from the silicon atom of the Pd-O-Si type complex at the reactant side (labelled as **act_sil_1** in Figure 3.2.23). In the transition state, the O-Si distance is 2.96 Å. The transition state structure is thus rather early, with a very small energy difference between **act_sil_1** and **act_sil_TS1**. However, the transition state lies 53.9 kcal/mol higher than the most stable structure, which is **Sil_1**. This can be understandable in the sense that **Sil_1** and **act_sil_1** have very different geometries. Indeed, in order to activate the silicon atom, one Pd-O bond should be first cleaved, and the silanolate generated should then move towards the silicon atom which is more than 5 Å away. This appears geometrically extremely challenging, and a barrier of more than 50 kcal/mol looks reasonable for such a move. At the product side, the phenyl group has been transferred to the metal

center, and the $(Me)_2Si=O$ unit has been caught by the additional silanolate to form a linear dimer. The oxygen atom of the $(Me)_2Si=O$ unit is still bound at the palladium, at 2.04 Å. This is thermodynamically favoured, and **act_sil_2** lies 46.9 kcal/mol lower than the transition state, but still 7.0 kcal/mol higher than **Sil_1**. The overall energy barrier is then prohibitively high, and definitively inconsistent with an activated process of a reaction occurring at room temperature.[215]

However, the possibility for the complex **Sil_1** to be present in the reaction media is low. The presence of a ligand on the metal center should greatly stabilize the process and the palladium catalyst contains a phosphine ligand. We computed thus a similar activated mechanism, but with a phosphine ligand.

3.2.5.4 Transmetalation step starting with the (Ph)(L)Pd(OSi(Me$_2$)Ph) complex, with L = R$_3$P. Added silanolate in an activated process

Figure 3.2.24 reports two transition state structures of an activated transmetalation with a phosphine (model system) ligand. The free energies reported below are relative to the separated reactants, namely **Conf_1** and **Silanolate**.

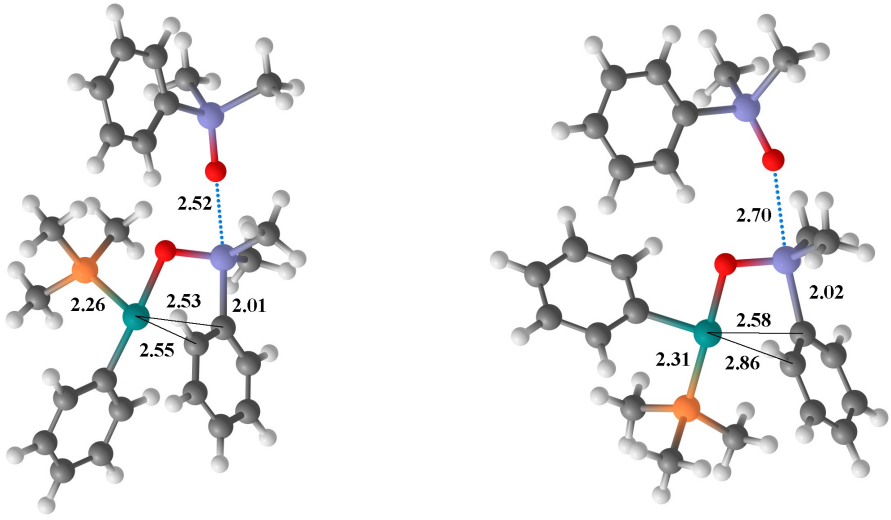

act_sil_phos_TS1 ***act_sil_phos_TS_trans***

-6.0 2.6

Figure 3.2.24 Transition state structures of an activated transmetalation on a (Ph)(Me$_3$P)Pd(OSi(Me$_2$)Ph) complex. Energy values are free energy (in kcal/mol) relative to the separated reactants: **Conf_1** and an anionic silanolate.

The pathway is detailed in Figure 3.2.25 where we can observe the very low barrier of the activated mechanism. Note that we chose to represent the pathway using **act_sil_phos_TS_trans**, and not **act_sil_phos_TS1** which is 8.6 kcal/mol lower in energy. However, we are confident that the same ideas and conceptual views

detailed below should be applicable for both isomers. **act_sil_phos_TS_trans** lies then 4.8 kcal/mol higher than the complex **act_sil_phos_2_trans**, and is only 2.6 kcal/mol higher than the separated reactants (Pd-O-Si type complex in the **Conf_1** arrangement and the silanolate). As expected, this process is extremely exothermic, **act_sil_phos_3_trans** being stabilized by more than 50 kcal/mol compared to the separated reactants. However, a very stable complex with two silanolates bound to the palladium has been found, labelled as **act_sil_phos_1_trans**. This complex is more stable than the separated reactants by more than 39 kcal/mol, and consequently, the real barrier for the activated transmetalation is of 42 kcal/mol. The additional silanolate prefers to bind to palladium rather than to the silicon. Such a barrier is too high to account for the experimental conditions reported for the activated mechanism.

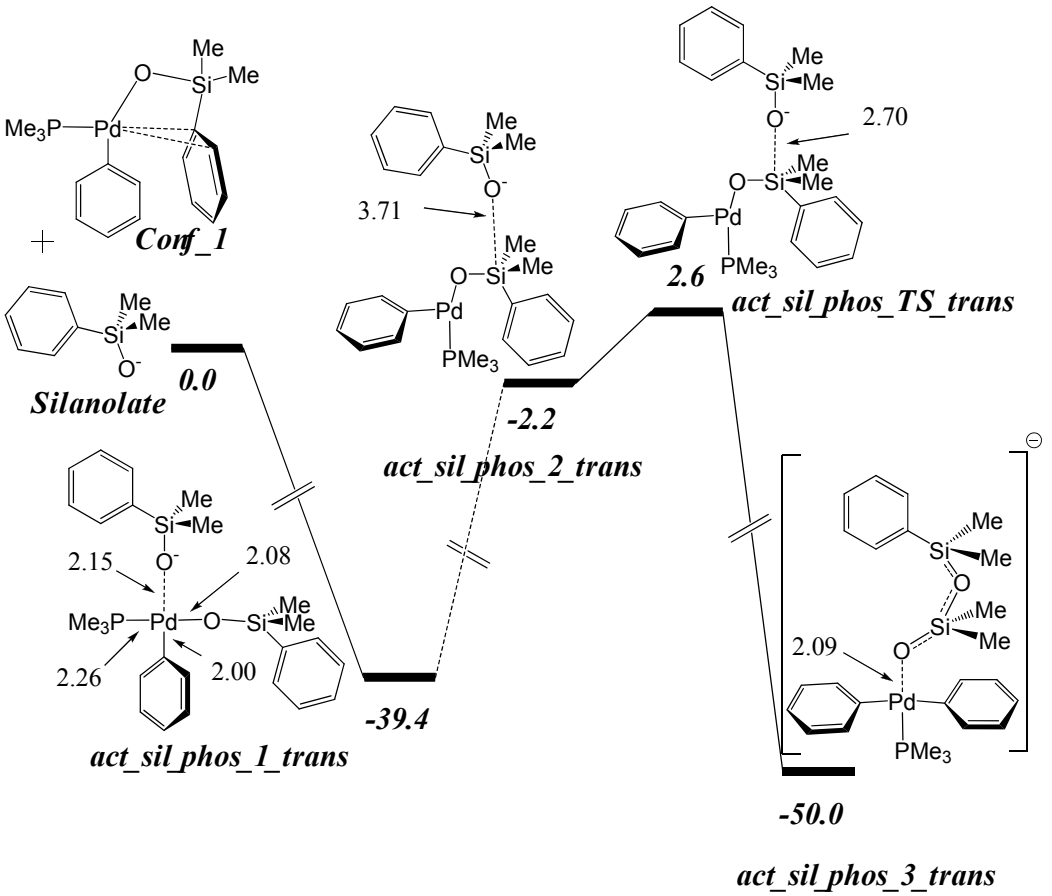

Figure 3.2.25 Silanolate activated transmetalation profile. Free energy values in kcal/mol. All these complexes (except **Conf_1**) are negatively charged.

However, raises the question of the probability to find two silanolates bound to the palladium at the same time. Each of these species is indeed accompanied by its corresponding cation (Cs^+, K^+, or Na^+), and the silanolate might bind better the cation than the palladium. We also note that the cation of the first silanolate which formed the Pd-O-Si type complex is likely to be near the negatively charged

oxygen. Since the cation is rather bulky (especially Cs^+, which is the cation which affords the fastest reactions), it might prevent a second silanolate to approach the metal center. The bulky group of the phosphine (not computed for this process) should increase again this steric hindrance. The second silanolate (the activating silanolate) might well be near the silicon atom, and far from the metal center. Consequently, the presence of the highly stable **act_sil_phos_1_trans** complex in solution can be questioned. Following this argumentation, the activated mechanism has a very low barrier, in agreement with the experimental data.

Finally, we would like to mention that such transition states corresponding to the attack of the negatively charged silanolate onto the silicon atom were very difficult to compute, and many convergence problems have been found.

3.2.6 Effect of the released siloxane. Computation of an autocatalytic reaction

We then considered the role of the siloxane moiety on the reaction. As depicted in several figures along this manuscript (see for instance Figure 3.1.1), the transmetalation step is concomitant with the release of the $(Me)_2Si=O$ unit from the Pd-O-Si type complex. This unit is very likely to polymerize, and the experimental characterization of this phenomenon is difficult. We envisioned the possibility for one of the siloxane units to activate the Pd-O-Si type complex, in a similar way to the one we proposed for dba. We used the highly constrained dimer of the siloxane unit, which would be present in the reaction media after a simple dimerization of two released siloxane units. A schematic representation of this hypothesis is given in Figure 3.2.26. The idea is that the silanone ($(Me)_2Si=O$) released after a first non-activated transmetalation step would immediately dimerize to form a dimeric form of a siloxane. Then, this species could attack the Pd-O-Si type complex (in this subsection we computed a complex generated from a bisphosphine aryl catalyst and an alkenyl silanolate) to form the product of transmetalation ready for the reductive elimination step, together with the release of a trimeric siloxane. This would be considered as a transmetalation step activated by a dimeric form of the siloxane.

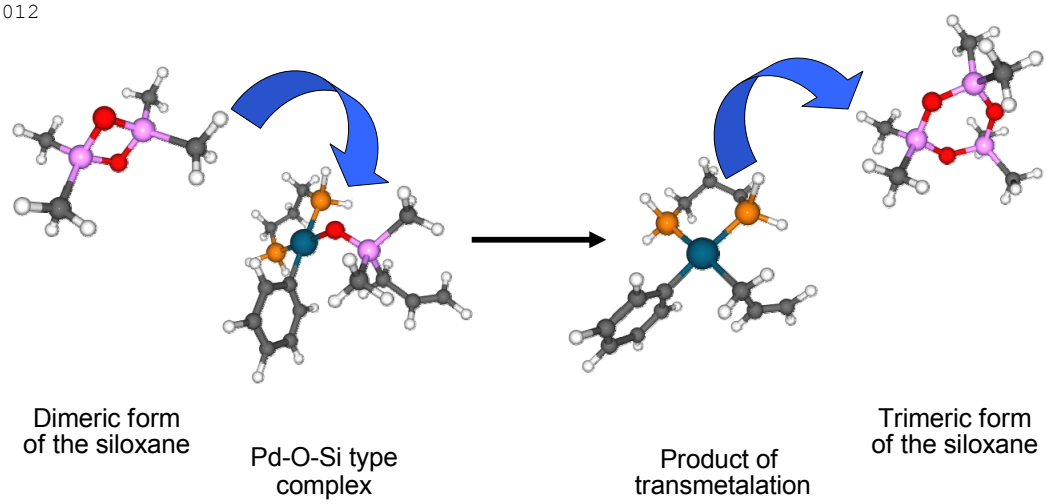

Figure 3.2.26 Schematic representation of the attack of the siloxane dimer to the Pd-O-Si type complex.

Figure 3.2.27 shows the computed profile for this activated mechanism. The profile can be described as a four step process. First, the dimeric siloxane is approaching, forming a weak interaction with the oxygen atom of the Pd-O-Si complex (**2_dim**). Then, the four-membered ring rotates (**3_dim**) and subsequently opens to form a trimeric form still bound to the complex (**4_dim**). Then the trimeric form of the silanone is released, together with formation of the product of transmetalation. The general pathway is very easy (the highest transition state **TS23_dim** is only 11.1 kcal/mol higher than the starting complex) and thermodynamically extremely favoured (46.6 kcal/mol lower than the starting complex).

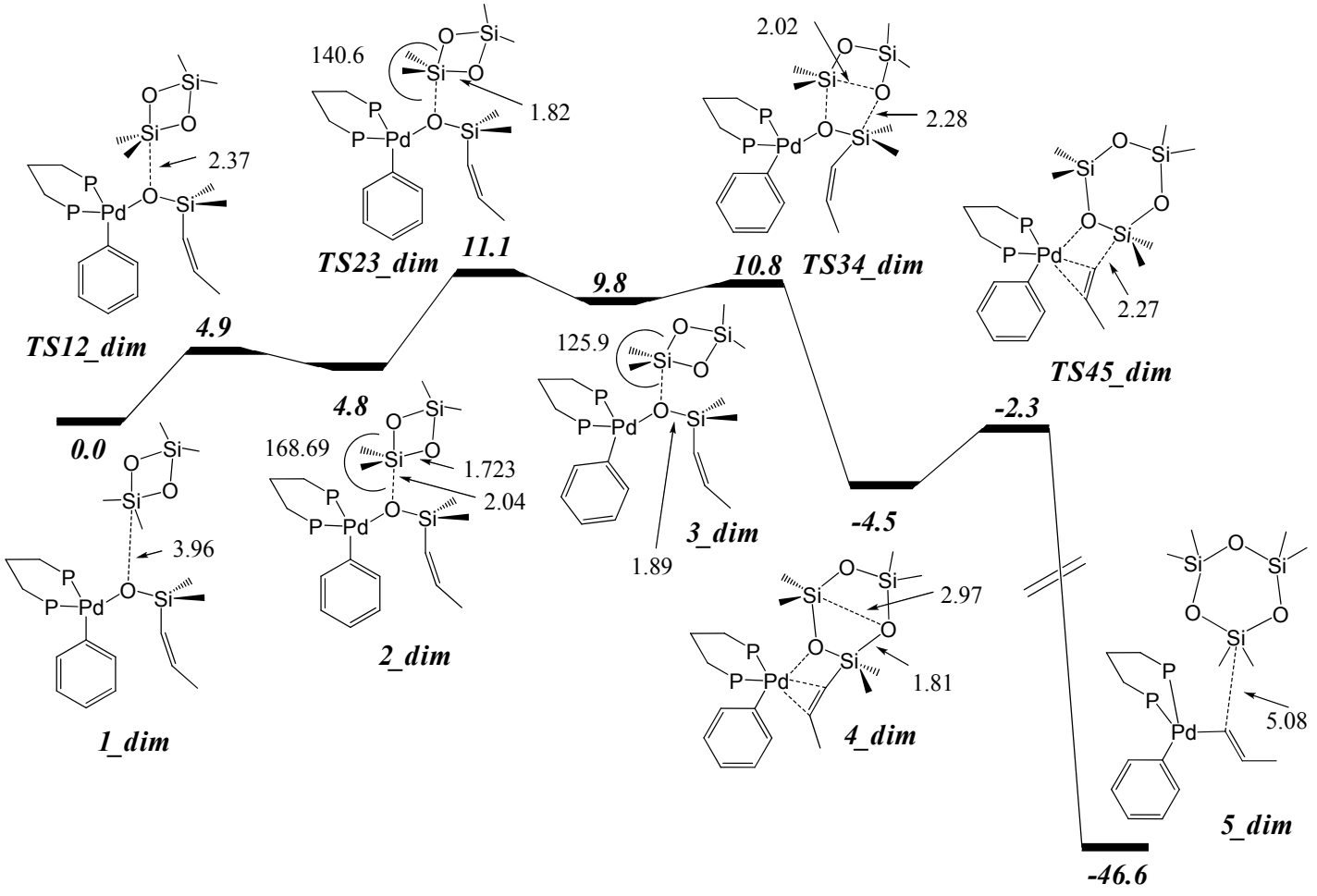

Figure 3.2.27 Dimeric siloxane assisted transmetalation step. Free energies in kcal/mol.

Nevertheless, contrary to other activating species (such as dba), the dimeric form of the siloxane is not present in the reaction media when the reaction starts. Indeed, it can be formed only after release of two $(Me)_2Si{=}O$ units, which means that a first transmetalation should occur beforehand to allow the presence of this activator. This particular configuration is typical from an autocatalytic reaction. Figure 3.2.28 depicts a refined and hypothetic catalytic cycle where the siloxane released would have a positive effect on the transmetalation.

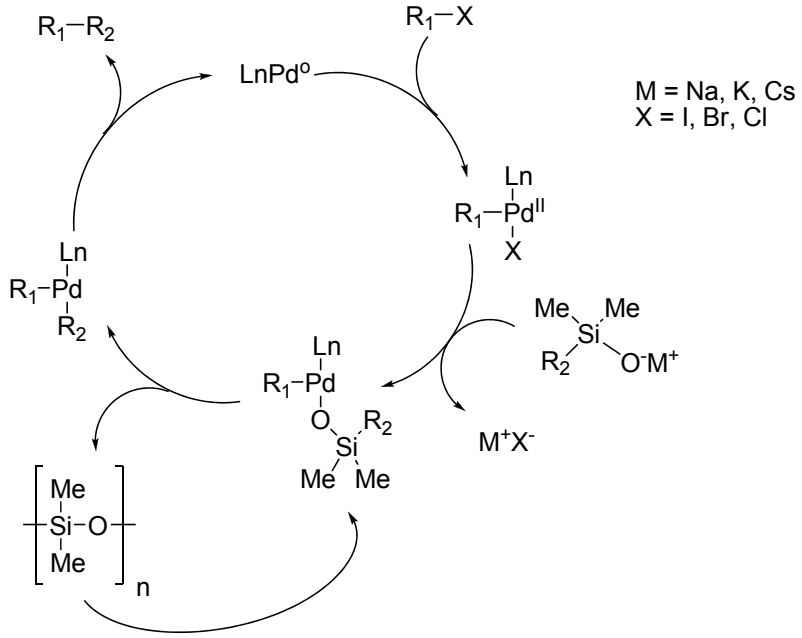

Figure 3.2.28 Catalytic cycle of the cross-coupling of silanolates taking into account the autocatalytic role of the released siloxane.

Such autocatalytic reactions are well-described and one of their features is the sigmoïdal shape of the curves obtained when kinetic studies are undertaken. As shown in Figure 3.2.29, the reaction proceeds slowly at the beginning because the main catalyst is not present in the reaction media. Then, once this catalyst (in our case we consider the hypothetic role of the siloxane released) is formed in a sufficient amount, the reaction speeds up. In other words, the rate of reaction would increase when the concentration of the siloxane increases.

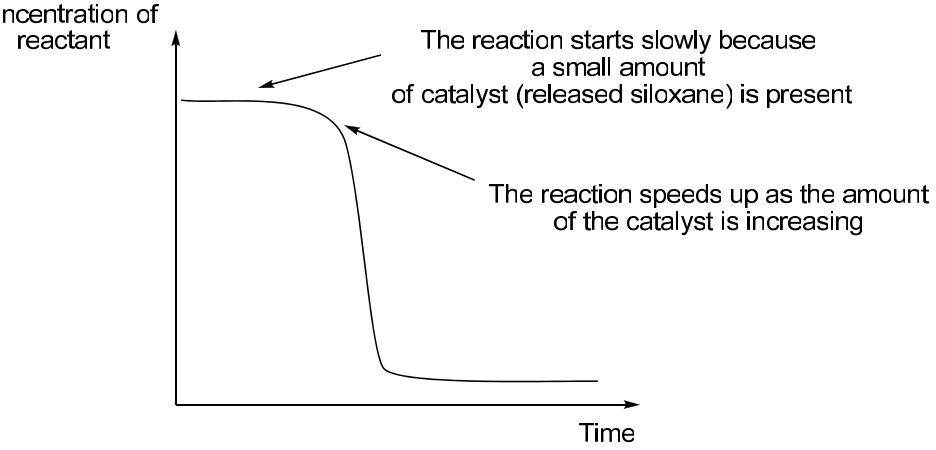

Figure 3.2.29 Typical curve of an autocatalytic reaction.

A number of examples can be found in the literature for heterogeneous and homogeneous autocatalytic reactions.[251, 252] All of them show sigmoïdal curves similar to the one depicted in Figure 3.2.29. However, this typical curve is completely absent in our case. All the kinetic studies carried out showed well-behaved kinetics.[215] Following this, the profile depicted in Figure 3.2.27 appears computationally accessible but the experimental data prevents its viability. We suspect that the problem in our model is that the dimer is a too reactive model for the polymer. Nevertheless, this profile is instructive because it shows that the polymerization of the $(Me)_2Si{=}O$ unit is a very easy process.

3.2.7 Concluding remarks

We clarified the dba-activated mechanism for the cross-coupling of crotyl silanolates. A new possible mode of action of dba through its carbonyl was discovered, and the π-olefinic character of the ligand was confirmed. The barriers obtained for the dba-activated mechanism are consistent with the experimental conditions required.
The selectivity issues of the cross-coupling of crotyl silanolates was explored, and the crucial role of the interconversion process could be confirmed. We proposed an explanation for the beneficial role of chloroform for the coupling of heterocyclic silanolates. A dichlorocarbene effect is believed to take advantage of the particular configuration of the Pd-O-Si type complex generated from heterocyclic silanolates. No such effects should be observed with Pd-O-Si type complexes generated from crotyl silanolates due to the η^2 interaction which takes place between the β and γ carbons and the metal center.
The beneficial role of the silanolate in excess under catalytic conditions was rationalized with the very low barriers obtained for that activated mechanism. We thus successfully computed the case of an activation of the silicon atom by an additional silanolate molecule. The calculations suggest that the phosphine dissociation is not required in the silanolate-activated process.

UNIVERSITAT ROVIRA I VIRGILI
COMPUTATIONAL STUDY OF C-H BOND CLEAVAGE AND C-C BOND FORMATION PROCESSES CATALYZED BY TRANSITION METAL COMPLEXES
Abel Jean Serge Locati
DL:T. 278-2012

Chapter 4

Conclusions

Our computational studies have led to a better understanding of the general reactivity of $TpNbCH_3(c\text{-}C_3H_5)(MeCCMe)$ and related complexes, in particular of their activity towards C-H activation. A computational method for the characterization of C-C agostic interactions in a series of niobium complexes, based on calculation of NMR coupling constants, has been proposed and satisfactorily evaluated in collaboration with the experimental group of Prof. Etienne. The reactivity of $TpNbCH_3(c\text{-}C_3H_5)(MeCCMe)$ with benzene has been fully characterized, with calculation of a full energy profile going through a η^2 cyclopropene intermediate, and satisfactory comparison of the computed profile with experimental kinetic analysis. The selectivity for sp^3 C-H (alkyl) or sp^2 C-H (aryl) activation of the same complex when confronted with several dimethylbenzenes has been rationalized. The methyl groups happens to play a critical role, with aryl activation favoured only when no *ortho* methyl groups are present in the ring. The conditions where competing migration processes, without intermolecular C-H activation, take place has been also investigated, and a mechanism through a niobium hydride has been characterized.

Our study on the palladium-catalyzed cross-coupling of silicon reagents leads to a better understanding of the reaction mechanism. The introduction of the real system in the computational treatment was found mandatory, calculations with smaller model phosphines produced qualitatively different results. We were able to compute reaction profiles for transmetalation in both the unactivated and the activated mechanisms for phenyl silanolate reactants. A variety of possibilities were evaluated for the unactivated mechanism, including carbometalation and rearrangement to Pd-Si-O type species, and the favoured one is the direct transfer of aryl from silicon to palladium. Phosphine dissociation appears likely, in the case of bisphosphines involving the decoordination of one of the arms. The presence of the halide ligand in the metal coordination sphere lowers the transmetalation barrier. In the activated mechanism, the coordination of the additional silanolate to the ligand creates a hypervalent silicon center, lowering the reaction barriers, which fits well with the experimental rates. The counter anion and/or the halide ligand must play a decisive role in the activated mechanism, preventing the simultaneous binding of two silanolates to the metal center.

Our calculations also explain the beneficial role of using $Pd(dba)_2$ as pre-catalyst for this cross-coupling processes, as well as selectivity issues when allyl and crotyl silanolates are used. The carbonyl of dba plays a major role in the activation of the silicon center, while the ligand coordinates palladium through its double bonds. Similar roles can be played by benzoquinone or carbon dioxide. Our study on allyl and crotyl silanolates confirms the critical role of the interconversion process, especially in the case of the ortho-ester substituted system. The beneficial role of chloroform in the coupling of heteroaromatic silanolates is due to the formation of very stable species between the Pd-O-Si type complex and a dichlorocarbene during the transmetalation.

References

1. Von Ragué Schleyer, P., *Encyclopedia of Computational Chemistry* **1998**, John Wiley & Sons.
2. Cramer, C. J., *Essentials of Computational Chemistry* **2002**, John Wiley & Sons.
3. Van Santen, R. A.; Sautet, P. E., *Computational methods in catalysis and materials science* **2009**, Wiley-VCH.
4. Siegel, J. B.; Zanghellini, A.; Lovick, H. M.; Kiss, G.; Lambert, A. R.; Clair, J. L. S.; Gallaher, J. L.; Hilvert, D.; Gelb, M. H.; Stoddard, B. L.; Houk, K. N.; Michael, F. E.; Baker, D., *Science* **2010,** 329, (5989), 309-313.
5. Dinner, A. R.; Sali, A.; Smith, L. J.; Dobson, C. M.; Karplus, M., *Trends in Biochemical Sciences* **2000,** 25, (7), 331-339.
6. Maseras, F.; Lledós, A. E., *Computational modeling of homogeneous catalysis* **2002**, Springer.
7. Morokuma, K.; Musaev, D. G., *Computational modeling for homogeneous and enzymatic catalysis* **2008**, Wiley-VCH.
8. Maseras, F.; Morokuma, K., *J. Comput. Chem.* **1995,** 16, (9), 1170-1179.
9. Dapprich, S.; Komaromi, I.; Byun, K. S.; Morokuma, K.; Frisch, M. J., *Journal of Molecular Structure-Theochem* **1999,** 461, 1-21.
10. Jiang, L.; Althoff, E. A.; Clemente, F. R.; Doyle, L.; Rothlisberger, D.; Zanghellini, A.; Gallaher, J. L.; Betker, J. L.; Tanaka, F.; Barbas, C. F.; Hilvert, D.; Houk, K. N.; Stoddard, B. L.; Baker, D., *Science* **2008,** 319, (5868), 1387-1391.
11. Rothlisberger, D.; Khersonsky, O.; Wollacott, A. M.; Jiang, L.; DeChancie, J.; Betker, J.; Gallaher, J. L.; Althoff, E. A.; Zanghellini, A.; Dym, O.; Albeck, S.; Houk, K. N.; Tawfik, D. S.; Baker, D., *Nature* **2008,** 453, (7192), 190-U4.
12. Tomasi, J.; Mennucci, B.; Cammi, R., *Chem. Rev.* **2005,** 105, (8), 2999-3093.
13. Hartwig, J. F., *Organotransition metal chemistry* **2010**, University Science Books.

14. Periana, R. A.; Bhalla, G.; Tenn, W. J.; Young, K. J. H.; Liu, X. Y.; Mironov, O.; Jones, C. J.; Ziatdinov, V. R., *J. Mol. Catal. A: Chem.* **2004,** 220, (1), 7-25.
15. Diaz-Requejo, M. M.; Perez, P. J., *Chem. Rev.* **2008,** 108, (8), 3379-3394.
16. Crabtree, R. H., *The Organometallic Chemistry of the Transition Metals* **2005**, fourth ed., John Wiley & Sons, New York.
17. Bergman, R. G., *Science* **1984,** 223, (4639), 902-908.
18. Labinger, J. A.; Bercaw, J. E., *Nature* **2002,** 417, (6888), 507-514.
19. Bergman, R. G., *Nature* **2007,** 446, (7134), 391-393.
20. Shilov, A. E.; Shul'pin, G. B., *Chem. Rev.* **1997,** 97, (8), 2879-2932.
21. Chatt, J.; Davidson, J. M., *J. Chem. Soc.* **1965**, 843.
22. Shilov, A. E.; Shteinman, A. A., *Coord. Chem. Rev.* **1977,** 24, (2-3), 97-143.
23. Periana, R. A.; Taube, D. J.; Evitt, E. R.; Loffler, D. G.; Wentrcek, P. R.; Voss, G.; Masuda, T., *Science* **1993,** 259, (5093), 340-343.
24. Periana, R. A.; Taube, D. J.; Gamble, S.; Taube, H.; Satoh, T.; Fujii, H., *Science* **1998,** 280, (5363), 560-564.
25. Balcells, D.; Clot, E.; Eisenstein, O., *Chem. Rev.* **2010,** 110, (2), 749-823.
26. Dedieu, A., *Chem. Rev.* **2000,** 100, (2), 543-600.
27. Niu, S. Q.; Hall, M. B., *Chem. Rev.* **2000,** 100, (2), 353-405.
28. Lin, Z. Y., *Coord. Chem. Rev.* **2007,** 251, (17-20), 2280-2291.
29. Janowicz, A. H.; Bergman, R. G., *J. Am. Chem. Soc.* **1982,** 104, (1), 352-354.
30. Janowicz, A. H.; Bergman, R. G., *J. Am. Chem. Soc.* **1983,** 105, (12), 3929-3939.
31. Arndtsen, B. A.; Bergman, R. G.; Mobley, T. A.; Peterson, T. H., *Acc. Chem. Res.* **1995,** 28, (3), 154-162.
32. Burger, P.; Bergman, R. G., *J. Am. Chem. Soc.* **1993,** 115, (22), 10462-10463.
33. Jones, W. D.; Feher, F. J., *Acc. Chem. Res.* **1989,** 22, (3), 91-100.
34. Bi, S. W.; Zhang, Z. W.; Zhu, S. F., *Chem. Phys. Lett.* **2006,** 431, (4-6), 385-389.
35. Boutadla, Y.; Davies, D. L.; Macgregor, S. A.; Poblador-Bahamonde, A. I., *Dalton Trans.* **2009**, (30), 5820-5831.
36. Thompson, M. E.; Baxter, S. M.; Bulls, A. R.; Burger, B. J.; Nolan, M. C.; Santarsiero, B. D.; Schaefer, W. P.; Bercaw, J. E., *J. Am. Chem. Soc.* **1987,** 109, (1), 203-219.
37. Sherer, E. C.; Cramer, C. J., *Organometallics* **2003,** 22, (8), 1682-1689.
38. Vastine, B. A.; Hall, M. B., *J. Am. Chem. Soc.* **2007,** 129, (40), 12068-12069.
39. Perutz, R. N.; Sabo-Etienne, S., *Angew. Chem., Int. Ed.* **2007,** 46, (15), 2578-2592.
40. Walsh, P. J.; Hollander, F. J.; Bergman, R. G., *J. Am. Chem. Soc.* **1988,** 110, (26), 8729-8731.

41. Bailey, B. C.; Fan, H. J.; Baum, E. W.; Huffman, J. C.; Baik, M. H.; Mindiola, D. J., *J. Am. Chem. Soc.* **2005,** 127, (46), 16016-16017.
42. Bailey, B. C.; Fan, H. J.; Huffman, J. C.; Baik, M. H.; Mindiola, D. J., *J. Am. Chem. Soc.* **2007,** 129, (28), 8781-8793.
43. Braga, A. A. C.; Maseras, F.; Urbano, J.; Caballero, A.; Diaz-Requejo, M. M.; Perez, P. J., *Organometallics* **2006,** 25, (22), 5292-5300.
44. Caballero, A.; Despagnet-Ayoub, E.; Diaz-Requejo, M. M.; Diaz-Rodriguez, A.; Gonzalez-Nunez, M. E.; Mello, R.; Munoz, B. K.; Ojo, W. S.; Asensio, G.; Etienne, M.; Perez, P. J., *Science* **2011,** 332, (6031), 835-838.
45. Davies, D. L.; Donald, S. M. A.; Macgregor, S. A., *J. Am. Chem. Soc.* **2005,** 127, (40), 13754-13755.
46. Garcia-Cuadrado, D.; Braga, A. A. C.; Maseras, F.; Echavarren, A. M., *J. Am. Chem. Soc.* **2006,** 128, (4), 1066-1067.
47. Stuart, D. R.; Fagnou, K., *Science* **2007,** 316, (5828), 1172-1175.
48. Clot, E.; Eisenstein, O., *Struc. Bond.* **2004,** 113, 1-36.
49. Brookhart, M.; Green, M. L. H.; Parkin, G., *Proc. Natl. Acad. Sci. USA* **2007,** 104, (17), 6908-6914.
50. Chirik, P. J.; Dalleska, N. F.; Henling, L. M.; Bercaw, J. E., *Organometallics* **2005,** 24, (11), 2789-2794.
51. Ivin, K. J.; Rooney, J. J.; Stewart, C. D.; Green, M. L. H.; Mahtab, R., *J. Chem. Soc.-Chem. Commun.* **1978**, (14), 604-606.
52. Brookhart, M.; Green, M. L. H., *J. Organomet. Chem.* **1983,** 250, (1), 395-408.
53. Brookhart, M.; Green, M. L. H.; Wong, L. L., *Prog. Inorg. Chem.* **1988,** 36, 1-124.
54. Maseras, F.; Crabtree, R. H., *Inorganica Chimica Acta* **2004,** 357, (1), 345-346.
55. Scherer, W.; McGrady, G. S., *Angew. Chem., Int. Ed.* **2004,** 43, (14), 1782-1806.
56. Metal-Catalyzeed Cross-Coupling Reaction (Eds.:A. De Meijere, F. D., *Wiley-VCH, Weinheim* **2004**.
57. de Vries, J. G., *Can. J. Chem.* **2001,** 79, (5-6), 1086-1092.
58. Nicolaou, K. C.; Bulger, P. G.; Sarlah, D., *Angew. Chem., Int. Ed.* **2005,** 44, (29), 4442-4489.
59. Denmark, S. E.; Liu, J. H. C., *Angew. Chem., Int. Ed.* **2010,** 49, (17), 2978-2986.
60. Ullmann, F.; Bielecki, J., *Ber. Dtsch. Chem. Ges.* **1901,** 34, 2174-2185.
61. Fanta, P. E., *Synthesis-Stuttgart* **1974**, (1), 9-21.
62. Mizoroki, T.; Mori, K.; Ozaki, A., *Bulletin of the Chemical Society of Japan* **1971,** 44, (2), 581.
63. Heck, R. F.; Nolley, J. P., *J. Org. Chem.* **1972,** 37, (14), 2320-&.
64. Heck, R. F., *Acc. Chem. Res.* **1979,** 12, (4), 146-151.
65. Glaser, C., *Ber. Dtsch. Chem. Ges.* **1869,** 2, 422-424.
66. Glaser, C., *Ann. Chem. Pharm.* **1870,** 154, 137-171.
67. Eglinton, G.; Galbraith, A. R., *Chem. Ind. (London)* **1956**, 737-738.

68. Hay, A. S., *J. Org. Chem.* **1962,** 27, (9), 3320-&.
69. Sonogashira, K.; Tohda, Y.; Hagihara, N., *Tetrahedron Lett.* **1975**, (50), 4467-4470.
70. Siemsen, P.; Livingston, R. C.; Diederich, F., *Angew. Chem., Int. Ed.* **2000,** 39, (15), 2633-2657.
71. Miyaura, N.; Yamada, K.; Suzuki, A., *Tetrahedron Lett.* **1979,** 20, (36), 3437-3440.
72. Braga, A. A. C.; Morgon, N. H.; Ujaque, G.; Lledos, A.; Maseras, F., *J. Organomet. Chem.* **2006,** 691, (21), 4459-4466.
73. Braga, A. A. C.; Ujaque, G.; Maseras, F., *Organometallics* **2006,** 25, (15), 3647-3658.
74. Braga, A. A. C.; Morgon, N. H.; Ujaque, G.; Maseras, F., *J. Am. Chem. Soc.* **2005,** 127, (25), 9298-9307.
75. Miyaura, N.; Suzuki, A., *Chem. Rev.* **1995,** 95, (7), 2457-2483.
76. Milstein, D.; Stille, J. K., *J. Am. Chem. Soc.* **1978,** 100, (11), 3636-3638.
77. Stille, J. K., *Angew. Chem., Int. Ed.* **1986,** 25, (6), 508-523.
78. Echavarren, A. M.; Stille, J. K., *J. Am. Chem. Soc.* **1987,** 109, (18), 5478-5486.
79. Negishi, E.; King, A. O.; Okukado, N., *J. Org. Chem.* **1977,** 42, (10), 1821-1823.
80. Negishi, E. I., *Acc. Chem. Res.* **1982,** 15, (11), 340-348.
81. Hartwig, J. F., *Nature* **2008,** 455, (7211), 314-322.
82. Hartwig, J. F., *Acc. Chem. Res.* **1998,** 31, (12), 852-860.
83. Hartwig, J. F.; Kawatsura, M.; Hauck, S. I.; Shaughnessy, K. H.; Alcazar-Roman, L. M., *J. Org. Chem.* **1999,** 64, (15), 5575-5580.
84. Muci, A. R.; Buchwald, S. L., *Cross-Coupling Reactions* **2002,** 219, 131-209.
85. Kosugi, M.; Kameyama, M.; Migita, T., *Chem. Lett.* **1983**, (6), 927-928.
86. Tokuyama, H.; Yokoshima, S.; Yamashita, T.; Fukuyama, T., *Tetrahedron Lett.* **1998,** 39, (20), 3189-3192.
87. Hatanaka, Y.; Hiyama, T., *J. Org. Chem.* **1988,** 53, (4), 918-920.
88. Denmark, S. E., *J. Org. Chem.* **2009,** 74, (8), 2915-2927.
89. Hassan, J.; Sevignon, M.; Gozzi, C.; Schulz, E.; Lemaire, M., *Chem. Rev.* **2002,** 102, (5), 1359-1469.
90. Xue, L. Q.; Lin, Z. Y., *Chem. Soc. Rev.* **2010,** 39, (5), 1692-1705.
91. Shen, X. Q.; Jones, G. O.; Watson, D. A.; Bhayana, B.; Buchwald, S. L., *J. Am. Chem. Soc.* **2010,** 132, (32), 11278-11287.
92. Kozuch, S.; Martin, J. M. L., *ACS Catalysis* **2011,** 1, (4), 246-253.
93. Balcells, D.; Maseras, F.; Keay, B. A.; Ziegler, T., *Organometallics* **2004,** 23, (11), 2784-2796.
94. Backtorp, C.; Norrby, P. O., *J. Mol. Catal. A: Chem.* **2010,** 328, (1-2), 108-113.
95. Ariafard, A.; Yates, B. F., *J. Am. Chem. Soc.* **2009,** 131, (39), 13981-13991.
96. Sugiyama, A.; Ohnishi, Y. Y.; Nakaoka, M.; Nakao, Y.; Sato, H.; Sakaki, S.; Hiyama, T., *J. Am. Chem. Soc.* **2008,** 130, (39), 12975-12985.

97. Ahlquist, M.; Fristrup, P.; Tanner, D.; Norrby, P. O., *Organometallics* **2006,** 25, (8), 2066-2073.
98. McMullin, C. L.; Jover, J.; Harvey, J. N.; Fey, N., *Dalton Trans.* **2010,** 39, (45), 10833-10836.
99. Low, J. J.; Goddard, W. A., *J. Am. Chem. Soc.* **1986,** 108, (20), 6115-6128.
100. Hartwig, J. F., *Inorg. Chem.* **2007,** 46, (6), 1936-1947.
101. Ananikov, V. P.; Musaev, D. G.; Morokuma, K., *Eur. J. Inorg. Chem.* **2007**, (34), 5390-5399.
102. Perez-Rodriguez, M.; Braga, A. A. C.; Garcia-Melchor, M.; Perez-Temprano, M. H.; Casares, J. A.; Ujaque, G.; de Lera, A. R.; Alvarez, R.; Maseras, F.; Espinet, P., *J. Am. Chem. Soc.* **2009,** 131, (10), 3650-3657.
103. Glorius, F., *Angew. Chem., Int. Ed.* **2004,** 43, (26), 3364-3366.
104. Johnson, J. B.; Rovis, T., *Angew. Chem., Int. Ed.* **2008,** 47, (5), 840-871.
105. Amatore, C.; Broeker, G.; Jutand, A.; Khalil, F., *J. Am. Chem. Soc.* **1997,** 119, (22), 5176-5185.
106. Amatore, C.; Jutand, A., *Coord. Chem. Rev.* **1998,** 178, 511-528.
107. Amatore, C.; Jutand, A.; Meyer, G.; Atmani, H.; Khalil, F.; Chahdi, F. O., *Organometallics* **1998,** 17, (14), 2958-2964.
108. Amatore, C.; Jutand, A.; Khalil, F.; Mbarki, M. A.; Mottier, L., *Organometallics* **1993,** 12, (8), 3168-3178.
109. Littke, A. F.; Fu, G. C., *Angew. Chem., Int. Ed.* **1998,** 37, (24), 3387-3388.
110. Littke, A. F.; Fu, G. C., *Angew. Chem., Int. Ed.* **2002,** 41, (22), 4176-4211.
111. Littke, A. F.; Dai, C. Y.; Fu, G. C., *J. Am. Chem. Soc.* **2000,** 122, (17), 4020-4028.
112. Lu, Z.; Fu, G. C., *Angew. Chem., Int. Ed.* **2010,** 49, (37), 6676-6678.
113. Lu, Z.; Wilsily, A.; Fu, G. C., *J. Am. Chem. Soc.* **2011,** 133, (21), 8154-8157.
114. Chen, X.; Engle, K. M.; Wang, D. H.; Yu, J. Q., *Angew. Chem., Int. Ed.* **2009,** 48, (28), 5094-5115.
115. Fermi, E., *Rend. Accad. Naz. Lincei* **1927,** 6, 602-607.
116. Thomas, L., *Proc. Cambridge Philos. Soc.* **1927,** 23, 542-548.
117. Slater, J. C., *Phys. Rev.* **1951,** 81, (3), 385-390.
118. Hohenberg, P.; Kohn, W., *Phys. Rev. B* **1964,** 136, 864-871.
119. Kohn, W.; Sham, L. J., *Phys. Rev.* **1965,** 140, (4A), 1133-1138.
120. Koch, W.; Holthausen, M. C., *A chemist's Guide to Density Functional Theory, Second Edition, Wiley-VCH* **2001**.
121. Dirac, P. A. M., *Proc. Cambridge Philos. Soc.* **1930,** 26, 376-385.
122. Tao, J. M.; Perdew, J. P., *J. Chem. Phys.* **2005,** 122, (11), 7.
123. Kurth, S.; Perdew, J. P.; Blaha, P., *Int. J. Quantum Chem.* **1999,** 75, (4-5), 889-909.
124. Becke, A. D., *Phys. Rev. A* **1988,** 38, (6), 3098-3100.
125. Becke, A. D., *J. Chem. Phys.* **1992,** 96, (3), 2155-2160.
126. Becke, A. D., *J. Chem. Phys.* **1992,** 97, (12), 9173-9177.
127. Becke, A. D., *J. Chem. Phys.* **1993,** 98, (7), 5648-5652.
128. Becke, A. D., *J. Chem. Phys.* **1996,** 104, (3), 1040-1046.

129. Perdew, J. P., *Phys. Rev. B* **1986,** 33, (12), 8822-8824.
130. Perdew, J. P.; Burke, K.; Ernzerhof, M., *Phys. Rev. Lett.* **1996,** 77, (18), 3865-3868.
131. Perdew, J. P.; Chevary, J. A.; Vosko, S. H.; Jackson, K. A.; Pederson, M. R.; Singh, D. J.; Fiolhais, C., *Phys. Rev. B* **1992,** 46, (11), 6671-6687.
132. Lee, C. T.; Yang, W. T.; Parr, R. G., *Phys. Rev. B* **1988,** 37, (2), 785-789.
133. Adamo, C.; Barone, V., *J. Chem. Phys.* **1999,** 110, (13), 6158-6170.
134. Tao, J. M.; Perdew, J. P.; Staroverov, V. N.; Scuseria, G. E., *Phys. Rev. Lett.* **2003,** 91, (14), 4.
135. Zhao, Y.; Truhlar, D. G., *Theo. Chem. Acc.* **2008,** 120, (1-3), 215-241.
136. Schwabe, T.; Grimme, S., *Phys. Chem. Chem. Phys.* **2007,** 9, (26), 3397-3406.
137. Sousa, S. F.; Fernandes, P. A.; Ramos, M. J., *J. Phy. Chem. A* **2007,** 111, (42), 10439-10452.
138. Perdew, J. P.; Ruzsinszky, A.; Constantin, L. A.; Sun, J. W.; Csonka, G. I., *J. Chem. Theory Comput.* **2009,** 5, (4), 902-908.
139. Tsuzuki, S.; Luthi, H. P., *J. Chem. Phys.* **2001,** 114, (9), 3949-3957.
140. Zhao, Y.; Truhlar, D. G., *Acc. Chem. Res.* **2008,** 41, (2), 157-167.
141. Grimme, S., *J. Comput. Chem.* **2006,** 27, (15), 1787-1799.
142. Hohenstein, E. G.; Chill, S. T.; Sherrill, C. D., *J. Chem. Theory Comput.* **2008,** 4, (12), 1996-2000.
143. Simon, L.; Goodman, J. M., *Org. Biomol. Chem.* **2011,** 9, (3), 689-700.
144. Trofimen.S, *J. Am. Chem. Soc.* **1966,** 88, (8), 1842-&.
145. Trofimenko, S., *Scorpionates: The Coordination of Poly(pyrazolyl)borate Ligands* **1999**, Imperial College Press: London.
146. Trofimenko, S., *J. Chem. Educ.* **2005,** 82, (11), 1715-1720.
147. Trofimenko, S., *Chem. Rev.* **1993,** 93, (3), 943-980.
148. Etienne, M., *Coord. Chem. Rev.* **1996,** 156, 201-236.
149. Lein, M., *Coord. Chem. Rev.* **2009,** 253, (5-6), 625-634.
150. Tomaszewski, R.; Hyla-Kryspin, I.; Mayne, C. L.; Arif, A. M.; Gleiter, R.; Ernst, R. D., *J. Am. Chem. Soc.* **1998,** 120, (12), 2959-2960.
151. Harvey, B. G.; Mayne, C. L.; Arif, A. M.; Ernst, R. D., *J. Am. Chem. Soc.* **2005,** 127, (47), 16426-16435.
152. Brayshaw, S. K.; Green, J. C.; Kociok-Kohn, G.; Sceats, E. L.; Weller, A. S., *Angew. Chem., Int. Ed.* **2006,** 45, (3), 452-456.
153. Brayshaw, S. K.; Sceats, E. L.; Green, J. C.; Weller, A. S., *Proc. Natl. Acad. Sci. USA* **2007,** 104, (17), 6921-6926.
154. Chaplin, A. B.; Weller, A. S., *Organometallics* **2010,** 29, (10), 2332-2342.
155. Vigalok, A.; Rybtchinski, B.; Shimon, L. J. W.; Ben-David, Y.; Milstein, D., *Organometallics* **1999,** 18, (5), 895-905.
156. Goldfuss, B.; Schleyer, P. V.; Hampel, F., *J. Am. Chem. Soc.* **1996,** 118, (48), 12183-12189.
157. Gandelman, M.; Shimon, L. J. W.; Milstein, D., *Chem.-Eur. J.* **2003,** 9, (18), 4295-4300.

158. Jaffart, J.; Etienne, M.; Reinhold, M.; McGrady, J. E.; Maseras, F., *Chem. Comm.* **2003**, (7), 876-877.
159. Jaffart, J.; Mathieu, R.; Etienne, M.; McGrady, J. E.; Eisenstein, O.; Maseras, F., *Chem. Comm.* **1998**, (18), 2011-2012.
160. Jaffart, J.; Etienne, M.; Maseras, F.; McGrady, J. E.; Eisenstein, O., *J. Am. Chem. Soc.* **2001,** 123, (25), 6000-6013.
161. Pantazis, D. A.; McGrady, J. E.; Besora, M.; Maseras, F.; Etienne, M., *Organometallics* **2008,** 27, (6), 1128-1134.
162. Etienne, M.; McGrady, J. E.; Maseras, F., *Coord. Chem. Rev.* **2009,** 253, (5-6), 635-646.
163. Gaussian 03, R. C., Frisch, M. J.; Trucks, G. W.; Schlegel, H. B.; Scuseria, G. E.; Robb, M. A.; Cheeseman, J. R.; Montgomery, Jr., J. A.; Vreven, T.; Kudin, K. N.; Burant, J. C.; Millam, J. M.; Iyengar, S. S.; Tomasi, J.; Barone, V.; Mennucci, B.; Cossi, M.; Scalmani, G.; Rega, N.; Petersson, G. A.; Nakatsuji, H.; Hada, M.; Ehara, M.; Toyota, K.; Fukuda, R.; Hasegawa, J.; Ishida, M.; Nakajima, T.; Honda, Y.; Kitao, O.; Nakai, H.; Klene, M.; Li, X.; Knox, J. E.; Hratchian, H. P.; Cross, J. B.; Bakken, V.; Adamo, C.; Jaramillo, J.; Gomperts, R.; Stratmann, R. E.; Yazyev, O.; Austin, A. J.; Cammi, R.; Pomelli, C.; Ochterski, J. W.; Ayala, P. Y.; Morokuma, K.; Voth, G. A.; Salvador, P.; Dannenberg, J. J.; Zakrzewski, V. G.; Dapprich, S.; Daniels, A. D.; Strain, M. C.; Farkas, O.; Malick, D. K.; Rabuck, A. D.; Raghavachari, K.; Foresman, J. B.; Ortiz, J. V.; Cui, Q.; Baboul, A. G.; Clifford, S.; Cioslowski, J.; Stefanov, B. B.; Liu, G.; Liashenko, A.; Piskorz, P.; Komaromi, I.; Martin, R. L.; Fox, D. J.; Keith, T.; Al-Laham, M. A.; Peng, C. Y.; Nanayakkara, A.; Challacombe, M.; Gill, P. M. W.; Johnson, B.; Chen, W.; Wong, M. W.; Gonzalez, C.; and Pople, J. A.; Gaussian, Inc., Wallingford CT, **2004**.
164. Hay, P. J.; Wadt, W. R., *J. Chem. Phys.* **1985,** 82, (1), 299-310.
165. Wadt, W. R.; Hay, P. J., *J. Chem. Phys.* **1985,** 82, (1), 284-298.
166. Ehlers, A. W.; Bohme, M.; Dapprich, S.; Gobbi, A.; Hollwarth, A.; Jonas, V.; Kohler, K. F.; Stegmann, R.; Veldkamp, A.; Frenking, G., *Chem. Phys. Lett.* **1993,** 208, (1-2), 111-114.
167. Hehre, W. J.; Ditchfield, R.; Pople, J. A., *J. Chem. Phys.* **1972,** 56, (5), 2257-2261.
168. Francl, M. M.; Pietro, W. J.; Hehre, W. J.; Binkley, J. S.; Gordon, M. S.; Defrees, D. J.; Pople, J. A., *J. Chem. Phys.* **1982,** 77, (7), 3654-3665.
169. Ditchfie.R, *Molecular Physics* **1974,** 27, (4), 789-807.
170. Jaffart, J.; Cole, M. L.; Etienne, M.; Reinhold, M.; McGrady, J. E.; Maseras, F., *Dalton Trans.* **2003**, (21), 4057-4064.
171. Boulho, C.; Keys, T.; Coppel, Y.; Vendier, L.; Etienne, M.; Locati, A.; Bessac, F.; Maseras, F.; Pantazis, D. A.; McGrady, J. E., *Organometallics* **2009,** 28, (4), 940-943.
172. Bax, A.; Freeman, R.; Frenkiel, T. A.; Levitt, M. H., *J. Magn. Reson.* **1981,** 43, (3), 478-483.
173. Autschbach, J., *Struct. Bond.* **2004,** 112, 1-48.
174. Solans-Monfort, X.; Eisenstein, O., *Polyhedron* **2006,** 25, (2), 339-348.

175. Jankowski, P.; Kamienskatrela, K.; Minksztym, K.; Wicha, J., *J. Organomet. Chem.* **1993,** 460, (1), 15-18.
176. Kamienska-Trela, K.; Bernatowicz, P.; Luttke, W.; Machinek, R.; Traetteberg, M., *Magn. Reson. Chem.* **2002,** 40, (10), 640-646.
177. Oulie, P.; Boulho, C.; Vendier, L.; Coppel, Y.; Etienne, M., *J. Am. Chem. Soc.* **2006,** 128, (50), 15962-15963.
178. Gaussian 09, R. A., Frisch, M. J.; Trucks, G. W.; Schlegel, H. B.; Scuseria, G. E.; Robb, M. A.; Cheeseman, J. R.; Scalmani, G.; Barone, V.; Mennucci, B.; Petersson, G. A.; Nakatsuji, H.; Caricato, M.; Li, X.; Hratchian, H. P.; Izmaylov, A. F.; Bloino, J.; Zheng, G.; Sonnenberg, J. L.; Hada, M.; Ehara, M.; Toyota, K.; Fukuda, R.; Hasegawa, J.; Ishida, M.; Nakajima, T.; Honda, Y.; Kitao, O.; Nakai, H.; Vreven, T.; Montgomery, Jr., J. A.; Peralta, J. E.; Ogliaro, F.; Bearpark, M.; Heyd, J. J.; Brothers, E.; Kudin, K. N.; Staroverov, V. N.; Kobayashi, R.; Normand, J.; Raghavachari, K.; Rendell, A.; Burant, J. C.; Iyengar, S. S.; Tomasi, J.; Cossi, M.; Rega, N.; Millam, N. J.; Klene, M.; Knox, J. E.; Cross, J. B.; Bakken, V.; Adamo, C.; Jaramillo, J.; Gomperts, R.; Stratmann, R. E.; Yazyev, O.; Austin, A. J.; Cammi, R.; Pomelli, C.; Ochterski, J. W.; Martin, R. L.; Morokuma, K.; Zakrzewski, V. G.; Voth, G. A.; Salvador, P.; Dannenberg, J. J.; Dapprich, S.; Daniels, A. D.; Farkas, Ö.; Foresman, J. B.; Ortiz, J. V.; Cioslowski, J.; Fox, D. J. Gaussian, Inc., Wallingford CT, **2009**.
179. Andrae, D.; Haussermann, U.; Dolg, M.; Stoll, H.; Preuss, H., *Theoretica Chimica Acta* **1990,** 77, (2), 123-141.
180. Marenich, A. V.; Cramer, C. J.; Truhlar, D. G., *J. Phys. Chem. B* **2009,** 113, (18), 6378-6396.
181. Schrock, R. R., *J. Am. Chem. Soc.* **1974,** 96, (21), 6796-6797.
182. Schrock, R. R., *Acc. Chem. Res.* **1979,** 12, (3), 98-104.
183. Adams, C. S.; Legzdins, P.; McNeil, W. S., *Organometallics* **2001,** 20, (23), 4939-4955.
184. Adams, C. S.; Legzdins, P.; Tran, E., *J. Am. Chem. Soc.* **2001,** 123, (4), 612-624.
185. Adams, C. S.; Legzdins, P.; Tran, E., *Organometallics* **2002,** 21, (7), 1474-1486.
186. Cheon, J.; Rogers, D. M.; Girolami, G. S., *J. Am. Chem. Soc.* **1997,** 119, (29), 6804-6813.
187. Coles, M. P.; Gibson, V. C.; Clegg, W.; Elsegood, M. R. J.; Porrelli, P. A., *Chem. Comm.* **1996**, (16), 1963-1964.
188. Tsang, J. Y. K.; Buschhaus, M. S. A.; Legzdins, P., *J. Am. Chem. Soc.* **2007,** 129, (17), 5372-5373.
189. Tsang, J. Y. K.; Buschhaus, M. S. A.; Graham, P. M.; Semiao, C. J.; Semproni, S. P.; Kim, S. J.; Legzdins, P., *J. Am. Chem. Soc.* **2008,** 130, (11), 3652-3663.
190. Debad, J. D.; Legzdins, P.; Lumb, S. A.; Batchelor, R. J.; Einstein, F. W. B., *J. Am. Chem. Soc.* **1995,** 117, (11), 3288-3289.
191. Legzdins, P.; Lumb, S. A., *Organometallics* **1997,** 16, (9), 1825-1827.

192. Debad, D.; Legzdins, P.; Lumb, S. A.; Rettig, S. J.; Batchelor, R. J.; Einstein, F. W. B., *Organometallics* **1999,** 18, (17), 3414-3428.
193. Ng, S. H. K.; Adams, C. S.; Legzdins, P., *J. Am. Chem. Soc.* **2002,** 124, (32), 9380-9381.
194. Ng, S. H. K.; Adams, C. S.; Hayton, T. W.; Legzdins, P.; Patrick, B. O., *J. Am. Chem. Soc.* **2003,** 125, (49), 15210-15223.
195. Kissounko, D.; Epshteyn, A.; Fettinger, J. C.; Sita, L. R., *Organometallics* **2006,** 25, (2), 531-535.
196. Buchwald, S. L.; Watson, B. T.; Huffman, J. C., *J. Am. Chem. Soc.* **1987,** 109, (8), 2544-2546.
197. Boulho, C.; Oulie, P.; Vendier, L.; Etienne, M.; Pimienta, V.; Locati, A.; Bessac, F.; Maseras, F.; Pantazis, D. A.; McGrady, J. E., *J. Am. Chem. Soc.* **2010,** 132, (40), 14239-14250.
198. Templeton, J. L., *Adv. Organomet. Chem.* **1989,** 29, 1-100.
199. Etienne, M.; Mathieu, R.; Donnadieu, B., *J. Am. Chem. Soc.* **1997,** 119, (14), 3218-3228.
200. Erker, G., *J. Organomet. Chem.* **1977,** 134, (2), 189-202.
201. Pamplin, C. B.; Legzdins, P., *Acc. Chem. Res.* **2003,** 36, (4), 223-233.
202. Cockcroft, J. K.; Gibson, V. C.; Howard, J. A. K.; Poole, A. D.; Siemeling, U.; Wilson, C., *J. Chem. Soc.-Chem. Commun.* **1992**, (22), 1668-1670.
203. McLain, S. J.; Schrock, R. R.; Sharp, P. R.; Churchill, M. R.; Youngs, W. J., *J. Am. Chem. Soc.* **1979,** 101, (1), 263-265.
204. Buijink, J. K. F.; Kloetstra, K. R.; Meetsma, A.; Teuben, J. H.; Smeets, W. J. J.; Spek, A. L., *Organometallics* **1996,** 15, (10), 2523-2533.
205. Hartwig, J. F.; Andersen, R. A.; Bergman, R. G., *J. Am. Chem. Soc.* **1989,** 111, (7), 2717-2719.
206. Buchwald, S. L.; Nielsen, R. B., *Chem. Rev.* **1988,** 88, (7), 1047-1058.
207. Eyring, H., *J. Chem. Phys.* **1935,** 3, (2), 107-115.
208. Wada, K.; Pamplin, C. B.; Legzdins, P., *J. Am. Chem. Soc.* **2002,** 124, (33), 9680-9681.
209. Wada, K.; Pamplin, C. B.; Legzdins, P.; Patrick, B. O.; Tsyba, I.; Bau, R., *J. Am. Chem. Soc.* **2003,** 125, (23), 7035-7048.
210. Rappe, A. K.; Casewit, C. J.; Colwell, K. S.; Goddard, W. A.; Skiff, W. M., *J. Am. Chem. Soc.* **1992,** 114, (25), 10024-10035.
211. Carbo, J. J.; Crochet, P.; Esteruelas, M. A.; Jean, Y.; Lledos, A.; Lopez, A. M.; Onate, E., *Organometallics* **2002,** 21, (2), 305-314.
212. Grimme, S., *J. Comput. Chem.* **2004,** 25, (12), 1463-1473.
213. Denmark, S. E.; Regen, C. S., *Acc. Chem. Res.* **2008,** 41, (11), 1486-1499.
214. Denmark, S. E.; Sweis, R. F., *J. Am. Chem. Soc.* **2004,** 126, (15), 4876-4882.
215. Denmark, S. E.; Smith, R. C., *J. Am. Chem. Soc.* **2010,** 132, (4), 1243-1245.
216. Denmark, S. E.; Baird, J. D., *Chem.-Eur. J.* **2006,** 12, (19), 4954-4963.
217. Denmark, S. E.; Sweis, R. F.; Wehrli, D., *J. Am. Chem. Soc.* **2004,** 126, (15), 4865-4875.

218. Denmark, S. E.; Werner, N. S., *J. Am. Chem. Soc.* **2008,** 130, (48), 16382-16393.
219. Denmark, S. E.; Smith, R. C.; Chang, W. T. T.; Muhuhi, J. M., *J. Am. Chem. Soc.* **2009,** 131, (8), 3104-3118.
220. Denmark, S. E.; Ober, M. H., *Adv. Synth. Catal* **2004,** 346, (13-15), 1703-1714.
221. Otsuka, S.; Yoshida, T.; Matsumoto, M.; Nakatsu, K., *J. Am. Chem. Soc.* **1976,** 98, (19), 5850-5858.
222. Dai, C. Y.; Fu, G. C., *J. Am. Chem. Soc.* **2001,** 123, (12), 2719-2724.
223. Stambuli, J. P.; Incarvito, C. D.; Buhl, M.; Hartwig, J. F., *J. Am. Chem. Soc.* **2004,** 126, (4), 1184-1194.
224. Clark, T.; Chandrasekhar, J.; Spitznagel, G. W.; Schleyer, P. V., *J. Comput. Chem.* **1983,** 4, (3), 294-301.
225. Sun, H. Y.; Gorelsky, S. I.; Stuart, D. R.; Campeau, L. C.; Fagnou, K., *J. Org. Chem.* **2010,** 75, (23), 8180-8189.
226. Casado, A. L.; Espinet, P., *Organometallics* **1998,** 17, (5), 954-959.
227. Henriksen, S. T.; Tanner, D.; Skrydstrup, T.; Norrby, P. O., *Chem.-Eur. J.* **2010,** 16, (31), 9494-9501.
228. Spies, P.; Frohlich, R.; Kehr, G.; Erker, G.; Grimme, S., *Chem.-Eur. J.* **2008,** 14, (1), 333-343.
229. Sameera, W. M. C.; Maseras, F., *Phys. Chem. Chem. Phys.* **2011,** 13, (22), 10520-10526.
230. Denmark, S. E.; Regens, C. S., *Acc. Chem. Res.* **2008,** 41, (11), 1486-1499.
231. Carrow, B. P.; Hartwig, J. F., *J. Am. Chem. Soc.* **2010,** 132, (1), 79-81.
232. Tan, Y. C.; Hartwig, J. F., *J. Am. Chem. Soc.* **2011,** 133, (10), 3308-3311.
233. Denmark, S. E.; Baird, J. D.; Regens, C. S., *J. Org. Chem.* **2008,** 73, (4), 1440-1455.
234. Denmark, S. E.; Werner, N. S., *J. Am. Chem. Soc.* **2010,** 132, (10), 3612-3620.
235. Fairlamb, I. J. S., *Org. Biomol. Chem.* **2008,** 6, (20), 3645-3656.
236. Fairlamb, I. J. S.; Kapdi, A. R.; Lee, A. F., *Org. Lett.* **2004,** 6, (24), 4435-4438.
237. Hatanaka, Y.; Ebina, Y.; Hiyama, T., *J. Am. Chem. Soc.* **1991,** 113, (18), 7075-7076.
238. Ohmiya, H.; Makida, Y.; Tanaka, T.; Sawamura, M., *J. Am. Chem. Soc.* **2008,** 130, (51), 17276-17277.
239. Cardenas, D. J.; Echavarren, A. M., *New J. Chem.* **2004,** 28, (3), 338-347.
240. Hayashi, S.; Hirano, K.; Yorimitsu, H.; Oshima, K., *J. Am. Chem. Soc.* **2006,** 128, (7), 2210-2211.
241. Yoshikai, N.; Zhang, S. L.; Nakamura, B., *J. Am. Chem. Soc.* **2008,** 130, (39), 12862-12863.
242. Yamanaka, M.; Kato, S.; Nakamura, E., *J. Am. Chem. Soc.* **2004,** 126, (20), 6287-6293.
243. Denmark, S. E.; Almstead, N. G., *J. Mex. Chem. Soc.* **2009,** 53, (3), 174-192.

244. Denmark, S. E.; Nguyen, S. T., *Org. Lett.* **2009,** 11, (3), 781-784.
245. Denmark, S. E.; Smith, R. C., *Synlett* **2006**, (18), 2921-2928.
246. Hine, J., *J. Am. Chem. Soc.* **1950,** 72, (6), 2438-2445.
247. Doering, W. V. E.; Laflamme, P., *J. Am. Chem. Soc.* **1956,** 78, (20), 5447-5448.
248. Doering, W. V.; Hoffmann, A. K., *J. Am. Chem. Soc.* **1954,** 76, (23), 6162-6165.
249. Han, J. L.; Ong, C. W., *Tetrahedron* **2005,** 61, (6), 1501-1507.
250. Moss, R. A.; Zhang, M.; Krogh-Jespersen, K., *Org. Lett.* **2009,** 11, (9), 1947-1950.
251. Begum, R. A.; Chanda, N.; Ramakrishna, T. V. V.; Sharp, P. R., *J. Am. Chem. Soc.* **2005,** 127, (39), 13494-13495.
252. Barrios-Landeros, F.; Carrow, B. P.; Hartwig, J. F., *J. Am. Chem. Soc.* **2008,** 130, (18), 5842-5843.

Annex 1

Part of the results presented in this PhD thesis have appeared in the following publications:

1. C-C Coupling Constants, J(CC), Are Reliable Probes for alpha-C-C Agostic Structures Boulho, C.; Keys, T.; Coppel, Y.; Vendier, L.; Etienne, M.; Locati, A.; Bessac, F.; Maseras, F.; Pantazis, D. A.; McGrady, J. E., *Organometallics* **2009,** 28, (4), 940-943
(related to the results reported in Chapter 2 section 1)

2. Copper(I)-Olefin Complexes: The Effect of the Trispyrazolylborate Ancillary Ligand in Structure and Reactivity Martin, C.; Munoz-Molina, J. M.; Locati, A.; Alvarez, E.; Maseras, F.; Belderrain, T. R.; Perez, P. J., *Organometallics* **2010**, 29, (16), 3481-3489
(results not reported in the PhD tesis)

3. C-H Bond Activation of Benzene by Unsaturated η^2-Cyclopropene and η^2-Benzyne Complexes of Niobium Boulho, C.; Oulie, P.; Vendier, L.; Etienne, M.; Pimienta, V.; Locati, A.; Bessac, F.; Maseras, F.; Pantazis, D. A.; McGrady, J. E., *J. Am. Chem. Soc.* **2010,** 132, (40), 14239-14250
(related to the results reported in Chapter 2 section 2)

4. Aromatic versus Benzylic CH Bond Activation of Alkylaromatics by a Transient η^2-Cyclopropene Complex Boulho, C.; Vendier, L.; Etienne, M.; Locati, A.; Maseras, F., *Organometallics* **2011,** 30, (15), 3999-4007
(related to the results reported in Chapter 2 section 3)